2001

Premixed ammonia-methane-air combustion.

Kenneth R. C. Mann
University of Windsor

INFORMATION TO USERS

This manuscript has been reproduced from the microfilm master. UMI films the text directly from the original or copy submitted. Thus, some thesis and dissertation copies are in typewriter face, while others may be from any type of computer printer.

The quality of this reproduction is dependent upon the quality of the copy submitted. Broken or indistinct print, colored or poor quality illustrations and photographs, print bleedthrough, substandard margins, and improper alignment can adversely affect reproduction.

In the unlikely event that the author did not send UMI a complete manuscript and there are missing pages, these will be noted. Also, if unauthorized copyright material had to be removed, a note will indicate the deletion.

Oversize materials (e.g., maps, drawings, charts) are reproduced by sectioning the original, beginning at the upper left-hand corner and continuing from left to right in equal sections with small overlaps.

Photographs included in the original manuscript have been reproduced xerographically in this copy. Higher quality 6" x 9" black and white photographic prints are available for any photographs or illustrations appearing in this copy for an additional charge. Contact UMI directly to order.

ProQuest Information and Learning
300 North Zeeb Road, Ann Arbor, MI 48106-1346 USA
800-521-0600

PREMIXED AMMONIA-METHANE-AIR COMBUSTION

By

Kenneth R.C. Mann

A Thesis
Submitted to the Faculty of Graduate Studies and Research
through Environmental Engineering
in Partial Fulfillment of the Requirements for
the Degree of Master of Applied Science at the
University of Windsor

Windsor, Ontario, Canada

2000

Abstract

To better understand the effects of ammonia as a fuel additive, both the adiabatic burning velocities and combustion emissions were determined for premixed methane-air and ammonia-methane-air flat flames. The experimental results of this work were compared to chemical kinetic (CHEMKIN III) and thermodynamic (STANJAN) simulations as well as literature values. The literature provided limited information on emissions from ammonia-methane-air flames. There was also a lack of information regarding the burning velocities of these mixtures.

A flat flame burner was built on the basis of the design of the perforated plate burner of van Maaren et al. [1993]. This burner facilitated the direct measurement of the adiabatic burning velocity based on the measurement of the unburned gas velocity. Using a 5-gas analyzer and a chimney, NO, NO_2, CO, CO_2 and O_2 emissions from various mixtures of ammonia-methane-air were determined. The burning velocity data for methane-air mixtures was found to be in good agreement with the literature and chemical kinetic simulations. For additions of 1% to 4% ammonia in the fuel, both the experimental observations and kinetic simulations revealed premixed ammonia-methane-air flames yield lower burning velocities than pure methane-air flames and result in a significant increase in NO emissions. In agreement with Wendt et al. [1974], the formation of NO in these flames appeared to be independent of thermodynamic equilibrium.

To my family

Acknowledgements

The author would like to express his sincere gratitude to Dr. P. Henshaw and Dr. D. Ting for their excellent guidance and support throughout this project. The valuable assistance and support of Dr. C. Uykur is also greatly appreciated.

The author is also grateful for the help and advice of Dr. A. Gnyp and Dr. A Sobiesiak. Technical assistance from Mr. Bill Henderson and Mr. Pat Seguin is also acknowledged and appreciated.

The financial support of NSERC is also gratefully acknowledged.

Table of Contents

ABSTRACT III

ACKNOWLEDGEMENTS V

TABLE OF CONTENTS VI

LIST OF TABLES IX

LIST OF FIGURES X

NOMENCLATURE XII

1.0 INTRODUCTION 1

1.1 Objective 2

1.2 Scope 2

2.0 LITERATURE REVIEW 3

2.1 One-Dimensional Flat Flames 3

2.2 Burning Velocity Measurement 4
2.2.1 Non-stationary Flames 5
2.2.2 Stationary Flames 7

2.3 Flat Flame Burners 8
2.3.1 The Porous-Plug Burner [Botha et al., 1954] 8
2.3.2 The Perforated Plate Burner [van Maaren, 1994] 12

2.4 Effect of Ammonia Addition on NO Emissions from a Flat Flame Burner 15

3.0 SIMULATIONS 17

3.1 Equivalence Ratio Calculation for Simulations 17

3.2 Thermodynamics of NH_3-CH_4-air Combustion 19
3.2.1 Method of Equilibrium Calculation 19

3.3 Chemical Kinetic Simulations of NH_3-CH_4-air Combustion 21
3.3.1 CHEMKIN III Interpreter 22

4.0 MATERIALS AND METHODS 27

4.1 Apparatus 27
4.1.1 Burner 27
4.1.2 System 30

4.2 Methods 32
4.2.1 Protocol 32
4.2.2 Determination of Burning Velocity and Equivalence Ratio, ϕ 33
4.2.3 Determining the Ammonia Content of the Fuel 35
4.2.4 Measuring Emissions 36
4.2.5 Measurement of Ammonia Breakthrough 37

5.0 RESULTS AND DISCUSSION 39

5.1 Burning Velocity 39

5.2 Emissions 43

5.3 Ammonia Break-through 55

6.0 CONCLUSIONS AND RECOMMENDATIONS 57

REFERENCES 60

APPENDIX A: REACTANT COEFFICIENTS FOR SIMULATIONS 63

Lean Conditions 63

Rich Conditions 64

APPENDIX B: THE GRI MECHANISM VERSION 3.0 65

APPENDIX C: FLAT FLAME BURNER DESIGN 79

APPENDIX D: SAMPLE CALCULATIONS 84

Equivalence Ratio, ϕ 84

Adiabatic Burning Velocity, S_u 86

Calculation of Ammonia Content in the Fuel 86

APPENDIX E: UNCERTAINTY ANALYSIS 87
Uncertainty in Measuring ϕ 87

Uncertainty in Measuring S_u 89
Uncertainty in NH_3% in fuel 91

APPENDIX F: CALIBRATION OF FLOWMETERS **92**

APPENDIX G: MEASUREMENT RANGE AND ACCURACY OF THE IMR 5-GAS ANALYZER **97**

APPENDIX H: OBSERVED FLAME PROPERTIES **98**

FLAME PHOTOGRAPHS **99**

APPENDIX I: THERMODYNAMIC COMPARISON OF CH_4-AIR AND NH_3-CH_4-AIR COMBUSTION **102**

APPENDIX J: AMMONIA BREAK-THROUGH LOWER LIMIT OF DETECTION **105**

VITA AUCTORIS **107**

List of Tables

Table A 1 Stoichiometric coefficients for NH_3-CH_4-Air lean mixtures 63
Table A 2 Stoichiometric coefficients for NH_3-CH_4-Air rich mixtures 64

Table D 1 Sample data for calculation of equivalence ratio. 84
Table D 2 Flow rate calculation. 84
Table D 3 Pressure and temperature corrected flowrates. 85

Table E 1 Typical uncertainty in equivalence ratio. 89
Table E 2 Typical uncertainty in equivalence ratio with ammonia addition 89
Table E 3 Uncertainty in measuring S_u. 90
Table E 4 Uncertainty in S_u with ammonia addition 91
Table E 5 Uncertainty in measuring the ammonia content of the fuel 91

Table F 1 Flowrate calibration equations. 93
Table F 2 Atmospheric pressure at calibration conditions. 93

Table G 1 IMR 5-Gas Analyzer accuracy and measurement range 97

Table H 1 Observed characteristics for CH_4-Air and NH_3-CH_4-Air flames 98

Table I 1 STANJAN equilibrium products for stoichiometric CH_4-Air 103
Table I 2 STANJAN equilibrium products for stoichiometric NH_3-Air 103
Table I 3 STANJAN equilibrium products for stoichiometric $0.2NH_3$-CH_4-Air 103

List of Figures

Figure 2. 1 The one-dimensional combustion wave. 3
Figure 2. 2 The burner stabilized flat flame. 9
Figure 2. 3 Perforated plate burner design of van Maaren, [1994]. 13
Figure 2. 4 Adiabatic condition of the perforated burner plate [van Maaren, 1994] 14

Figure 3. 1 Flowchart of general STANJAN analysis 20
Figure 3. 2 Axial temperature direction in a burner stabilized flat flame 22
Figure 3. 3 Experimental and simulation axial temperature profile comparison. 26

Figure 4. 1 Section through the experimental flat flame burner. 28
Figure 4. 2 The flat flame burner. 28
Figure 4. 3 Schematic of experimental layout. 31
Figure 4. 4 Experimental set-up for ammonia breakthrough testing. 38

Figure 5. 1 Comparison of methane-air burning velocities obtained by various workers 40
Figure 5. 2 Experimental and Simulation adiabatic burning velocity data for CH_4-air and NH_3-CH_4-air mixtures 42
Figure 5. 3 Comparison of adiabatic burning velocity results for 0% and 4% ammonia addition 42
Figure 5. 4 Experimental NO emissions from NH_3-CH_4-air flames. 43
Figure 5. 5 Comparison of experimental and simulation values for NO production in CH_4-air and NH_3-CH_4-air flames 44
Figure 5. 6 Effect of burner plate on axial temperature profiles [van Maaren et al. 1993]. 46
Figure 5. 7 Radical formation in the preheat zone of a stoichiometric NH_3-CH_4-air laminar flame. 47
Figure 5. 8 Comparison of experimental, simulation and thermodynamic results to the experimental data of Wendt et al., [1974]. 48
Figure 5. 9 Experimental results for NO_2 production in CH_4-air and NH_3-CH_4-air flat flames. 53
Figure 5. 10 Simulation results for NO_2 production in CH_4-air and NH_3-CH_4-air flat flames. 53
Figure 5. 11 Effect of ammonia addition on CO emissions from CH_4-air flat flames. 54
Figure 5. 12 Comparison of experimental and simulation results for ammonia break-through in NH_3-CH_4-air flat flames. 56

Figure C 1 Aluminum Burner Plate 79
Figure C 2 Burner Head 80
Figure C 3 Burner mixing chamber and distribution plate 81
Figure C 4 Burner cooling jacket 82
Figure C 5 Burner bottom cover plate 83

Figure F. 1 Flowrate calibration curve for the air flowrate 93
Figure F. 2 Pressure calibration curve for air. 94
Figure F. 3 Flowrate calibration curve for methane 94
Figure F. 4 Pressure calibration curve for methane. 95
Figure F. 5 Flowrate calibration curve for 5%-NH_3-air 95
Figure F. 6 Pressure calibration curve for 5%-NH_3-air 96

Figure H 1 Photograph of a CH_4-air adiabatic flat flame at ϕ=0.7. 99
Figure H 2 Photograph of a CH_4-air adiabatic flat flame at ϕ=0.9. 99
Figure H 3 Photograph of a CH_4-air flame with the unburned gas velocity > S_u 99
Figure H 4 Unburned gas flowrate greater than Su for a) CH_4-air rich flame, b) CH_4-air lean flame 100
Figure H 5 Photograph of 4% NH_3 addition flame for a) lean conditions and b) rich conditions 101

Nomenclature

ΔX_u = the distance the unburned gas travels with respect to the flame front
Δt = time increment
S_u = velocity of the unburned gas mixture relative to the flame front
Q_i = flow rate of species i
A = cross-sectional Area
V = unburned gas velocity
T_u = Unburned gas temperature
ϕ = equivalence ratio
Po = unburned gas pressure
S_u'= non-adiabatic burning velocity
Su = adiabatic burning velocity
Tb'= non-adiabatic flame temperature
q = heat loss
C_n = concentration corrected to n% O_2,
C_x = concentration at actual % O_2,
n = % O_2 correction desired,
x = actual % O_2 in products.
x = spacial coordinate

$\dot{M}$ = mass flow rate (which is independent of x)
T = temperature
Y_k = mass fraction of the k^{th} species
p = pressure
u = velocity of the fluid mixture
ρ = mass density
W_k = molecular weight of the k^{th} species
W= mean molecular weight of the mixture
R = universal gas constant
λ = the thermal conductivity of the mixture
c_p = constant pressure heat capacity of the mixture
c_{pk} = constant pressure heat capacity of the k^{th} species
$\dot{\omega}_k$ = the molar rate of production by chemical reaction of the k^{th} species per unit volume
h_k = the specific enthalpy of the k^{th} species
V_k = the diffusion velocity of the k^{th} species
A = the cross-sectional area of the stream tube encompassing the flame (unity by default)

1.0 Introduction

A growing awareness of the severity of the global pollution problem in the combustion community has prompted many studies aimed at decreasing the emissions from combustion processes [Cooper et al., 1994; Glassman, 1996; Borman et al., 1998;]. Though other energy sources exist, it will likely be some time before they are refined to a point where they can replace fossil fuels [Cooper et al., 1991]. Until such a time, research aimed at minimizing the harmful emissions from combustion applications is of great importance.

It is well known that common combustion products such as nitrogen oxides (NO_x) and carbon dioxide (CO_2) contribute greatly to problems such as acid rain and global warming. To reduce NO_x emissions from stationary combustion applications, it is possible to use ammonia (NH_3) injection into the combustion products. Two methods have been proven, selective catalytic reduction (SCR) at temperatures of 300 to 430K and selective non-catalytic reduction (SNCR) at temperatures of about 1100 to 1400K [Roslyakov et al., 1989].

Combustion of gaseous streams that contain ammonia occurs in the disposal of waste gases from anaerobic digesters, flaring of natural gas, and chemical and petroleum processing plants. Since the combustion of fuels containing ammonia is likely to lead to a significant NO_x air pollution problem, it is important to determine the conditions when this problem might be minimized. It is also useful to examine the variables that effect

NO_x production, and evaluate combustion modifications to minimize nitrogen oxide emissions [Wendt et al., 1974].

Ammonia may meet one of several fates during combustion. Under fuel lean conditions it may be oxidized to give equilibrium concentrations of NO or its conversion may be kinetically controlled to give production of NO which is independent of equilibrium. Under fuel rich conditions, some ammonia may not be oxidized at all, or it may be partially oxidized to NO and N_2 where product concentrations are independent of equilibrium.

1.1 Objective

The focus of this thesis was to investigate the effect that premixed ammonia addition to methane-air combustion has on emissions (NO_x and CO) and laminar burning velocity.

1.2 Scope

To accomplish this, a flat flame burner was built to provide a means of measuring adiabatic laminar burning velocities and emissions in laboratory-scale one-dimensional (1-D) flat flames. In addition, thermodynamic and kinetic simulations of the combustion were conducted and compared to the experimental results.

2.0 Literature Review

2.1 One-Dimensional Flat Flames

The one-dimensional (1-D) flame, as shown in figure 2.1, is one of the most frequently studied flames in combustion research due to its well-defined structure and properties. Flat flame burners are often used to stabilize premixed laminar flames to study the chemical kinetics of combustion. These stationary flat flames can essentially be considered 1-dimensional (the dimension being the distance from the burner plate) and allow explicit experimental measurements of temperature and species profiles. Further, burning velocity is often used to characterize the combustion of various fuel-oxidizer combinations. In addition, the ability to model chemical kinetics and transport processes in these flames is very important for understanding the combustion process, interpreting experimental data, and predicting flame properties.

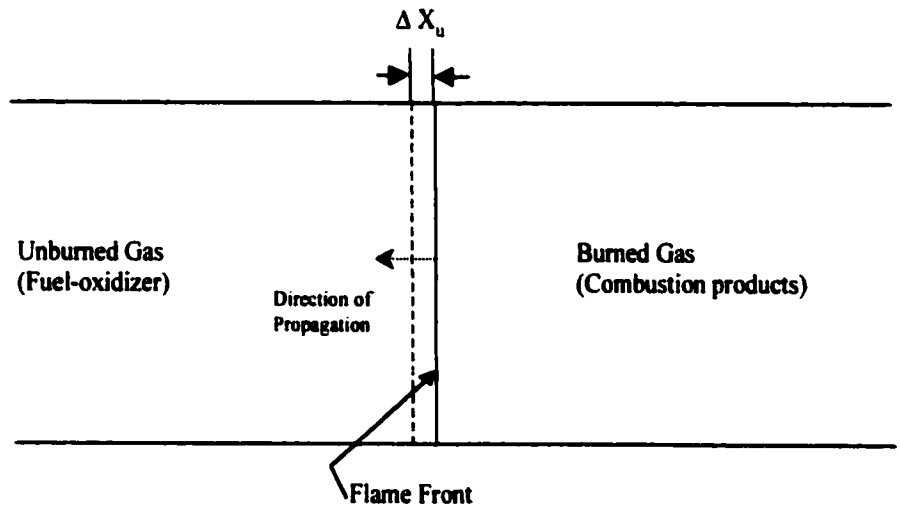

Figure 2. 1 The one-dimensional combustion wave.

The 1-D combustion wave propagates by thermal and molecular (radicals) diffusion. These transport processes control its velocity. Figure 2.1 illustrates that, the laminar burning velocity of a 1-D flame, S_u, is the velocity of the unburned gas mixture relative to the flame front and can be expressed as:

$$S_u = \frac{\Delta X_u}{\Delta t} \tag{2.1}$$

where ΔX_u is the distance the unburned gas travels with respect to the flame front in time, Δt.

It should be noted that in reality, true 1-D flames are impossible to create due to inevitable heat losses and flow non-uniformity which result in flame unevenness. However, with careful design, situations that approximate 1-D flames can be accomplished. Properly designed flat flame burners have proven to be good approximations [van Maaren et al.,1994; Fristrom, 1995; Glassman, 1996].

2.2 Burning Velocity Measurement

Burning velocity is a physicochemical constant for a given combustible mixture. As described by equation 2.1 it is the velocity, relative to the unburnt gas, with which a plane, one-dimensional flame front travels along the normal to its surface [Andrews & Bradley, 1972a]. Though its theoretical definition is straight forward, its experimental measurement is quite involved.

Methods of measuring burning velocity involve the use of two flame types: non-stationary flames, where the flame passes through a quiescent gas, and stationary flames where the flame is held stationary relative to the laboratory.

2.2.1 Non-stationary Flames

Some popular methods of measuring burning velocities with non-stationary flames are as follows:

Tube Method:

This was one of the first methods used originally by Bunsen [1866] in which the flame propagation speed was determined by measuring the amount of time it takes a flame to propagate through a tube of known length. The tube was typically open at the ignition end and closed at the other. As technology progressed, high-speed photographic techniques enabled flame front propagation to be photographed [Mallard and Le Chatelier, 1883]. It was determined that with this technique the flame propagation speed was not equal to the burning velocity. To improve this method for determination of burning velocity, successive experimentation lead to the use of orifice plates at the burned and unburned ends of the tube to reduce pressure waves and thus stabilize the flame. Viscous drag forces of the burnt gas at the wall cause the flame front to be distorted. Even if photography of the flame reveals that it is a true ellipsoid, accurate determination of the flame surface area is near impossible. More recently, a technique created by Raezer and Olsen [1962] produces propagating flat flames in a tube which reduce the error in measurement of flame surface area. In this method the flame propagationspeed is equal to the burning velocity, but only when the unburnt gas velocity

and rise of temperature and pressure are equal to zero [Andrews and Bradley, 1972; Fristrom, 1995].

Contained Explosions:

With this method a contained explosive mixture is ignited centrally, and the rate of propagation of the spherical flame front in space is measured. Both the pressure rise of the combustion chamber and photography of the growing flame ball can be used. Due to the complexity of this type of combustion, i.e. the changing pressure, temperature and flame radius, calculation of burning velocity is quite involved. If the flame thickness is neglected and gas ideality implied, the burning velocity can be calculated from the time rate of change of diameter obtained by photography [Andrews and Bradley, 1972; Fristrom, 1995].

Constant-Pressure Measurements

Typically, a combustible gas mixture is isolated from its surroundings by means of a flexible membrane such as a soap bubble. The mixture is then centrally ignited and the flame propagation (spherical) can be visualized by photographic methods. Since the gas consumed by the spherical flame expands during combustion, the measurements describe the expansion velocity. Derivation of the burning velocity from the expansion velocity requires that the density change across the flame front is known along with a correction for finite flame thickness. Assuming a model with constant flame thickness, these results are generally extrapolated to large diameters where the flame approximates a one-dimensional plane [Andrews and Bradley, 1972; Fristrom, 1995].

2.2.2 Stationary Flames

If the flame propagation can be matched by an opposing flow, then the burning velocity of a stationary flame (fixed in laboratory coordinates) can be determined. Producing a burner stabilized laminar flame of any measurable geometry can do this.

In earlier work, by Gouy [1879], conical flames were used for burning velocity measurements. In this method the gas velocity normal to a conical flame must be measured. As well, it is assumed that all the premixed gas passes through the flame. Determining the surface area of the flame front, A, and knowing the flow rate of the unburned gas, Q, burning velocity can be calculated from V=Q/A. However, this method is inaccurate due to difficulty in determining the surface area of the flame since in reality it is not truly conical. Determination of burning velocity from flame angles is another method available. Again many inaccuracies can arise with this approach due to optical measurement of angles and pressure and temperature variations in the flame that are not accounted for. Other methods involving flame area methods such as the slot burner method are limited by flame instabilities and error in estimating the flame front area normal to the unburned gas flow [Andrews and Bradley, 1972a, b; Fristrom, 1995]. To reduce these errors, properly designed burners can create flat flames which allow for accurate measurement of burning velocity.

2.3 Flat Flame Burners

Constant velocity profiles of unburned gas can be created using flow straightening methods. With a uniform velocity profile, at low velocities with heat extraction from the flame, a flat stationary flame can be created a short distance downstream of the burner. Assuming all the unburned gas passes through the flame, and because of the ease in determining the flat flame surface area, the burning velocity can easily be determined by the unburned gas velocity based on V=Q/A.

A number of flat flame burner designs can be found in the literature. The first flat flame burner was that of Powling [1949]. However, Powling's burner design was such that flat flames could only be created in a small burning velocity range. In 1954, a new burner was introduced, the porous-plug burner [Botha et al., 1954].

2.3.1 The Porous-Plug Burner [Botha et al., 1954]

The key feature of this burner is a water-cooled disk of porous bronze through which the combustible material is passed. Since the porosity of the disk is fine, the emerging gas stream can be considered uniform. When the gas downstream of the disk is ignited, the flame that is formed will travel upstream if the stream velocity is less than the burning velocity or downstream if the stream velocity is greater. If the burning velocity and stream velocity are exactly matched the flame remains fixed in space in a plane normal to the direction of flow. This balancing becomes impossible when the burning velocity exceeds about 12 cm/s.

The method of Botha et al. [1954] does not require that the flame and stream velocities be balanced. Figure 2.3 helps to illustrate this point. The stream velocity, V, is simply set to a value less than the burning velocity. This causes the flame to travel upstream towards the water-cooled disk. As the flame approaches the disk it begins to transfer heat, q, to the disk, which due to the water-cooling, does not rise in temperature more than a few degrees. However, the temperature of the burned gases is greatly reduced (T_b'), and consequently the burning velocity is reduced (S_u'). As a result the flame rapidly and automatically takes up a position of equilibrium a short distance away from the disk, where it looses just enough heat for the stream velocity to equal the burning velocity, S_u'. This is less than the adiabatic burning velocity, S_u.

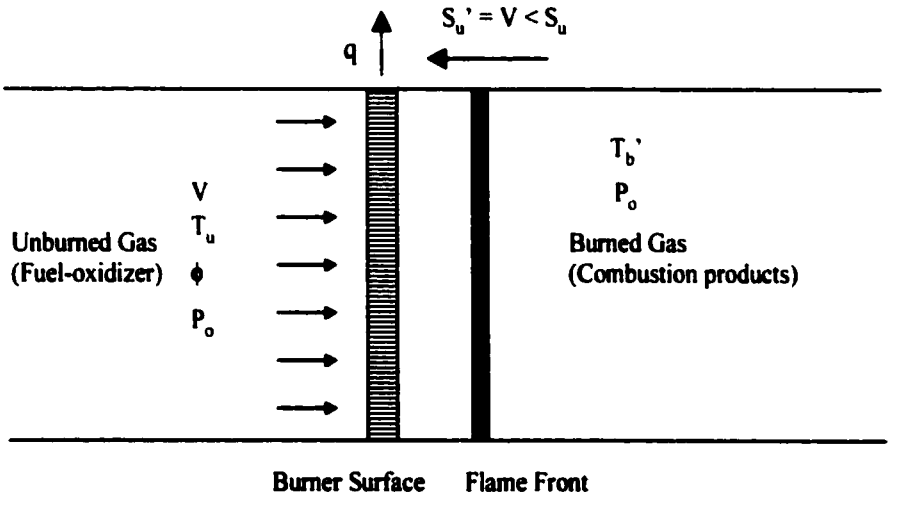

Figure 2. 2 The burner stabilized flat flame.

Since the heat carried away by the cooling water through the disk is measured, the burning velocity can be calculated by V=(total flow)/Area. Knowing total unburned gas flow and flat flame area, it is therefore possible to plot burning velocity vs. heat carried

away for a given mixture ratio. It is by extrapolating from these curves to zero heat loss that the adiabatic burning velocity can be determined. Clearly when the stream velocity is small in comparison to the burning velocity, a large amount of heat is removed from the disk, when the stream velocity is increased to approach the laminar adiabatic burning velocity of the uncooled mixture, the heat transfer rate to the porous metal disk decreases. Usually when the stream velocity equals or exceeds the adiabatic burning velocity the flame does not remain planar, but distorts into a non-laminar state. Therefore the value of the stream velocity that corresponds to no heat transfer from the flame to the disk must be obtained by extrapolation.

Botha et al.'s burner does not give adiabatic flames, because the removal of heat by the porous disk is a necessary stabilizing mechanism. However it is believed that this stabilized flame is identical, in the decisive temperature region, with adiabatic flames giving the same fully burned state. The rate of chemical reaction is the same whether heat conducted in an upstream direction is in part removed by the cooling water or exclusively used in increasing the enthalpy of the oncoming gases.

Description of Burner Apparatus and Method

The burner used by Botha et al. consisted of a 51 mm (2") diameter flat flame burner tube with three concentric water jackets and was constructed of brass. Three sintered bronze disks (porous-plug) of diameter 51mm and 3mm thick (2" x 1/8") were soldered to the burner tube and created a uniform velocity profile at the burner nozzle.

The top bronze disk was soldered around its entire outer rim to form a good thermal contact with the outer water-jacket. The outer water-jacket extended over the entire outer burner tube and had a water inlet at the top and an outlet at the bottom. Measurements were taken in these inlets/outlets to determine the heat carried away by the disk. Cooling water was supplied by a constant level reservoir and a constant flow rate was supplied throughout a series of experiments. The rest of the tubes were packed with steel wool to help prevent explosion and aid in the mixing of the fuel and air. The inner cooling water jackets helped keep the unburned gas at a constant temperature. Copper-constantan thermocouples were placed in the disks to measure their radial temperature distribution.

Flow rates of fuel and air to the burner were also measured and controlled. At the start of each series of experiments a rich mixture was used and the fuel flow rate was backed off until a flat flame was observed. Then various pressure, temperature and flow rate readings were taken so that the burning velocity and heat removed by the disk could be determined. Then a different fuel air ratio was set keeping the same total flow rate. With a constant total flow rate the stream velocity was kept constant for the series of mixtures. The system was allowed to reach steady state and new data was recorded to determine the burning velocity and heat removed for the new mixture. This was repeated for every desired mixture ratio at the same total flow rate of unburned mixture. Then a new total flow was set using the same mixture ratios and the experiments were repeated. As the flow rate was increased the stream velocity was increased and the measured burning velocity approached the laminar adiabatic burning velocity.

2.3.2 The Perforated Plate Burner [van Maaren, 1994]

The main difference between the design of the perforated plate burner of van Maaren [1994] and that of Botha et al. [1954] is the use of a perforated burner plate in place of a porous plug. As mentioned in the previous section, the porous-plug style of Botha required that heat be extracted from the flame for stabilization, and extrapolation of results was necessary to determine the adiabatic burning velocity. Further, the porous-plug design does not allow measurements such as Laser Doppler Velocimetry (LDV) to be performed as the required particle seeding would clog the porous-plug. The perforated burner plate design of van Maaren [1994] solves these problems.

The perforated plate is the most important part of this burner design. A brass plate of radius 15 mm and a thickness of 2 mm with a hexagonal perforation pattern of 0.5 mm and a pitch of 0.7 mm was used. Using LDV, van Maaren et al. [1994] found the flow field created to be optimum for producing almost perfectly one-dimensional flames. On the upstream side of the plate, small thermocouples (0.1 mm) were soldered inside some of the perforations to monitor its radial temperature profile. The burner plate was mounted onto a burner head which was kept at a constant temperature of ~368 K for all experiments. Below the burner head was a plenum chamber which maintained the unburned mixture at a temperature of 298 K. Figure 2.3 illustrates the mechanics of the perforated plate burner design of van Maaren et al. [1994].

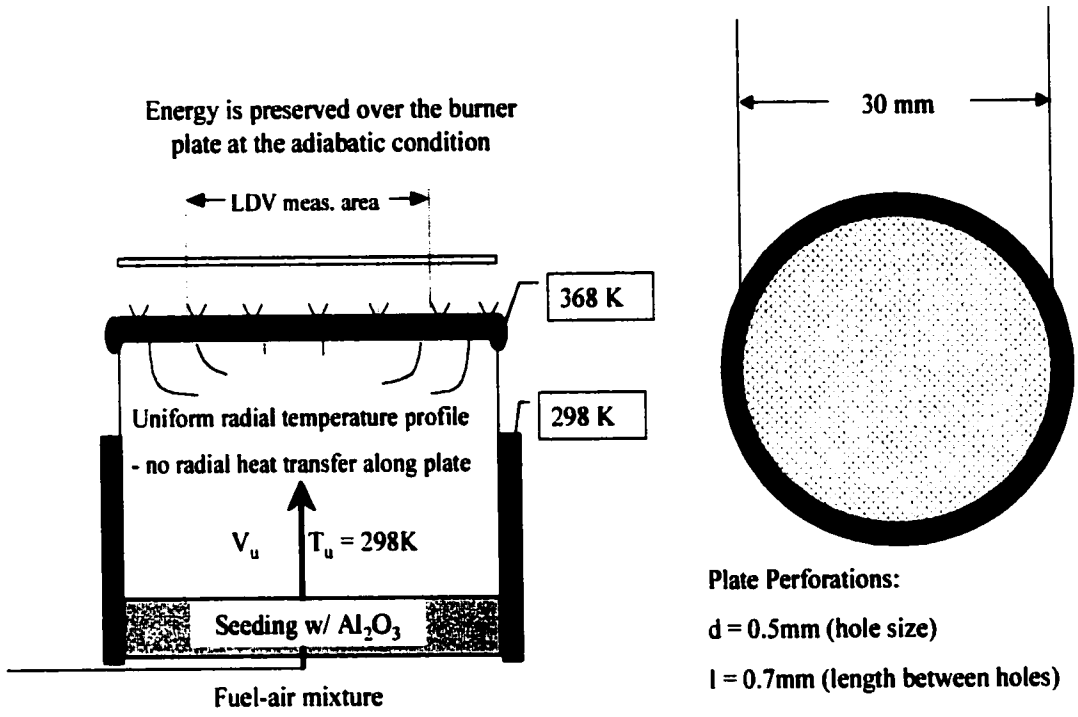

Figure 2. 3 Perforated plate burner design of van Maaren, [1994].

Since the brass burner plate has such a high thermal conductivity, it is very sensitive to small changes in heat loss from the flame. When the unburned gas flowrate is slightly lower than S_u the flame will approach the burner plate and thus the burner plate temperature will increase and be non-uniform with a thermal gradient toward the outside of the burner head. Conversely, when the unburned gas flowrate is slightly higher than S_u the flame will lift away from the burner plate causing the burner plate temperature to again become non-uniform, under which condition the burner plate will gain heat from the burner head. Only when the unburned gas velocity matches S_u will the radial temperature across the burner plate be uniform. Under these conditions there is no thermal gradient radially in the burner plate. Thus any heat extracted to stabilize the flame is transferred directly to the unburned gases as they pass through it. If any heat losses to the environment are neglected and the system boundaries for the adiabatic

condition are extended through the flame's pre-heat zone, the flame and burner plate together can be considered adiabatic [de Goey et al., 1993]. With this method the burning velocity of experimental adiabatic laminar flat flames can be measured accurately and directly with this burner without the need for extrapolation. Figure 2.4 illustrates the adiabatic conditions of the perforated burner plate [van Maaren, 1994].

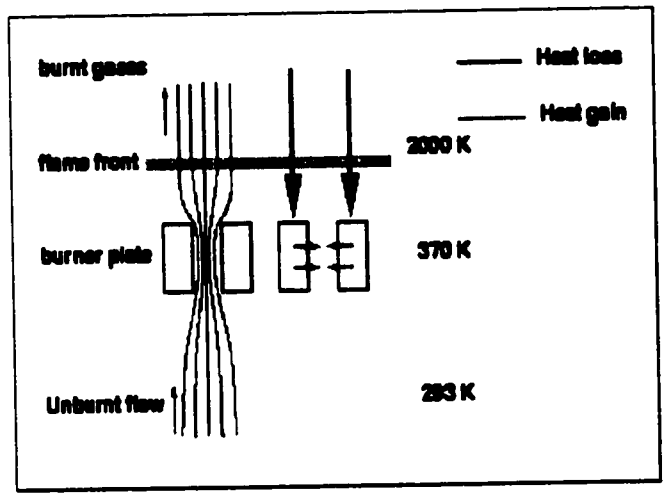

Figure 2. 4 Adiabatic condition of the perforated burner plate [van Maaren, 1994]

2.4 Effect of Ammonia Addition on NO Emissions from a Flat Flame Burner

Wendt et al. [1974] investigated a number of methods for burning ammonia to produce low NO_x emissions in both laboratory and field tests to answer the following questions:

1. Under what conditions is NH_3 oxidized to N_2 instead of NO?
2. Under fuel rich conditions, does NH_3 pass through the flame unreacted?
3. Which combustion modifications might lead to higher conversions of NH_3 to N_2 and lower conversions to NO?

A modified Meker burner (porous-plug burner with a flame stabilization grid) was used to establish an approximately flat premixed flame above a grid. A movable injector above the grid allowed for either secondary air or secondary fuel to be added at different locations above the primary flame. The burner was enclosed in a Pyrex chimney with an asbestos cap on it. Samples were drawn from a 23 mm inside diameter Vycor chimney protruding from the top. Analysis of NO_x was done by on-line instrumental methods using an electrochemical sensing device.

Wendt et al. [1974] found that the degree of conversion of ammonia to NO_x was a strong function of excess air, ammonia content in the fuel, and degree of mixing in the flame. In premixed laboratory flames it was found that the actual NO_x concentrations exceeded that of peak equilibrium values. In furnace diffusion flames it was discovered that the conversion of ammonia to NO_x was much less than that of premixed laboratory flames.

At substoichiometric fuel-air ratios all the ammonia appeared to pyrolize, forming N_2, and little NO_x was formed.

Wendt et al. [1974] determined that with 10% excess air and above, the effect of adding NH_3 on NO_x concentration was minimal. Below 10% excess air (fuel rich), the effect was very great. For higher percentages of NH_3 in the fuel, the conversion to NO_x was essentially zero when the flame was operated at approximatly 87% stoichiometric air. Under these fuel rich conditions the products were analyzed for unburned NH_3 and none could be found. This means that ammonia was being converted to N_2 even when little NO_x was formed, rather than passing through unreacted. The conversion of ammonia to NO_x was also shown to be heavily dependent on the ammonia content in the fuel. At the same fuel to air ratio higher ammonia/fuel percentages produce less conversion to NO_x. This means that although the absolute NO_x emission rate increases with increasing NH_3 in the fuel, the percent conversion decreases i.e. NH_3 has a self-inhibiting effect on its own oxidation. Under fuel rich conditions (<87% stoichiometric) low concentrations of NH_3 in the fuel give higher concentrations of NO_x than with higher concentrations of NH_3. The reason for this is that under fuel rich conditions, the amount of N_2 formed depends on the reaction of NH_3 both with itself and with NO_x that may have formed. This would tend to increase the N_2 (and decrease NO) with increasing NH_3.

Wendt et al. [1974] concluded that minimum NO_x formation occurs when burning as concentrated an ammonia stream as possible, at as fuel rich a condition as possible.

3.0 Simulations

This chapter is devoted to describing the thermodynamic and chemical kinetic simulations of NH_3-CH_4-air combustion used in this thesis.

3.1 Equivalence Ratio Calculation for Simulations

To represent stoichiometric, lean and fuel rich combustion, and taking care not to exceed the approximate flammability limits (of methane-air) the equivalence ratio, ϕ, was varied from 0.5 to 1.5 [Borman et al., 1998]. The equivalence ratio is defined as:

$$\phi = \frac{\left(\frac{F}{A}\right)_{actual}}{\left(\frac{F}{A}\right)_{stoich.}} \tag{3.1}$$

where $(F/A)_{actual}$ is the experimental ratio of the fuel to air on a molar, volume or mass basis and $(F/A)_{stioch.}$ is the theoretical ratio of fuel to air required for stoichiometric combustion.

The number of moles of air (x) required to satisfy the desired ϕ value, was determined first by calculating the required air for complete combustion using by the following stoichiometric chemical equation:

$$CH_4 + aNH_3 + x\,(O_2 + 3.76N_2) \rightarrow yH_2O + CO_2 + zN_2$$

The molar value of a was set to a constant value for each run, allowing the $\%NH_3$ in the fuel (CH_4 +NH_3) to be calculated by:

$$\%NH_3 = \frac{a}{1+a} \tag{3.2}$$

The value of x is the air required at the "stoichiometric" condition. A value of x_ϕ under rich or lean conditions at the same fuel composition was calculated from:

$$x_\phi = x \cdot \phi \tag{3.3}$$

where, x_ϕ is the air required for combustion at the desired equivalence ratio, ϕ. Values of x and x_ϕ for the fuel compositions used in this thesis are summarized in Appendix A.

Correction of Results

The computed post flame species concentrations were then reported on a dry basis corrected to 3% O_2. The dry basis was determined by recalculating the product mole fractions without including H_2O in the total number of moles. Concentrations were reported as parts per million (ppm). Oxygen correction was based on the general formula [Cooper et al., 1974]:

$$C_n = C_x\left(\frac{20.9-n}{20.9-x}\right) \tag{3.4}$$

where, C_n = concentration corrected to n% O_2,
C_x = concentration at actual % O_2,
n = % O_2 correction desired,
x = actual % O_2 in products.

The O_2 correction eliminates the dilution effect that excess air has on combustion product concentrations thus allowing for more meaningful comparison between data from different fuel-air conditions.

3.2 Thermodynamics of NH_3-CH_4-air Combustion

This section consists of a theoretical study of the chemical equilibrium thermodynamics involved in ammonia-methane-air combustion. Chemical equilibrium analysis was performed using the element potential method as calculated using the STANJAN computer program [Reynolds, 1986].

3.2.1 Method of Equilibrium Calculation

Element Potential Method

There are many methods available to solve chemical equilibrium problems. One is to use the concept of equilibrium constants, which requires identification of the set of reactions that take place to determine expressions for the associated equilibrium constants. It is then necessary to solve a system of non-linear algebraic equations to find the number of moles of each species at equilibrium. This can become a difficult and tedious task. Other methods used are based on the minimization of the Gibbs function and can also become quite difficult to solve with large systems based on the number of variables involved.

In the method of element potentials, the mole fractions of each species are related to quantities called element potentials. There is one element potential for each independent atom in the system, and these element potentials, plus the total number of moles in each phase, are the only variables that may be adjusted for the solution [Reynolds, 1986]. To simplify the problem of solving the chemical equilibria of large systems, it is preferred to use the element potential method.

STANJAN

The interactive program STANJAN [Reynolds, 1986] can be applied to solving chemical equilibrium problems. Developed at Stanford University, this program uses the element potential method and data from JANAF Thermo-chemical tables [JANAF, 1977]. For this project STANJAN version 3 was used. Figure 3.1 summarizes the general procedure for each STANJAN run used in this study.

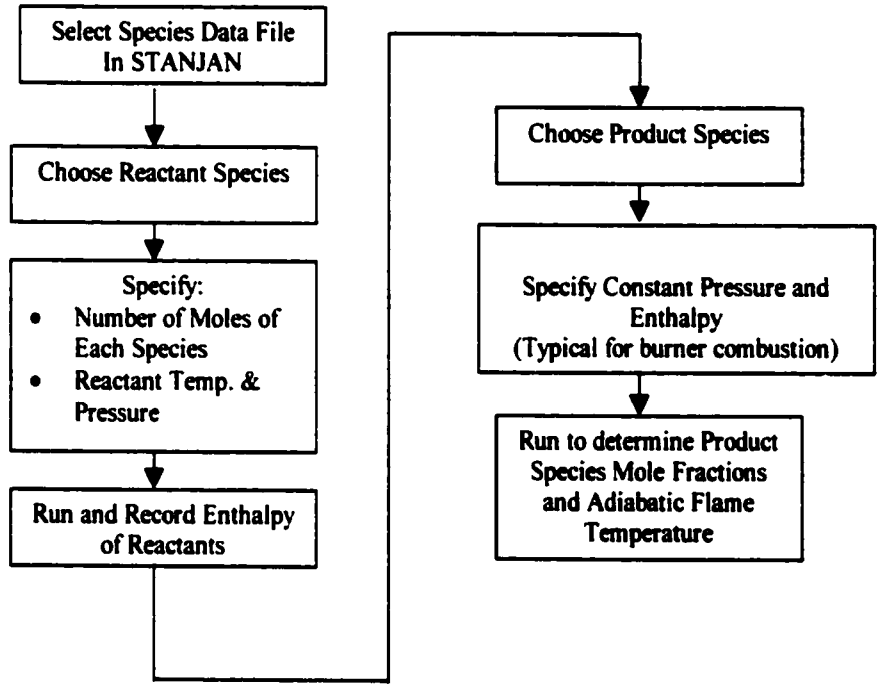

Figure 3. 1 Flowchart of general STANJAN analysis

Species Thermo-Chemical Data

Included with STANJAN is a program called JANFILE, which can be used to prepare data files for reactant or product species that are not found in the existing STANJAN data. The procedure for creating a data file using JANFILE is straightforward, requiring the user to input data from JANAF Thermo-chemical tables as requested by the program.

The reactant species for this investigation consisted of a mixture of Ammonia-methane-air. An existing data file (comb.sud) provided the necessary data for all the species except ammonia (NH_3). Therefore it was necessary to use JANFILE to create a data file for NH_3. To ensure that the Ammonia data file was created properly, a data file for a known species, methane, was created. STANJAN runs with the new file data were then compared to the existing file and were found to be in agreement.

3.3 Chemical Kinetic Simulations of NH_3-CH_4-air Combustion

With the computational power and speed available today, accurate 1-D flame data can be easily calculated on a personal computer by simultaneously solving sets of differential equations based on:

Elementary Reaction Kinetics (detailed reaction mechanisms)

+

Transport Equations (viscosity, thermal/molecular diffusion)

+

Continuity Equations (each species and overall)

+

Energy Equation

+

Species Equation

+

Equation of State

For situations where the reaction mechanisms are well known, as with methane, calculated results are credible and may be compared with experimental results.

3.3.1 CHEMKIN III Interpreter

The CHEMKIN software package is capable of predicting temperature and species profiles in two 1-D laminar premixed flame configurations, burner stabilized flames and freely propagating adiabatic flames.

The burner-stabilized flame with known mass flow rate configuration can be used when the temperature profile is known, or when the temperature profile is determined by the energy equation. The temperature profile is the temperature as a function of the axial distance from the reactants through the flame and into the products as shown in Figure 3.2.

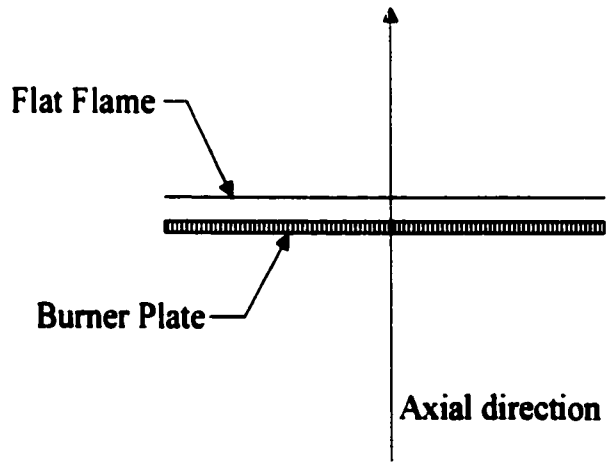

Figure 3. 2 Axial temperature direction in a burner stabilized flat flame

Although difficult to measure, if the temperature profile is obtained by experiment, then only the species transport equations are solved. However, in many flames there can be significant heat losses to the surrounding environment. These losses are typically unknown or of questionable origin and are therefore troublesome to model. Since the chemistry depends strongly on the temperature, it is very important to know the

temperatures accurately in order to draw conclusions about chemical kinetic behavior. Therefore, if a temperature profile can be measured accurately, then it is often better to use the measured temperature profile as opposed to the one calculated by the energy equation.

In a freely propagating adiabatic flame, there are no heat losses (by definition), and thus the temperature profile is computed from the energy equation. The flame propagation speed depends on the transport of heat, therefore predicting the temperature distribution is an integral part of the burning velocity calculation.

Premixed Flame Equations

The equations governing steady, constant pressure, one-dimensional flame propagation may be written as follows:

Continuity:

$$\dot{M} = \rho u A \tag{3.5}$$

Energy:

$$\dot{M}\frac{dT}{dx} - \frac{1}{c_p}\frac{d}{dx}\lambda A\frac{dT}{dx} + \frac{A}{c_p}\sum_{k=1}^{K}\rho Y_k V_k c_{pk}\frac{dT}{dx} + \frac{A}{c_p}\sum_{k=1}^{K}\dot{\omega}_k h_k W_k = 0, \tag{3.6}$$

Species:

$$\dot{M}\frac{dY_k}{dx} + \frac{d}{dx}(\rho A Y_k V_k) - A\dot{\omega}_k W_k = 0 \qquad (k = 1,...,K), \tag{3.7}$$

Equation of state:

$$\rho = \frac{p\bar{W}}{RT} \tag{3.8}$$

where,

x = spacial coordinate

$\dot{M}$ = mass flow rate (which is independent of x)

T = temperature

Y_k = mass fraction of the k^{th} species

p = pressure

u = velocity of the fluid mixture

ρ = mass density

W_k = molecular weight of the k^{th} species

W= mean molecular weight of the mixture

R = universal gas constant

λ = the thermal conductivity of the mixture

c_p = constant pressure heat capacity of the mixture

c_{pk} = constant pressure heat capacity of the k^{th} species

$\dot{\omega}_k$ = the molar rate of production by chemical reaction of the k^{th} species per unit volume

h_k = the specific enthalpy of the k^{th} species

V_k = the diffusion velocity of the k^{th} species

A = the cross-sectional area of the stream tube encompassing the flame (unity by default)

The net chemical production rate ω_k of each species results from competition between all the chemical reactions involving that species (reaction mechanism). It is presumed that each reaction proceeds according to the law of mass action and the forward rates are of the modified Arrhenius form,

$$k_f = AT^{\beta} \exp\left(\frac{-E_A}{RT}\right) \tag{3.9}$$

To solve these premixed flame equations a Fortran program called PREMIX, which uses a combination of Newton's method and time integration, is used. Further, two

preprocessors are used to solve a given problem. The CHEMKIN III Gas-phase Interpreter, processes the chemical reaction mechanism and the transport property preprocessor evaluates gas-phase multicomponent viscosities, thermal conductivities, diffusion coefficients, and thermal diffusion coefficients were used.

Using CHEMKIN III, with the post processing software PREMIX [Kee et al., 1998], and the well-known Gas Research Institute (GRI) kinetic mechanism for natural gas combustion [GRI, 1999], 1-Dimensional kinetic simulations were performed for various premixed NH_3-CH_4-air flames. Appendix B lists the reactions and parameters used in the GRI mechanism. The simulations provide data on emissions, burning velocity and flame temperature for various mixture stoichiometries. Since no experimental data are available for the temperature profiles across NH_3-CH_4-air flat flames, a freely propagating flame model was employed in place of a burner-stabilized model. As stated previously, the freely propagating flame model assumes adiabatic combustion and calculates its own temperature profile, thus there is some error when comparing these calculations to experimental results obtained under burner stabilized (altered temperature profile) conditions. However, the burner used in these experiments operates adiabatically and therefore may be compared to the freely propagating flame.

Comparison of Burner Stabilized and Freely Propagating Simulations

Figure 3.3 compares the experimental temperature profile obtained by Coherent Anti-Stokes Raman Spectroscopy (CARS) thermometry [van Maaren et al., 1999] to the freely propagating simulation for stoichiometric CH_4-air combustion. Figure 3.3 verifies that the temperature profile generated by the freely propagating simulation is in good agreement with the CARS measurements from the burner-stabilized flame of van Maaren et al. [1999].

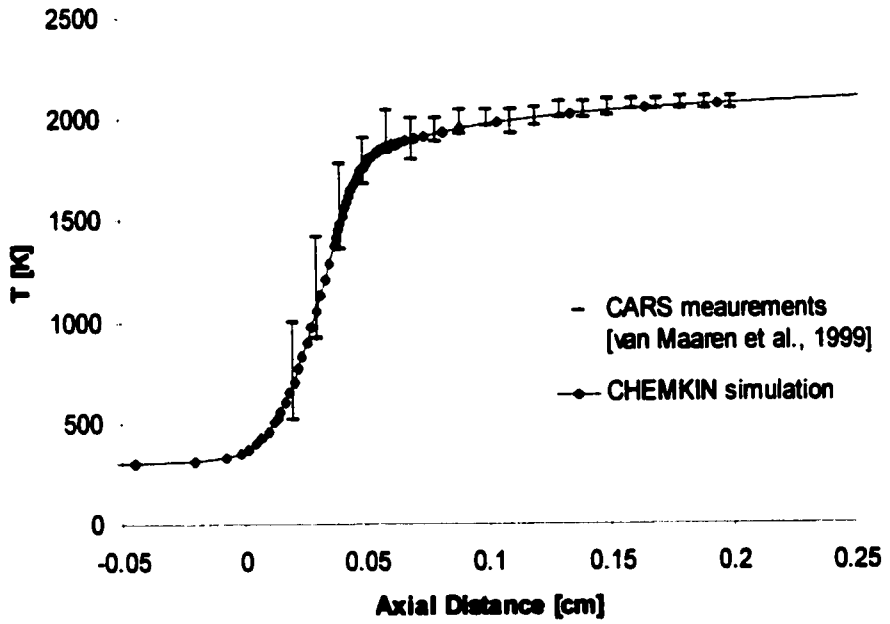

Figure 3. 3 Experimental and simulation axial temperature profile comparison.

4.0 Materials and Methods

4.1 Apparatus

4.1.1 Burner

A schematic drawing of the flat flame burner system used in this study is provided in Figure 4.1. A photograph of the burner is given in Figure 4.2. The basic design and principle of operation of this burner was modeled after the perforated plate flat flame burner design of van Maaren [1994] (described in section 2.3). The main modifications that were made to the van Maaren design for this work consisted of the use of different burner materials and a new method of heating the burner plate. As well, the burner used in this study has slightly different dimensions.

The most critical component of this type of burner is the perforated burner plate. In this work, an aluminum, as opposed to a brass burner plate was used due to the corrosive effects ammonia has on brass. Like van Marren's, the perforated aluminum burner plate has a diameter of 30mm. It was 2mm thick with a hexagonal perforation pattern of very small holes of diameter 0.5mm and pitch of 0.7mm. The function of the perforated burner plate is to provide enough thermal conductivity so that temperature variations across the burner surface are minimal. Since aluminum has a higher thermal conductivity than brass, this modification is an improvement. Van Maaren [1994] found that the best condition for stabilization of adiabatic methane-air flat flames over the entire range of flammability limits was to maintain a burner plate temperature of 363 to 398K. In this study, a new burner plate heating system consisting of an electric ring heating element and a temperature controller was used. With this system the edge of the burner plate

could quickly and easily be heated to the temperature of the middle of the burner plate so that there was no conductive heat loss from the burner plate.

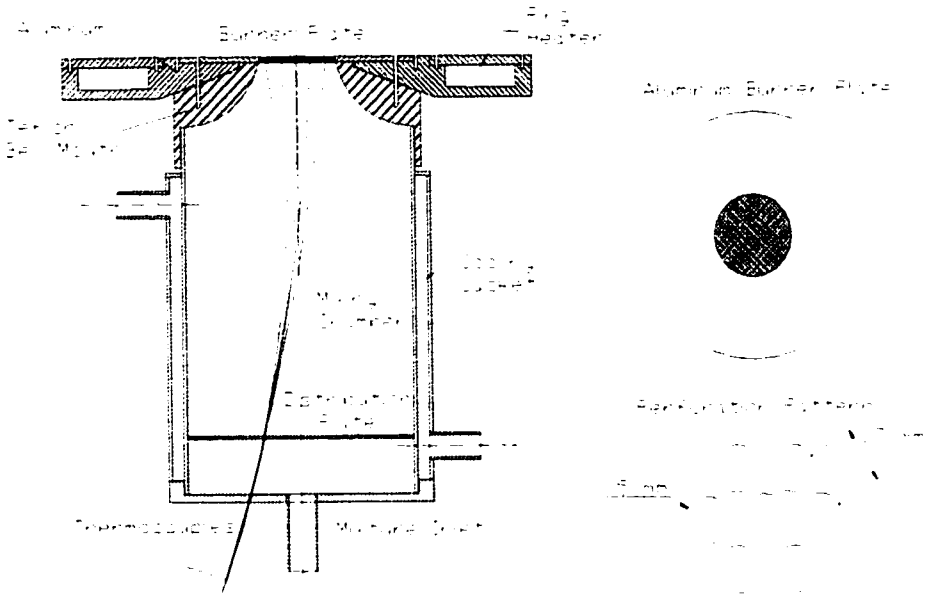

Figure 4. 1 Section through the experimental flat flame burner.

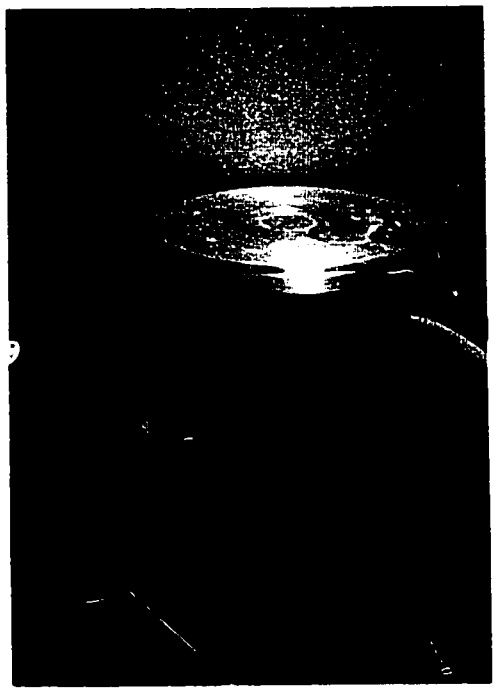

Figure 4. 2 The flat flame burner.

The body of the burner consists of a bell mouth, mixing chamber and cooling jacket. To help thermally insulate the mixing chamber from the heater burner plate, the bell mouth was constructed using Teflon. The bell mouth was designed based on the work of van Maaren [1994], wherein a 30 mm radius of curvature bell mouth with an exit orifice diameter of 30 mm (at the burner plate) provided a uniform velocity profile suitable for flat flames. The mixing chamber and distribution plate (mixing plate) helped to provide uniform flow, and sufficient mixing inside the burner. They were constructed from stainless steel to prevent ammonia corrosion. A cooling jacket surrounds the mixing chamber. Water at approximately 298K (from a constant temperature bath) was pumped through the cooling jacket in order to control the unburned gas temperature.

Along a diameter on the upstream side of the burner plate, 5 very fine (0.1mm) K-type thermocouples were fixed into selected holes. These thermocouples were used to measure the plate temperature during a given experiment so that the adiabatic condition could be determined. Small thermocouples were used to minimize any distortion of the flow profile. Detailed drawings of the burner are given in Appendix C.

4.1.2 System

Figure 4.3 illustrates the experimental layout of the apparatus used for this study. Methane with a purity of 99.9% (Prax-air Ultra-Pure) was supplied from a compressed gas cylinder. Air was supplied from the laboratory compressed air system which was passed through a fiberglass filter and a desiccant to ensure it was clean and dry. A mixture of 5.01% ammonia in air was purchased from Prax-air for use in the tests with premixed ammonia addition. Inert Tygon tubing was used to transport the gases to avoid any surface chemical reactions. The flow rates of the gases were controlled by needle valves and their flows were monitored by variable area flowmeters (rotameters). The line pressure and temperature of each gas was measured in front of each flowmeter using a manometer and thermocouples. A manometer measures the in-line pressure of each gas above atmospheric pressure. This was done so that any deviations in conditions from calibration could be monitored and corrected for at working conditions. The gas streams were then brought together with two Teflon 'Y' fittings. The gas mixture was then passed through a flash arrester consisting of a stainless steel cylinder containing small stainless steel ball bearings. This flash arrester would quench any flame that attempted to propagate back from the mixing chamber to protect the tanks and up-stream gas lines. It also provided extra mixing of the fuel and air before reaching the burner.

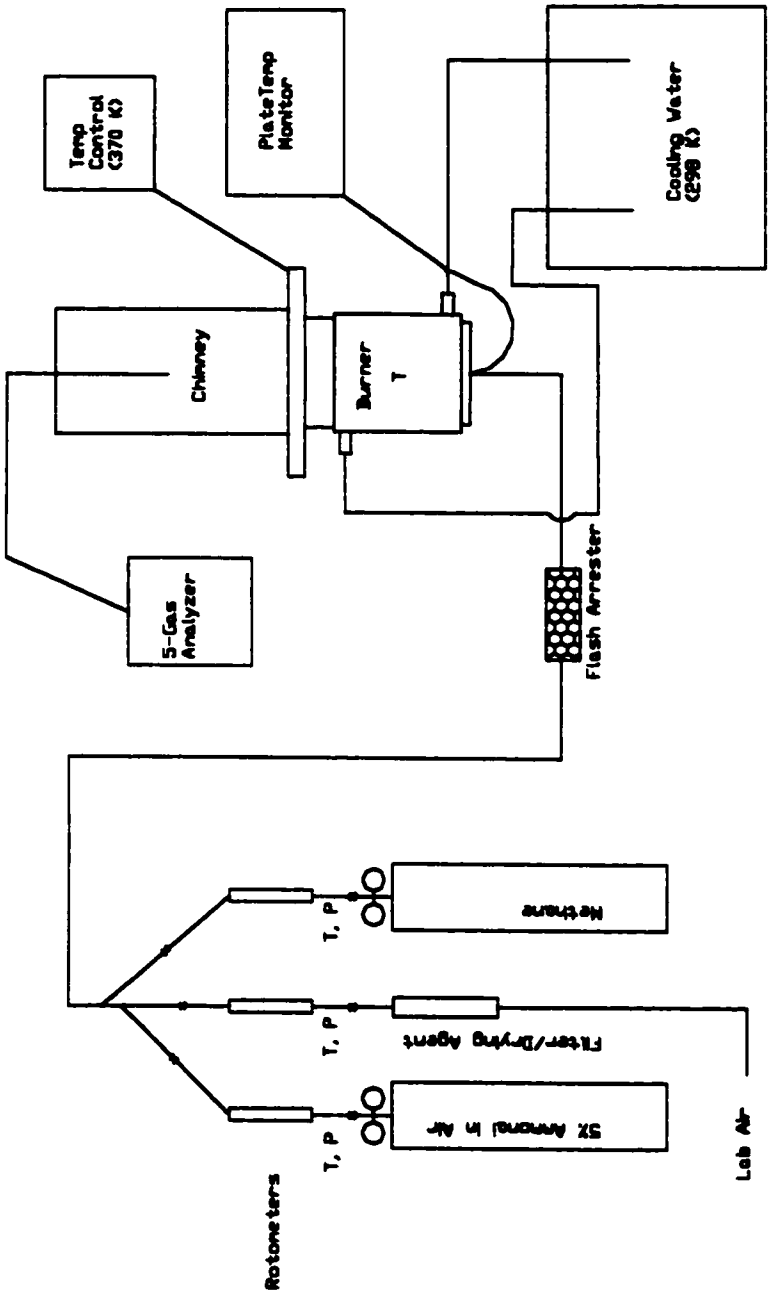

Figure 4.3 Schematic of experimental layout.

As mentioned in the previous section, the burner mixing chamber was cooled to approximately 298K by means of a constant temperature water bath equipped with a pump to supply a flow of water through the water jacket of the burner. The plate temperature of the burner was monitored by 5 small (0.1 mm) diameter K-type thermocouples with a digital readout. One additional thermocouple was positioned below the burner plate in the mixing chamber to measure the unburned gas temperature (T_u). As well, the burner plate temperature could be controlled and monitored using a ring heater and temperature controller. Finally an aluminum chimney with a diameter of 102 mm and a height of 318 mm with a stainless steel partial lid was placed around the flame when emissions samples were taken using the 9.5 mm (3/8 ") diameter stainless steel sampling probe which was fitted to the 5-Gas analyzer.

4.2 Methods

4.2.1 Protocol

Before starting a series of experiments the burner plate heater was set at 363K and the burner plate was allowed to reach equilibrium at the set temperature. A series of experiments was then started by igniting a rich mixture which burns as a "semi-diffusion" flame on top of the burner. In "semi-diffusion" flames, diffusion burning occurs downstream of the premixed flame front. The flow rates of the fuel and air were then carefully adjusted with needle valves until a flat flame formed above the burner surface. Further fine adjustments were made until the temperature profile radially along the burner plate was uniform (± 10K). At this point, the flow readings are recorded along with the pressures and temperatures at the flowmeters. As well, the barometric pressure and

unburned gas temperature were recorded. These steps were repeated for various fuel-air mixtures to cover the entire range of ϕ.

4.2.2 Determination of Burning Velocity and Equivalence Ratio, ϕ

In these experiments burning velocity and equivalence ratio are calculated based on measurement of the unburned gas flow rates. The general methodology for the determination of these parameters is described here. Sample calculations and tabulated experimental values for S_u and ϕ are given in Appendix D. Uncertainty analysis performed on these parameters is provided in Appendix E. Calibration data for the flowmeters used in the experiments are shown in Appendix F.

Burning Velocity

In these experiments the burning velocity of the flat flame front is calculated directly by measuring the total flowrate, temperature and pressure of the unburned gas. Since the area of the flat flame is approximated as equal to the burner plate diameter, the adiabatic burning velocity is calculated using equation 2.1 modified to the following form:

$$S_u = \frac{Q}{A} \tag{4.1}$$

where Q is the total flowrate of the unburned gas mixture (pressure and temperature corrected) and A is the area of the flat flame.

Equivalence Ratio

Experimentally, the equivalence ratio, ϕ was calculated based on the individual flowrates of the fuel and air. For pure methane-air combustion, ϕ was calculated using experimental volumetric flow rates according to:

$$\phi = \frac{\left(\frac{Q_{CH_4}}{Q_{Air}}\right)_{exp.}}{\left(\frac{F}{A}\right)_{stoich}} \tag{4.2}$$

where Q_{CH4} and Q_{Air} are the pressure and temperature corrected volumetric flow rates of the fuel and air respectively in L/min. Since the complete combustion of methane occurs according to:

$$CH_4 + 2(O_2 + 3.76N_2) \rightarrow CO_2 + 4H_20 + 7.52N_2$$

The stoichiometric value for the fuel to air ratio is calculated on a molar basis as:

$$\left(\frac{F}{A}\right)_{stoich} = \frac{1}{2(4.76)} = 0.105042 \tag{4.3}$$

Thus, knowing this value, ϕ is easily determined for each experimental run.

For cases where ammonia was added as a component of the fuel in addition to methane, calculation of ϕ was more involved. Since, for safety reasons, a compressed gas tank containing 5% ammonia in air was used to supply ammonia as a fuel additive, the stoichiometric equation for NH_3-CH_4-air combustion was written as:

$$CH_4 + a(0.05NH_3 + 0.95(O_2 + 3.76N_2)) + x(O_2 + 3.76N_2) \rightarrow CO_2 + bH_2O + cN_2$$

From this equation we can write:

$$\left(\frac{F}{A}\right)_{stoich.} = \frac{1+0.05a}{a(4.522)+x(4.76)} \tag{4.4}$$

To allow for the calculation of the stoichiometric fuel to air ratio, based on the volumetric flowrate of the 5% ammonia-air, a, an atom balance was performed on the stoichiometric equation. The stoichiometric fuel to air ratio can then be written as:

$$\left(\frac{F}{A}\right)_{stoich} = \frac{1+0.05Q_{actual5\%NH_3+Air}}{Q_{actual5\%NH_3+Air}\cdot(4.522)+\left[\frac{2+\left(\frac{4+0.15Q_{actual5\%NH_3+Air}}{2}\right)-1.9Q_{actual5\%NH_3+Air}}{2}\right]\cdot(4.76)} \tag{4.5}$$

where $Q_{actual,5\%NH3+Air}$ and $Q_{actual,CH4}$ are the actual flowrates of the unburned gas streams of $5\%NH_3$+Air and CH_4. The expression for the experimental fuel to air ratio becomes:

$$\left(\frac{F}{A}\right)_{exp.} = \frac{Q_{CH_4}+0.05Q_{5\%NH_3+Air}}{Q_{Air}+0.95Q_{5\%NH_3+Air}} \tag{4.6}$$

Using equations 4.5 and 4.6, ϕ can be determined for any experimental condition, with or without ammonia addition. When the ammonia volumetric flowrate, a, is set to zero, equation 4.5 reduces to equation 4.3 and equation 4.6 reduces to equation 4.2.

4.2.3 Determining the Ammonia Content of the Fuel

Since the ammonia stream used in these experiments was a mixture of 5% ammonia in air, it was difficult to predetermine the resulting ammonia concentration in the fuel.

Instead, the $\%NH_3$ in the fuel was found after an adiabatic flame was created by substituting the flowrates of each gas stream into the following equation:

$$\%NH_3 \text{ in the fuel} = \frac{0.05Q_{actual,5\%NH_3+Air}}{Q_{actual,CH_4} + 0.05Q_{actual,5\%NH_3+Air}} \times 100 \quad (4.7)$$

For this reason it was necessary to organize the data for a desired ammonia concentration (1 – 4% NH_3 in the fuel) in bins. These bins were chosen such that the data for ammonia content of the fuel does not deviate more than ± 0.5% of the stated values. The uncertainty in the values calculated from equation 4.7 is shown in Appendix E.

4.2.4 Measuring Emissions

Analysis of the emissions from the various combustion conditions was performed using the IMR 2800 5-Gas analyzer [IMR, St Petersburg, FL]. The gas analyzer is capable of measuring NO, NO_2, CO, CO_2 and O_2 and reports the results on a dry basis. The analyzer utilizes electrochemical sensors for the determination of NO, NO_2, CO and O_2 concentrations. The analyzer calculates CO_2 concentrations based on the carbon content in the fuel and the measured O_2 concentration as follows:

$$CO_2 = CO_{2\max} \times \left(20.9 - \frac{O_{2meas.}}{20.9}\right) \quad (4.8)$$

where CO_{2max} is a constant given as 11.75 for methane and $O_{2meas.}$ is the percent oxygen measured at a given condition. The IMR gas analyzer is typically used in analysis of stack gas emissions and is therefore tailored to lean combustion situations (O_2 present in

emissions). For this reason equation 4.8 was modified to include the effects of CO under rich combustion conditions where oxygen is deficient according to:

$$CO_2 = CO_{2\max} \times \left(20.9 - \frac{O_{2meas.}}{20.9} \right) - CO_{meas.} \tag{4.9}$$

where $CO_{meas.}$ is the percent CO measured at the given condition.

Once an adiabatic flame was stabilized for a given combustion condition, sampling of the combustion products could begin. With the aluminum sampling chimney in place, the gas analyzer probe nozzle was placed approximately 10 cm from the burner surface. The analyzer draws a continuous sample of the combustion products through a filter and a condensate trap at approximately 1.6 L/min. The nature of the electrochemical sensors requires that the gas sample be drawn for at least 5 minutes for the most accurate measurement of the emissions. The accuracies and measurement ranges of the 5-gas analyzer are detailed in Appendix G.

4.2.5 Measurement of Ammonia Breakthrough

Using wet chemical analysis, tests were performed to check for ammonia which was not burned and "broke through" the flame to appear in the exhaust gases. This test was performed for lean, rich and stoichiometric flames with 1 and 4% ammonia addition to the fuel. Figure 4.3 illustrates the experimental setup which was employed. An impinger fitted with a 3 mm (1/8") stainless steel tubing sampling probe was filled with boric acid and an indicating solution. Using the house vacuum system, a continuous sample was bubbled through the boric acid and indicating solution at approximately 2 L/min and the total time of sampling was recorded. This flowrate was controlled by a needle valve and

monitored with a calibrated flowmeter. The sample was bubbled through the indicating solution until there was a color change (indicating the presence of NH_3) or until sufficient sample was collected to justify that there was essentially no ammonia present. If a color change occurred, the mixture was titrated to determine the ammonia concentration in the sample volume according to the Standard Methods, Method number 4500-NH_3 C, ammonia by boric acid titration [APHA, AWWA, WEF, 1995].

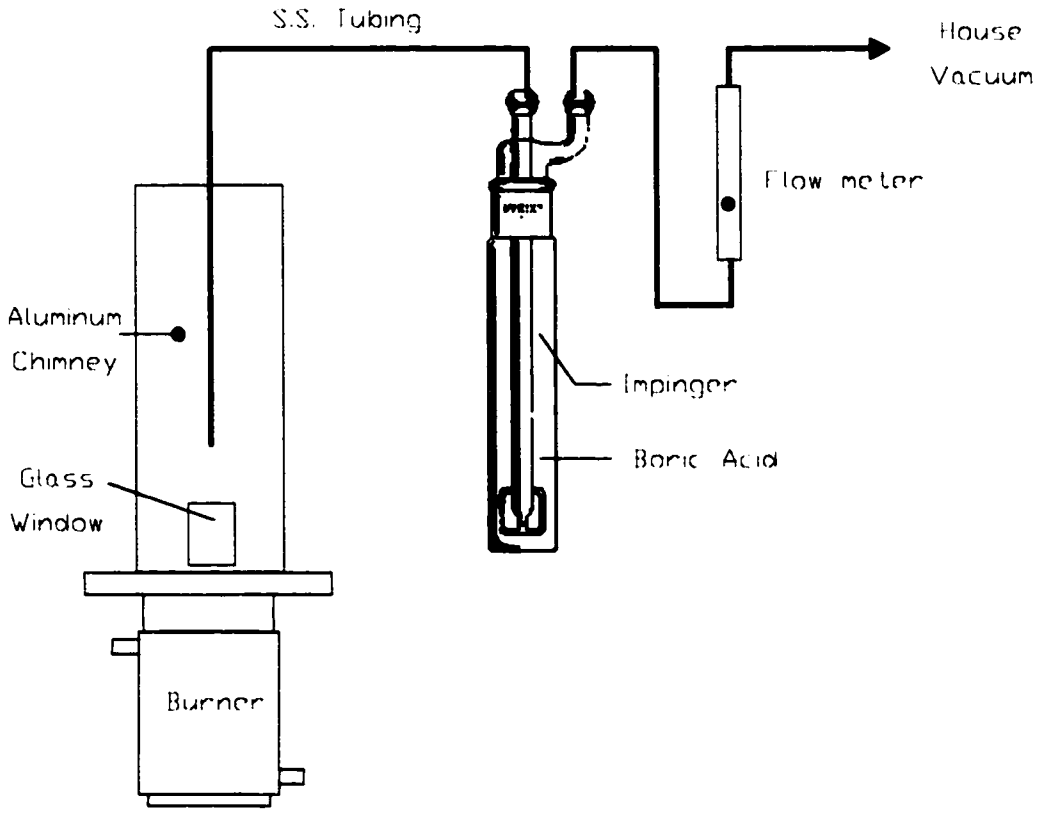

Figure 4. 3 Experimental set-up for ammonia breakthrough testing.

5.0 Results and Discussion

First, the experimental and simulation results for the adiabatic burning velocity of pure methane-air are compared to literature values. Since no adiabatic burning velocity data could be found in the literature for ammonia-methane-air mixtures these new values are compared only to simulation results. Measured NO concentrations are then compared to simulation and literature values for methane-air and ammonia-methane-air flames. The effect of ammonia addition to the fuel (methane) on CO emissions will be discussed and finally, ammonia break-through is investigated.

5.1 Burning Velocity

To illustrate the reliability of the burning velocity results obtained in this study, Figure 5.1 compares experimental values of burning velocity for pure methane-air to those found in the literature and to chemical kinetic simulations. The best method for the determination of adiabatic burning velocity is a subject of debate among combustion researchers. The experimental data of Law [1993] was determined by the opposed jet method. Gu et al. [2000] utilized photographic observations of spherically expanding flames propagating at constant pressure. Both of the aforementioned techniques require corrections for flame stretching [Law 1993; Gu et al., 2000]. Vagelopoulos et al. [1998] utilized a single jet-plate configuration with quasi-steady negative to positive stretch. Similar to the data from this study, the results of van Marren et al. [1994] were obtained using an adiabatic flat flame burner. As shown in Figure 5.1, the results from this work were within the range of values reported for lean combustion (ϕ<1) but were lower than those found by others for stoichiometric combustion (ϕ=1) and higher than others under

rich conditions (ϕ>1). The chemical kinetic simulations also confirmed the general shape of the burning velocity curve. The simulation results are in good agreement with the literature under rich conditions, but are somewhat higher for lean and stoichiometric combustion. The error bar in Figure 5.1 shows the maximum uncertainty in the measurement of ϕ and Su. As shown, the maximum uncertainty occurs at the most rich condition with an uncertainty in ϕ and S_u of approximately 4% (See Appendix E for details). Upon inspection of Figure 5.1, it is clear that considering the uncertainties in the measurements, the experimental data in this work are in good agreement with accepted literature values.

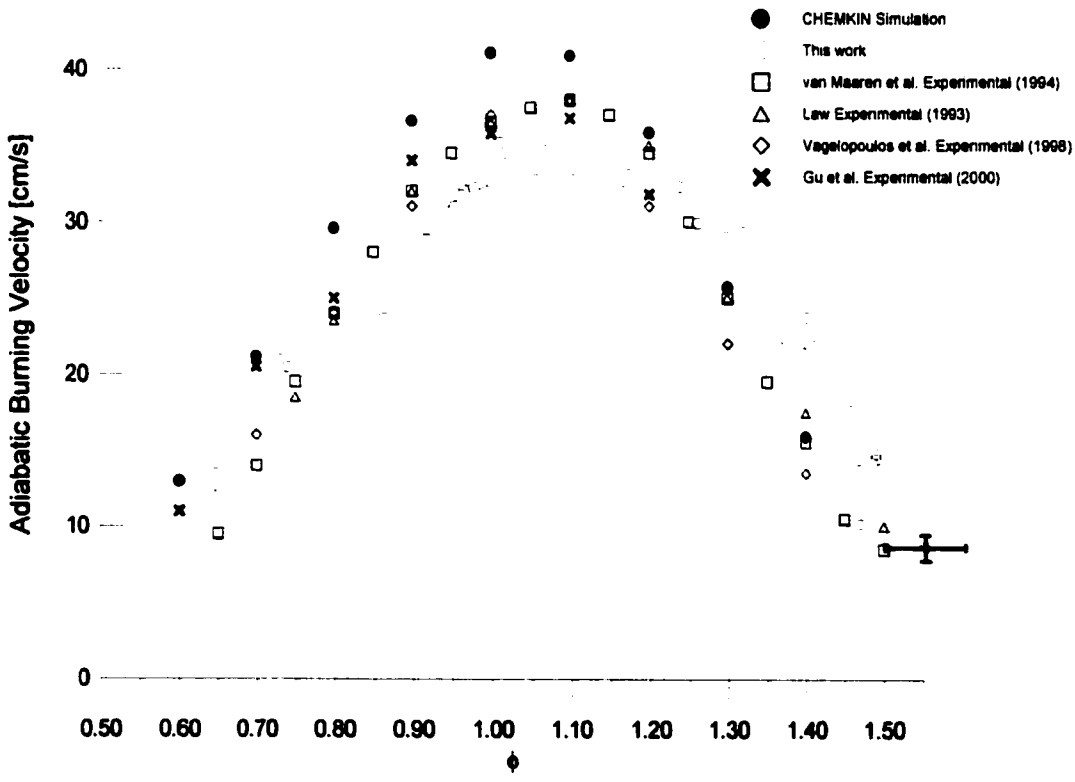

Figure 5. 1 Comparison of methane-air burning velocities obtained by various workers

Figure 5.2 shows all of the experimental and simulation adiabatic burning velocity data for pure CH_4-air and NH_3-CH_4-air mixtures in the range of 0 – 4% ammonia in the fuel. Both the simulation and experiments illustrate that ammonia addition to the fuel results in a decrease in burning velocity over the entire range of ϕ. In general higher ammonia concentrations in the fuel result in lower burning velocity. As illustrated earlier in Figure 5.1, the simulation results are higher than the experimental values for lean and stoichiometric combustion and are lower under rich conditions. For ϕ = 1.3 and 1.4, experimental and simulation results appear to be in agreement within the range of experimental uncertainty. To further illustrate this point, Figure 5.3 shows the same results but focuses on the extreme conditions of 0% and 4% ammonia in the fuel.

It should be mentioned that a slight change in flame diameter throughout the range of stoichiometries was observed. For near stoichiometric combustion, the use of the burner plate area as the flame area seems fairly reasonable. However, there is significant error in this assumption near the flammability limits as instabilities at the edges of the flame may cause the actual flame area to decrease. Appendix H gives photographs and descriptions of flame characteristics at lean, stoichiometric and rich conditions.

Since mixtures of ammonia-air burn very slowly and under some conditions are considered non-flammable, it is not surprising that the resulting burning velocities of ammonia-methane-air mixtures are lower than that of pure methane-air [Pfahl et al, 2000; Cooper et al., 1991; Cornelius et al., 1966].

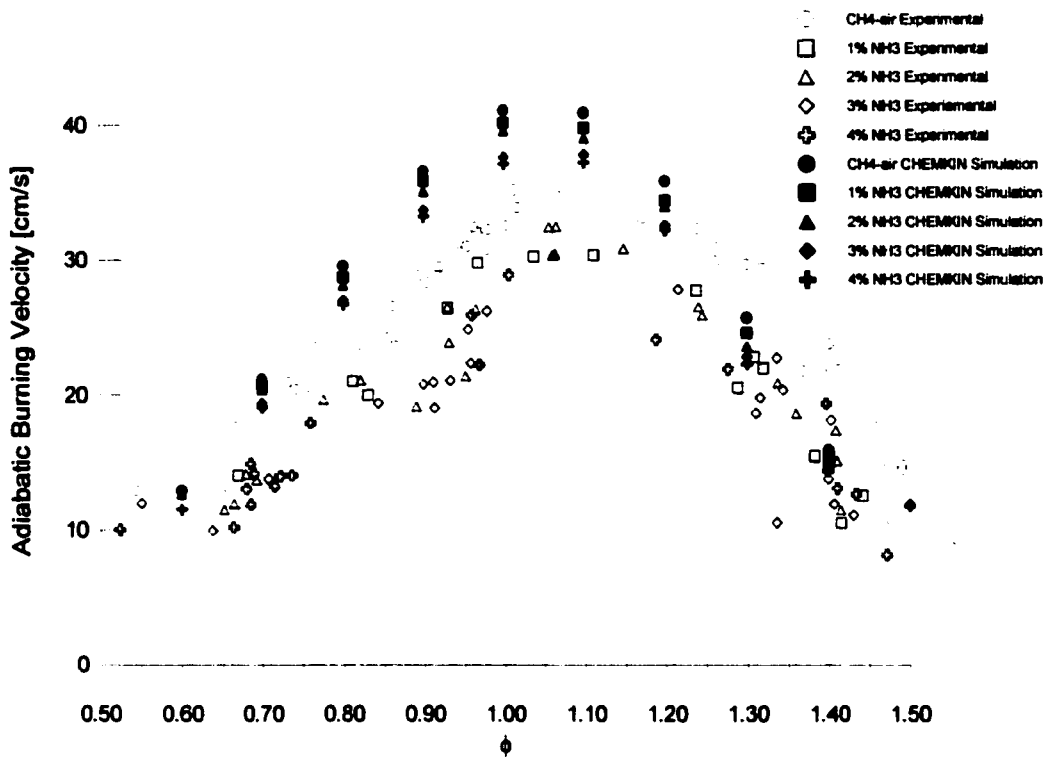

Figure 5. 2 Experimental and Simulation adiabatic burning velocity data for CH_4-air and NH_3-CH_4-air mixtures

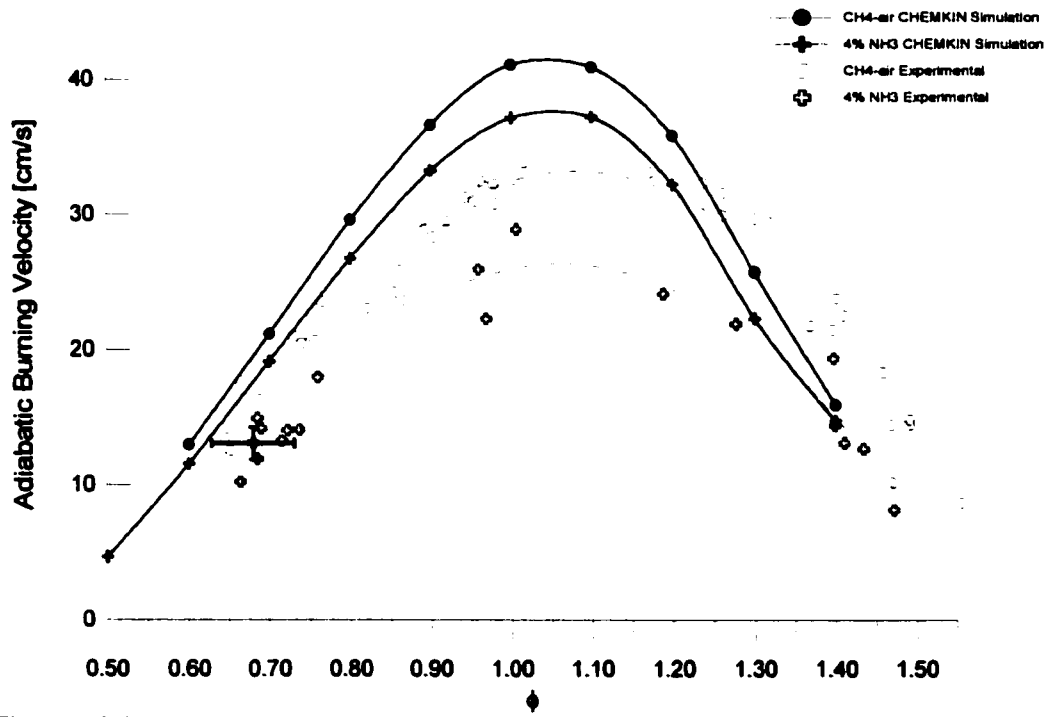

Figure 5. 3 Comparison of adiabatic burning velocity results for 0% and 4% ammonia addition

5.2 Emissions

Figure 5.4 shows experimental data for NO emissions for various combinations of premixed NH_3-CH_4-air flat flames. The data have been curve fitted to third order polynomials for the different NH_3-CH_4-air combinations and a second order polynomial for the pure CH_4-air flames. It is obvious from this figure that an increase in ammonia concentration in the fuel causes an increase in NO emissions for all mixtures of NH_3-CH_4-air that are flammable ($0.53 < \phi < 1.47$).

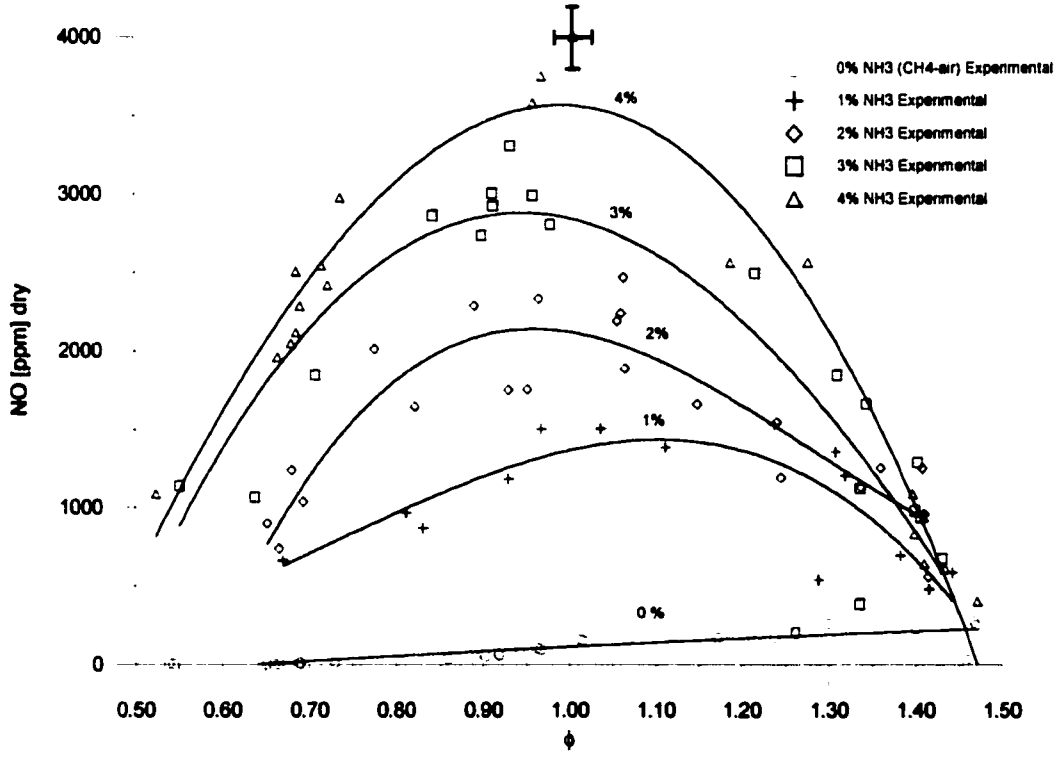

Figure 5. 4 Experimental NO emissions from NH_3-CH_4-air flames.

Figure 5.5 shows a comparison of the experimental NO emission data with simulation data calculated using CHEMKIN. The curves fitted to the data points shown in Figure 5.4 are repeated without the actual experimental data points for clarity.

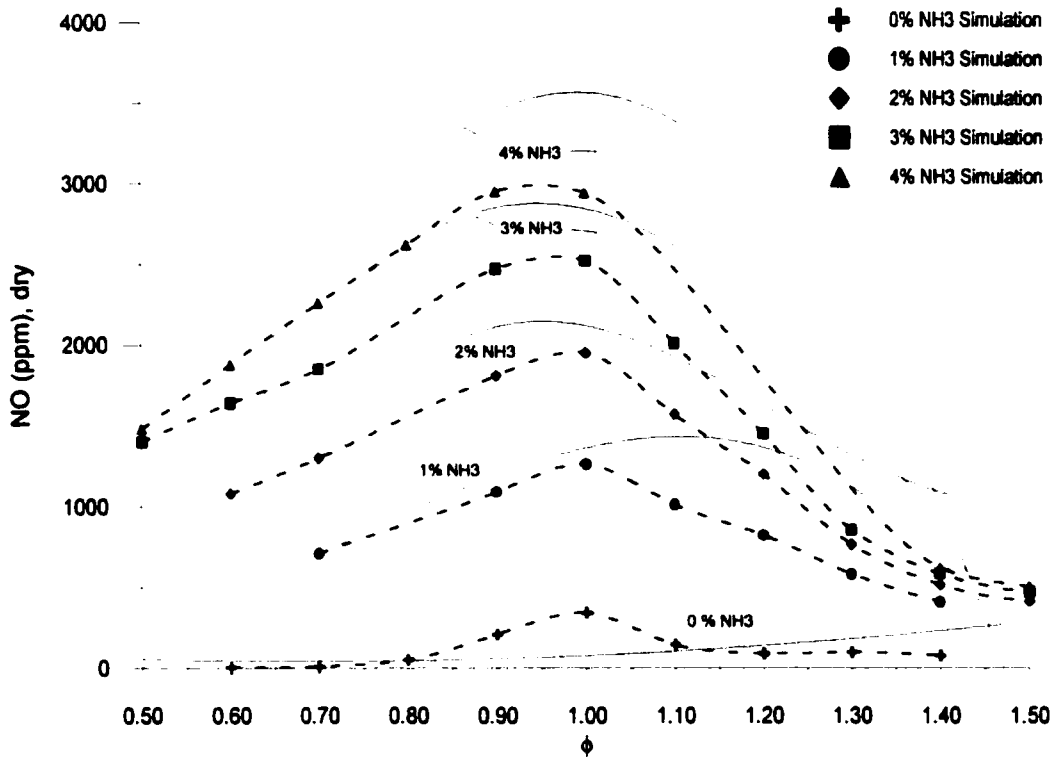

Figure 5. 5 Comparison of experimental and simulation values for NO production in CH_4-air and NH_3-CH_4-air flames

The simulation data follow the same general trend as found in the experiments. With increasing ammonia concentration in the fuel, an increase in NO production is shown over the entire range of flammability. Typically, lean combustion yields NO concentrations lower than those for stoichiometric conditions mainly due to the lower flame temperature. Lower than stoichiometric NO concentrations are also found on the rich side since there is an absence of oxygen for nitrogen oxidation under these conditions [Heywood, 1988]. This phenomenon is predicted by the simulations and is also reflected by the experiments.

The simulation results for NO production in NH_3-CH_4-air flames are generally lower than the experimental values except near the lean and rich combustion limits. This trend may be due to the effects of the burner plate intruding into the preheat zone* of the flame.

In Figure 5.6 part of a temperature profile, T(x), of a freely propagating adiabatic flame is represented by a solid line. The altered temperature profile, T(x'), of a burner-stabilized flame is shown as a dashed line as it passes through the burner plate of temperature, T_p. As shown in Chapter 3, the axial temperature profiles of freely propagating adiabatic flames (by simulation), and measurements of adiabatic burner-stabilized flames are in good agreement. Distance zero refers to the upstream end of the burner plate. The assumption made by de Goey and van Maaren et al. [1993], is that any small alterations of the temperature profile through the region of the burner plate will not ultimately change the true temperature profile (freely propagating flame) beyond the distance of the burner plate. Thus the T(x') and T(x) meet at the burner surface. As suggested by de Goey et al. [1993], the burner surface does intrude on the preheat zone of the flame front. This may interfere with radical formations in the preheat zone.

In Figure 5.7, simulation results for the stoichiometric combustion of NH_3-CH_4-air with 4% NH_3 in the fuel show that two important radicals OH and HO_2 [Glassman, 1996] as well as NO are present in the preheat zone. With burner-stabilized flames, the presence of the burner plate in this region may alter these species and thus the final species concentrations will be affected. In experiments, the average plate temperature was

* Region in front of a laminar flame defined by the distance from the initial temperature rise to the inflection point on the temperature profile.

approximately 363 K. Figure 5.7 illustrates that the burner plate does indeed extend into the preheat-zone where radicals are present.

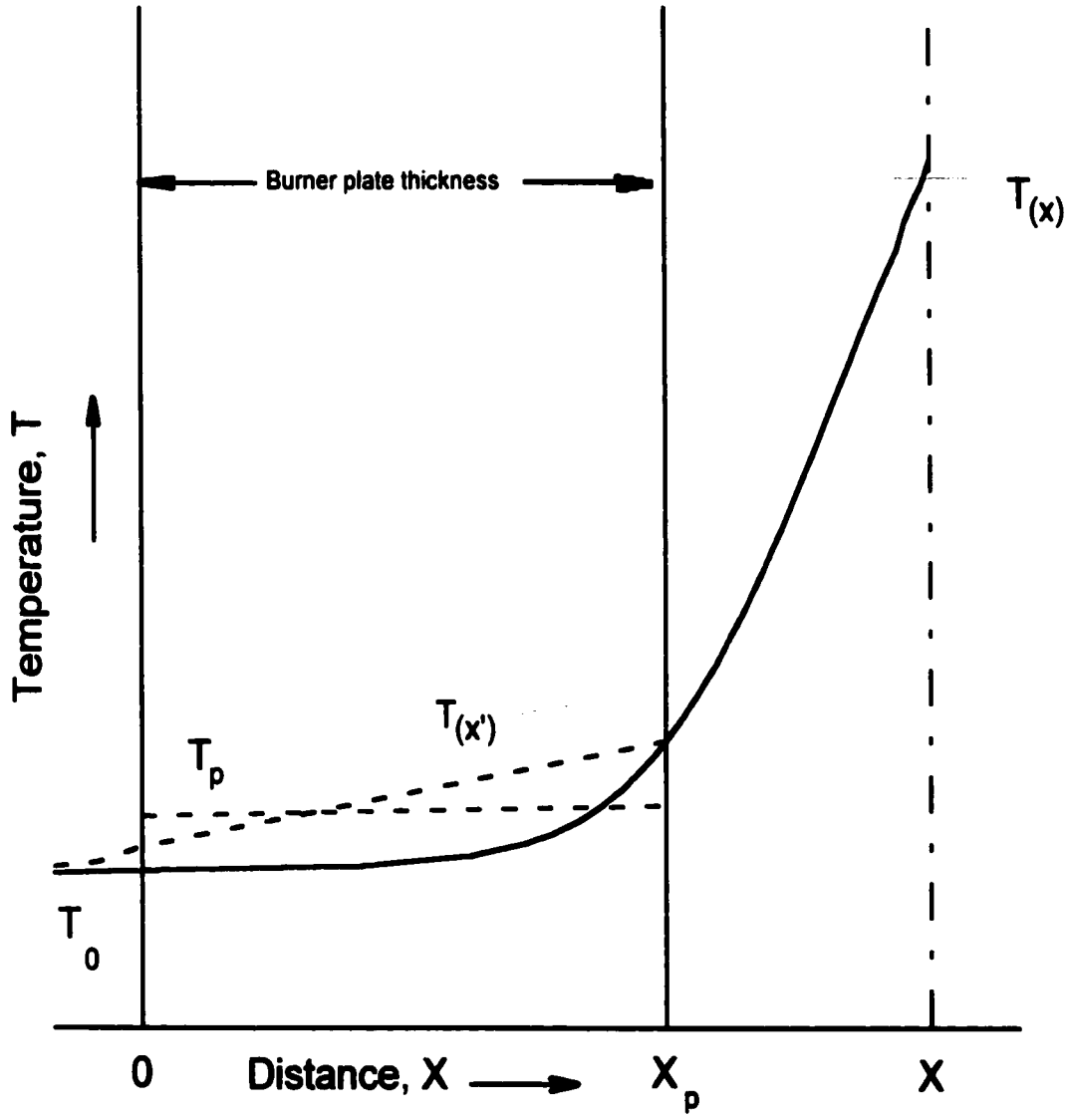

Figure 5. 6 Effect of burner plate on axial temperature profiles [van Maaren et al. 1993].

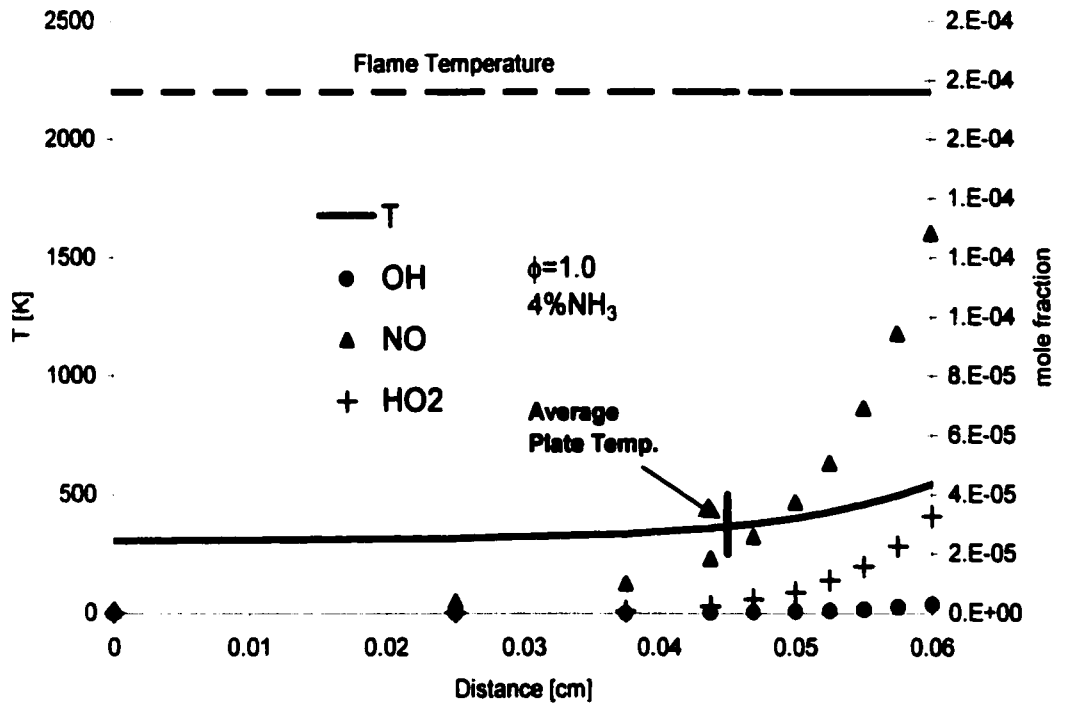

Figure 5. 7 Radical formation in the preheat zone of a stoichiometric NH_3-CH_4-air laminar flame.

In Figure 5.8, experimental, chemical kinetic and thermodynamic calculations from this study are compared to the experimental values of Wendt et al. [1974] with 1% and 5% ammonia addition to the fuel. For this figure the data were corrected to 3% oxygen to eliminate any dilution effects on product species concentration. When plotted on this semi-log plot (as done by Wendt), the experimental data from this work show small decreases in NO concentration on either side of stoichiometric combustion. As well, it should be mentioned here that the gap in experimental data for 5% ammonia addition occurs due to the inability of the gas analyzer to measure NO concentrations above 4000 ppm.

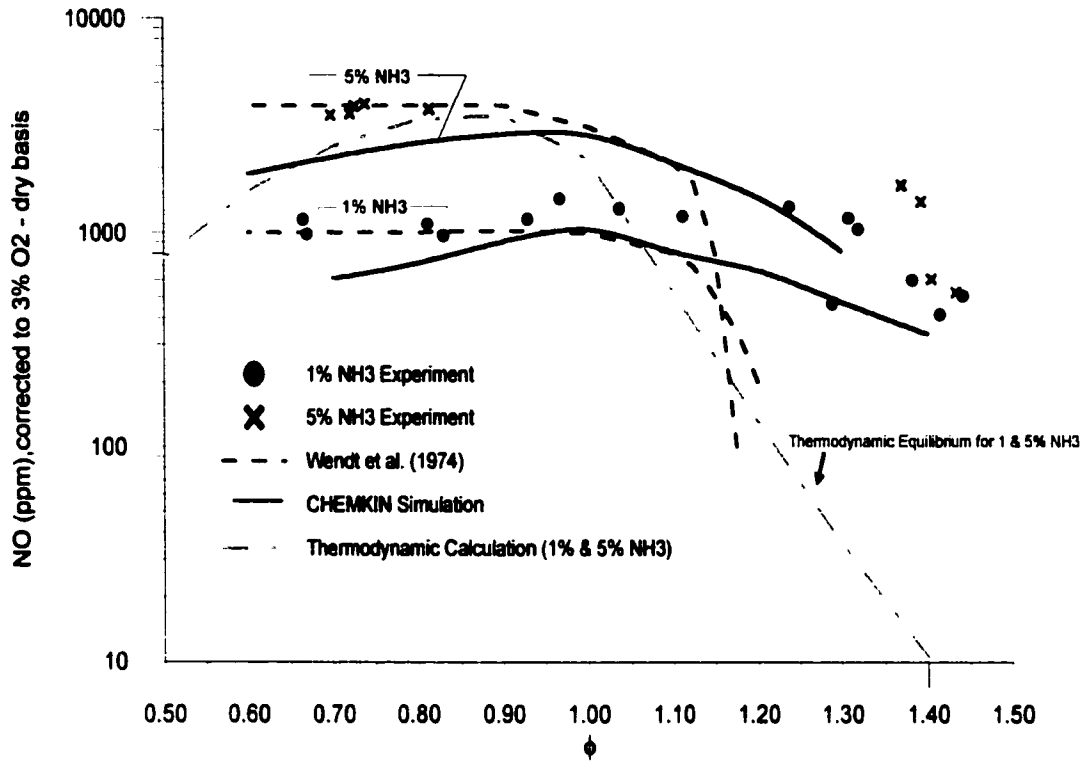

Figure 5. 8 Comparison of experimental, simulation and thermodynamic results to the experimental data of Wendt et al., [1974].

In this experimental study NO concentrations exceeded this limit for 5% ammonia addition near stoichiometric combustion. On the lean portion of this figure, the data from this study, the experimentation of Wendt et al. [1974] and the kinetic simulations are in good agreement. However, when considering rich combustion, the experimental data of Wendt et al. [1974] tend to deviate significantly from the experimental values and kinetic simulations provided by this work. In Wendt et al.'s study, it was determined that the best condition for NO reduction occurred at the richest condition possible, and with the highest amount of ammonia in the fuel (CH_4+NH_3) possible. The experimental data from the present study show that indeed, for a given amount of ammonia in the fuel, NO emissions are lowest at the rich limit, but the reduction in NO is not as dramatic as the results of Wendt et al. [1974] suggest. Further, this study provides evidence that for all

ammonia concentrations in the fuel, the resulting NO emissions will be higher than without ammonia, for all points within the combustion limits.

Comparison of Thermodynamic Properties of Ammonia and Methane

It is important to note that in theory the amount of NO produced per kJ of energy from ammonia is approximately equal to that of methane. In Appendix I, calculations demonstrate this equality using heat of formation data at 298K and NO concentrations at equilibrium with ϕ = 1.0. Methane-air produces more NO per mole of fuel than ammonia-air. However, when these NO concentrations are normalized by dividing by the fuels' respective heat of combustion (ΔH_{comb}), the results are nearly identical. Appendix I shows that pure ammonia-air combustion produces 2.59 ppmNO/kJ and methane-air produces 2.74 ppmNO/kJ; pure ammonia combustion produces approximately 5 percent less NO per kJ.

According to equilibrium calculations, burning pure ammonia-air to obtain the same amount of energy from combustion as methane-air would result in roughly the same amount of NO production. Also it seems logical that when ammonia is mixed with methane, less energy is released from combustion (compared with pure methane-air) due to the lower heating value of ammonia. As a result of a lower flame temperature, less NO should be formed. However, this doesn't happen in practice. The additional nitrogen added to the flame overcomes the effect of the lower temperature resulting in more NO being produced, not less.

Since ammonia is a non-carbon containing compound, a proportional decrease in CO and CO_2 (common greenhouse gases) concentrations is expected with ammonia addition to methane. Comparing the product CO and CO_2 data for CH_4-air to $0.2NH_3$-CH_4-air, thermodynamic calculations show reductions of 11.39% and 8.03% respectively. A sample calculation demonstrating this point is given in Appendix I.

Inspection of Figure 5.8 also reveals that NO formation seems to be somewhat independent of thermodynamics. The equilibrium calculations for 1 and 5% ammonia addition can be represented by the single curve as shown. Thus, as Wendt et al. found, thermodynamic equilibrium does not play an important role in the formation of NO. Equilibrium states are not achieved.

When comparing the results of Wendt et al. [1974] to this work it is important to consider the differences in the styles of the burners used. The flames generated by the burner used in this study are considered adiabatic i.e. no heat losses to the burner, whereas the burner used by Wendt et al. [1974] used heat loss as a method of flame stabilization. Since NO formation is sensitive to temperature changes [Glassman, 1996], it is probable that differences in NO measurements between the two burner designs may be partly attributed to differences flame temperature. Since Wendt's burner design used heat extraction from the flame for stabilization, the resulting lowered flame temperatures should yield lower NO formation than adiabatic flames. This appears to be the case in rich combustion when Wendt's results are compared to the simulations and experimental results of this work. In a previous thermodynamic study investigating the effect of heat extraction on

the emissions from CH_4-air and NH_3-CH_4-air flames, it was found that heat loss from the flame will result in a significant NO reduction [Mann et al., 1999].

There is some disagreement in NO production results between this work and that of Wendt et al. [1974] on the rich side of combustion. This discrepancy may be due to the nature of the sampling probe used in this work. Wendt et al. [1974] stated that the use of a stainless steel sampling probe could disrupt NO_x measurements, especially with rich combustion. As well, the sampling probe used in this work was not heated whereas Wendt et al. [1974] utilized a tape heater around a quartz probe to help maintain the integrity of the sample as it traveled to the analyzer. Further, Wendt et al. [1974] cooled the gas sample to ambient temperature before analysis. Though the experimental data for NO production in these experiments are in good agreement with the kinetic simulations, it is recommended that further work be performed with a cooled inert sampling probe such as quartz.

Figures 5.9 and 5.10 show simulation predictions and actual experimental values for NO_2 production in NH_3-CH_4-air flat flames. The general trend predicted by the simulation is similar to the experimental results. With lean combustion, increasing ammonia concentration in the fuel yields an increase in NO_2 production. However, the experimental results show higher values for NO_2 production by a factor of 30 to 40.

A possible explanation for the high experimental NO_2 values is that a 'cold flame' reaction may be occurring in the sampling probe. In cold flame regions, the chemical

reaction, $NO + HO_2 \rightarrow NO_2 + OH$ dominates kinetics and yields high NO_2 formation. The high NO_2 results give evidence that a reaction of this type may be occurring in the sampling probe.

Further, the experimental data also illustrate that NO_2 is also created in rich combustion whereas the simulation predicts no NO_2. It is suspected that the experimental data for NO_x (NO, NO_2) in rich combustion may deviate from the true values since catalysis by materials such as stainless steel is known to disturb NO_x measurements, especially when oxygen is deficient [Wendt et al., 1973]. The 5-Gas analyzer used for these measurements was designed (by the manufacturer) with a stainless steel sampling probe. It does seem that the NO and NO_2 measurements are higher than simulation values especially on the rich side where there is little oxygen. These effects could be avoided by using an inert sampling probe cooled to just above the dew point temperature with a smaller diameter that would quench the secondary cold flame NO_2 formation kinetics.

It should also be mentioned that simulations indicated that N_2O concentrations for methane-air combustion with 0% to 4% ammonia addition were no greater than 0.15 ppm.

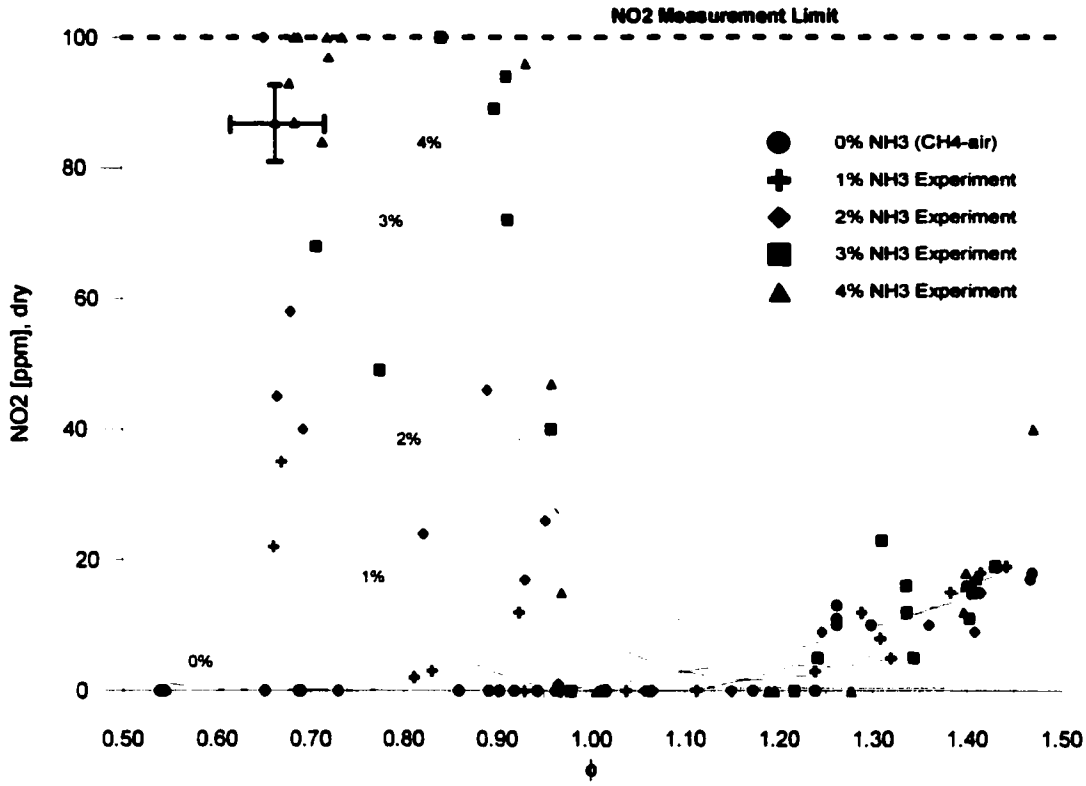

Figure 5. 9 Experimental results for NO_2 production in CH_4-air and NH_3-CH_4-air flat flames.

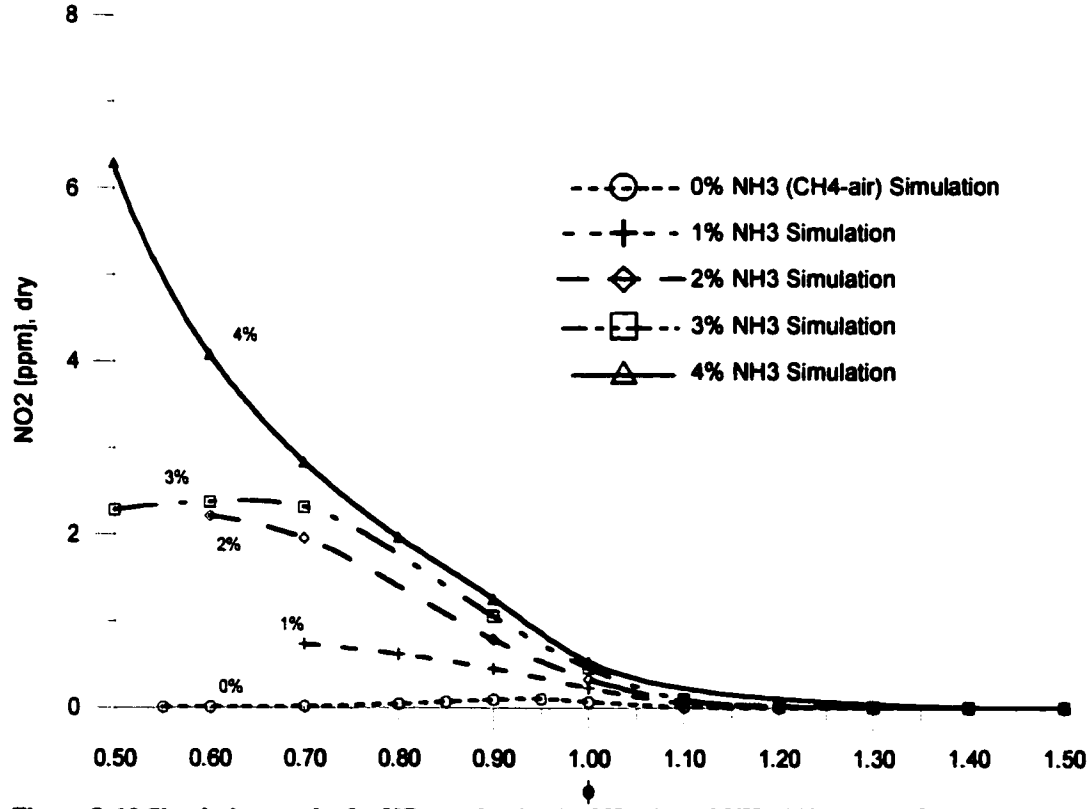

Figure 5. 10 Simulation results for NO_2 production in CH_4-air and NH_3-CH_4-air flat flames.

Another point to consider when using ammonia as a fuel additive, is whether or not there is any significant reduction in carbonaceous emissions, most importantly, carbon monoxide. Clearly when a non-carbonaceous fuel such as ammonia (NH_3) is added to a fuel such as methane (CH_4), there will be a decrease in carbonaceous emissions if only by dilution. The more ammonia that is added per mole of fuel, the less carbon there is available for oxidation. However, ammonia is a lower energy fuel, which means, when considering carbonaceous emissions, there is a trade-off between useful energy and emissions reduction. Figure 5.11 shows experimental and kinetic simulation data for methane-air combustion with and without ammonia addition.

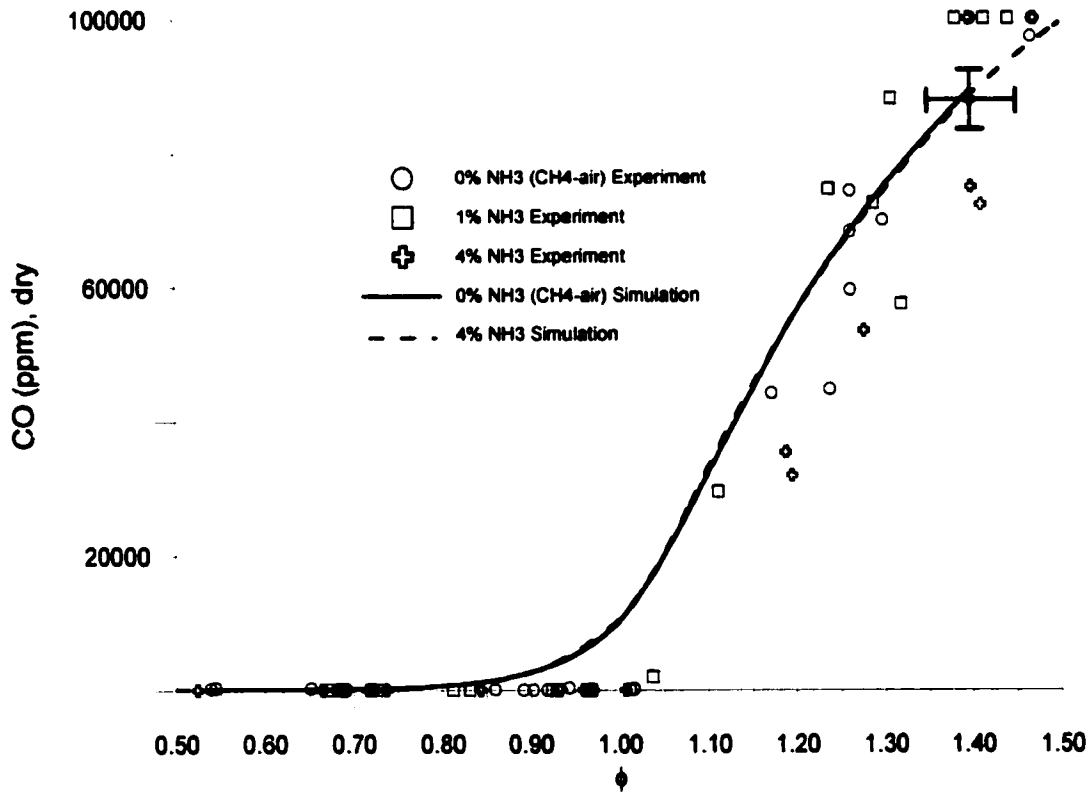

Figure 5. 11 Effect of ammonia addition on CO emissions from CH_4-air flat flames.

Upon examination of the CO emissions simulation curves it can be seen that there is, as expected, only a slight reduction in CO by addition of 4% NH_3 in the fuel. The 1% NH_3

addition simulation shows an even smaller reduction and is not shown here. The experimental scatter also shows that there is no significant CO reduction with the addition of up to 4% ammonia in the fuel. As stated previously, it is anticipated that the more ammonia added to the fuel the greater the reduction in CO. Contrary to thermodynamic predictions (Appendix I), Figure 5.11 illustrates that these reductions will be insignificant, resulting only from the dilution by the non-carbonaceous fuel additive, ammonia.

5.3 Ammonia Break-through

When using ammonia as a fuel or a fuel additive, it is important to consider whether or not there is any significant amount of unburned ammonia in the combustion products (break-through). Adding a component to a fuel that does not completely burn can give a false impression as to its effects on flame properties. As well, with the addition of ammonia it is important to check for break-through for the purpose of exposure and odour problems since ammonia is both highly toxic and has a pungent odour.

In Figure 5.12, experimental measurements for ammonia break-through are compared to simulation results for 1% and 4% NH_3 in the fuel. For the experimental measurement of NH_3, the lower limit of detection was 5 ppm (as shown in Appendix J). It should be mentioned that when NH_3 was not found the concentration was reported as 0 ppm in Figure 5.12. Experimentally, 1% and 4% NH_3 addition results show ammonia breakthrough at the lean and rich limits. With 4% NH_3 in the fuel, ammonia break-through was 50 ppm under lean combustion conditions and up to 30 ppm with rich combustion. Between these flammability limits, break-through was determined to be <5

ppm, in agreement with the simulations. On the rich side of combustion, the experimental and simulation results are also in good agreement. Both simulation and experimental data illustrate that ammonia addition to methane-air combustion can yield significant ammonia break-through at the rich combustion limits, with higher ammonia concentrations in the fuel giving higher ammonia break-through. For the experimental condition with 4%NH_3 in the fuel at ϕ=1.4, the ammonia break-through is of the order of 30ppm. This means that approximately 0.1% of the ammonia in the fuel broke through the flame front. This value exceeds the odour threshold of 17 ppm set by the American Industrial Hygiene Association (AIHA) [AIHA, 1989] and approaches the Time-Weighted Average (TWA) exposure value of 25 ppm set by the American Conference of Governmental Industrial Hygienists (ACGIH) [ACGIH, 2000].

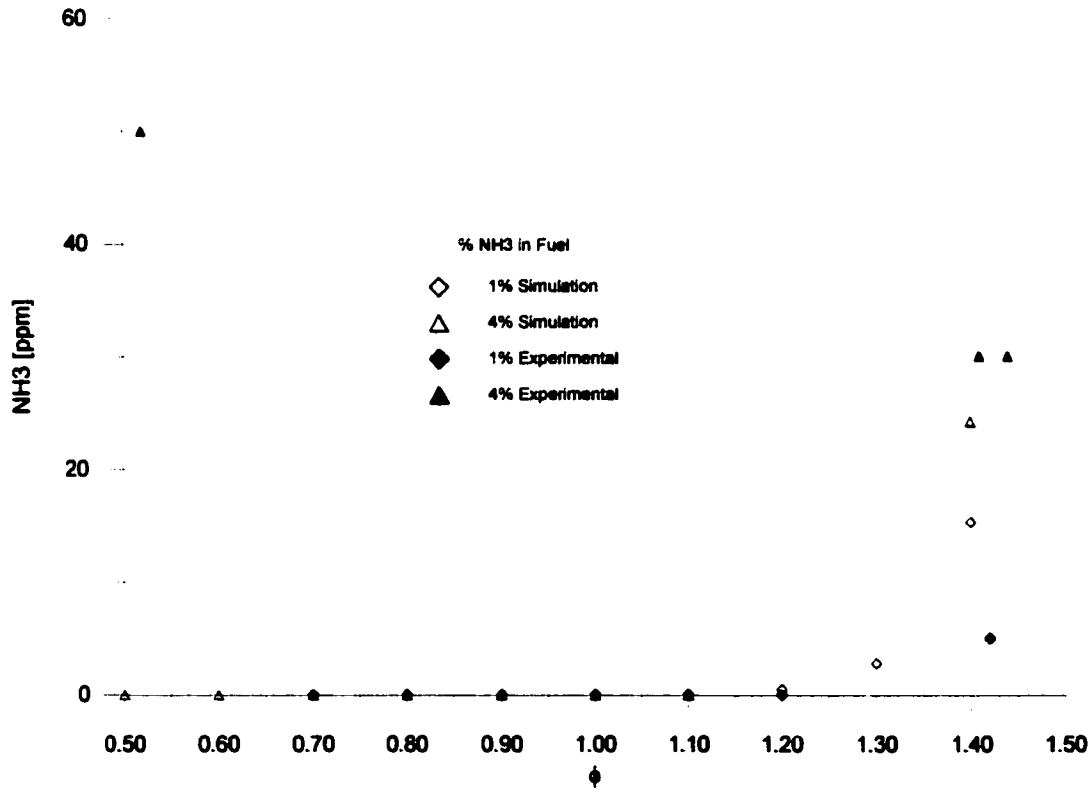

Figure 5. 12 Comparison of experimental and simulation results for ammonia break-through in NH_3-CH_4-air flat flames.

6.0 Conclusions and Recommendations

It is clear from this study that ammonia addition to the fuel in methane-air combustion results in a decrease in burning velocity and an increase in NO_x emissions. Over the entire range of flammability, as the concentration of ammonia in the fuel is increased, the burning velocity is reduced and NO emissions increase.

Ammonia has a lower heat of combustion than methane, and therefore the addition of ammonia to methane-air combustion results in a lowered flame temperatures. Since the formation of NO is temperature dependent, thermodynamic calculations show that ammonia addition to the fuel in premixed methane-air combustion slightly reduces NO emissions. However, in practice thermodynamic equilibrium is not achieved since the time scale is quite brief (~ ms) and therefore chemical kinetics determine the extent of the reaction. Thermodynamic analysis of NH_3-CH_4-Air combustion will not yield useful NO emission data. These findings are in agreement with Wendt et al. [1974].

The general trend exhibited by the chemical kinetic simulations for the production of NO are in good agreement with the experimental results of this work. This study shows that with ammonia addition, the production of NO is increased for lean, stoichiometric and rich mixtures. Contrary to the findings of Wendt et al. [1974], both the experiments and kinetic simulations of this work do not show a significant decrease in NO emissions with ammonia addition to very rich mixtures of methane-air.

It has also been demonstrated that carbonaceous emissions such as carbon monoxide (CO) are not significantly reduced by adding up to 4% ammonia to the fuel. Though thermodynamic equilibrium calculations show that with 2% ammonia CO can be reduced up to 11 %, the actual experiments and kinetic simulations show CO reduction to be insignificant.

The measurement of mixture stoichiometry and burning velocity were dependent on the accurate measurement of the unburned gas flowrates. Their accuracy can be improved through the use of mass flowmeters. The accuracy in determination of the percent ammonia in the fuel can also be improved by purchasing cylinders of premixed ammonia-methane. This would allow for greater ease in determining flame properties of ammonia-methane-air with specific ammonia additions.

Emissions measurements could be improved by using a sampling probe that will quench the reactions without condensing the water vapour or by using in-situ techniques.

It was observed that the flame area in this work varied slightly from stoichiometric conditions at the lean and rich limits. Since this dimension is critical in determining the burning velocity by the methods used in this investigation, it is recommended that a traveling microscope or other such measurement technique be used to determine the actual flame area in future work. It would be even more accurate to directly measure the unburned gas velocity in the center of the unburned gas stream by laser diagnostics.

In addition, continued work should include flame temperature measurements. With knowledge of experimental flame temperatures, the 'adiabatic' condition can be verified thus emissions and burning velocity results will have more validity.

Though the experimental set-up used in this study was adequate for measuring adiabatic burning velocity and emissions, a more accurate study of the possible correlation between the burner plate temperature and mixture stoichiometry is of interest.

References

American Conference of Governmental Industrial Hygienists (ACGIH), TLV's and BEI's, Threshold Limit Values for Chemical Substances and Physical Agents and Biological Exposure Indices, ACGIH, (2000)

American Industrial Hygiene Association (AIHA), Odour Thresholds for Chemicals with Established Occupational Heath Standards, AIHA, (1989)

Andrews, G.E., and Bradley, D., "Determination of Burning Velocities: A Critical Review", Combustion and Flame, Volume 18, 133-153, (1972)

Andrews, G.E., and Bradley, D., "The Burning Velocity of Methane-air Mixtures", Combustion and Flame, Volume 19, 275-288, (1972)

APHA, AWWA, WEF, Standard Methods for the Examination of Water and Waste Water, 19th Edition, 1995

Borman and Ragland, Combustion Engineering, McGraw-Hill, (1998)

Botha, J. P., and Spalding, D. B., "The laminar flame speed of propane/air mixtures with heat extraction from the flame", Proceedings of the Royal Society of London, Ser A, Vol 225, (1954)

Bunsen, R., "Bunsen Burner", Poggendorffs Ann. 131, 161, (1866)

Cooper, C.D., and Alley, F.C., Air Pollution Control, A Design Approach, Second Edition, Waveland Press Inc. (1994)

Cooper, J.R., Crookes, R.J. Mozafari, A., and Rose, J.W., "Ammonia as a Fuel for the IC Engine", Environmental Pollution 1, Indersciences Enterprises Limited, (1991)

Cornelius, W., Huellmantel, W.L., Mitchell, H.R., "Ammonia as an Engine Fuel", SAE Paper 650052, SAE Trans 74, 300-315, (1966)

de Goey, L.P.H., van Maaren, A., and Quax, R.M., "Stabilization of Adiabatic Premixed Laminar Flames on a Flat Flame Burner", Comb. Sci. Tech. 92, 1-3, 201, (1993)

Fristrom, R.M., Flame Structure and Processes, Oxford University Press, (1995)

Glassman, I., Combustion, Third Edition, Academic Press, (1996)

Gouy, G., "Measurement of Burning Velocity", Ann. Chim. Phys., 18, 27, (1879)

Gas Research Institute, GRI-Mechanism Version 3.0,
www.me.berkely.edu/gri_mech/overview.html

Gu, X. J., Haq, M. Z., Lawes, M., Wooley, R., "Laminar Burning Velocities and Markstein Lengths of Methane-Air Mixtures", Combustion and Flame 121:41-58, (2000)

Haywood, J. B., Internal Combustion Engineering Fundamentals, McGraw-Hill, (1988)

JANAF Thermochemical Tables, 2nd edition, (1977)

Kee, R.J., Rupley, F.M., and Meeks, E., CHEMKIN-PREMIX A Fortran Program for Modeling Steady Laminar One-Dimensional Premixed Flames, Reaction Design Sandia National Laboratories, (1998)

Law, C.K.. "A compilation of experimental data on laminar burning velocities", in Peters, N., Rogg, B., (ed.'s), Reduced kinetic mechanisms for applications in combustion systems, Lecture Notes in Physics 19, Springer Verlag, Berlin, (1993)

Mallard, E., Le Chatelier, L., "Combustion des mélanges gaseux explosives", Ann. Mines, 4, 274, (1883)

Mann, K., Henshaw, P., and Ting, D., "Combustion Thermodynamics of Ammonia/Methane/Air Mixtures", Combustion Institute Canadian Section 1999 Spring Technical Meeting, University of Alberta, Edmonton, Alberta, (1999)

Pfahl, U.J., Ross, M.C., Shepherd, J.E., Pasamehmetoglu, K.O., and Unal, C., "Flammability Limits, Ignition Energy, and Flame Speeds in H_2-CH_4-NH_3-N_2O-O_2-N_2 Mixtures", Combustion and Flame, 123:140-158, (2000)

Powling, J., "A new burner method for the determination of low burning velocities and limits of inflammability", Imperial College of Science and Technology, London, (1948)

Raezer, S.D., and Olsen, H.L., "Intermittent Thermometer, A New Method for Measuring Extreme Temperatures", Report CM 985, Applied Physics Laboratory/The Fohns Hopkins University, Laurel, MD, AD-252682, Armed Services Information Agency, Arlington Hall Station, VA, (1960)

Reynolds, W. C., The Element Potential Method for Chemical Equilibrium Analysis: Implementation of the Interactive Program STANJAN Version 3, Department of Mechanical Engineering, Stanford University, January (1986)

Roslyakov, P.V., Dvoinishnikov, V.A., Burkova, A.V., and Stepanova, E.N., "Controlling emissions of nitrogen oxides by introducing ammonia to combustion products", Thermal Engineering, 36, 9, (1989)

Vagelopoulos, C.M., and Egolfopoulos, F.N., "Direct Experimental Determination of Laminar Flame Speeds", Twenty-Seventh Symposium (International) on Combustion/The Combustion Institute, pp. 513-519, (1998)

van Maaren, A., Thung, D.S., and de Goey, L.P.H.. "Measurement of Flame Temperature and Adiabatic Burning Velocity of Methane/Air Mixtures", *Combust. Sci. and Tech.*, 96, pp. 327-344 (1993)

van Maaren, A. and de Goey, L.P.H.. "Stretch and The Adiabatic Burning Velocity of Methane- and Propane-Air Flames", *Combust. Sci. and Tech.*, 102, pp. 309-314 (1994)

van Maaren, A., One-Step Chemical Reaction Parameters for Premixed Laminar Flames, PhD Thesis, Eindhoven University of Technology, (1994)

Wendt, J. O. L.,. Sternling, C. V., and Matovich M. A, "Reduction of Sulfur Trioxide and Nitrogen Oxides by Secondary Fuel Injection", 14th Symposium (International) on Combustion, p 187, The Combustion Institute, (1973)

Wendt, J. O. L., and Sternling, C. V., "Effect of Ammonia in Gaseous Fuels on Nitrogen Oxide Emissions", Journal of the Air Pollution Control Association, Vol 24, No 11, (1974)

Appendix A: Reactant Coefficients for Simulations

Lean Conditions

Table A 1 Stoichiometric coefficients for NH_3-CH_4-Air lean mixtures

									mole fraction in reactants				
ϕ	N_{NH3}/N_{CH4}	N_{NH3}	N_{CH4}	N_{NH3}/N_{fuel}	N_{NH3}/N_{react}	x (moles of air)	(fuel/air)	N_{TReac}	CH_4	NH_3	O_2	N_2	NH_3 ppm
1	0.01	0.01	1	1%	0.09%	2.01	0.11	10.566	0.0946	0.0009	0.1900	0.7144	946
0.9	0.01	0.01	1	1%	0.09%	2.23	0.10	11.627	0.0860	0.0009	0.1918	0.7213	860
0.8	0.01	0.01	1	1%	0.08%	2.51	0.08	12.955	0.0772	0.0008	0.1937	0.7283	772
0.7	0.01	0.01	1	1%	0.07%	2.87	0.07	14.661	0.0682	0.0007	0.1956	0.7355	682
0.6	0.01	0.01	1	1%	0.06%	3.35	0.06	16.936	0.0590	0.0006	0.1976	0.7428	590
0.5	0.01	0.01	1	1%	0.05%	4.02	0.05	20.121	0.0497	0.0005	0.1995	0.7503	497
1	0.02	0.02	1	2%	0.19%	2.02	0.11	10.611	0.0942	0.0019	0.1899	0.7140	1885
0.9	0.02	0.02	1	2%	0.17%	2.24	0.10	11.677	0.0856	0.0017	0.1917	0.7209	1713
0.8	0.02	0.02	1	2%	0.15%	2.52	0.09	13.009	0.0769	0.0015	0.1936	0.7280	1537
0.7	0.02	0.02	1	2%	0.14%	2.88	0.07	14.722	0.0679	0.0014	0.1955	0.7352	1359
0.6	0.02	0.02	1	2%	0.12%	3.36	0.06	17.006	0.0588	0.0012	0.1975	0.7425	1176
0.5	0.02	0.02	1	2%	0.10%	4.03	0.05	20.203	0.0495	0.0010	0.1995	0.7500	990
1	0.03	0.03	1	3%	0.29%	2.02	0.11	10.662	0.0938	0.0029	0.1898	0.7135	2908
0.9	0.03	0.03	1	3%	0.26%	2.25	0.10	11.732	0.0852	0.0026	0.1916	0.7205	2642
0.8	0.03	0.03	1	3%	0.24%	2.53	0.09	13.069	0.0765	0.0024	0.1935	0.7276	2372
0.7	0.03	0.03	1	3%	0.21%	2.89	0.07	14.789	0.0676	0.0021	0.1954	0.7348	2096
0.6	0.03	0.03	1	3%	0.18%	3.37	0.06	17.082	0.0585	0.0018	0.1974	0.7422	1815
0.5	0.03	0.03	1	3%	0.15%	4.05	0.05	20.292	0.0493	0.0015	0.1994	0.7498	1528
1	0.04	0.04	1	4%	0.37%	2.03	0.11	10.703	0.0934	0.0037	0.1897	0.7132	3737
0.9	0.04	0.04	1	4%	0.34%	2.26	0.10	11.776	0.0849	0.0034	0.1915	0.7202	3397
0.8	0.04	0.04	1	4%	0.30%	2.54	0.09	13.119	0.0762	0.0030	0.1934	0.7273	3049
0.7	0.04	0.04	1	4%	0.27%	2.90	0.08	14.844	0.0674	0.0027	0.1954	0.7346	2695
0.6	0.04	0.04	1	4%	0.23%	3.38	0.06	17.145	0.0583	0.0023	0.1973	0.7420	2333
0.5	0.04	0.04	1	4%	0.20%	4.06	0.05	20.366	0.0491	0.0020	0.1994	0.7496	1964
1	0.05	0.05	1	5%	0.47%	2.04	0.11	10.749	0.0930	0.0047	0.1896	0.7128	4652
0.9	0.05	0.05	1	5%	0.42%	2.26	0.10	11.826	0.0846	0.0042	0.1914	0.7198	4228
0.8	0.05	0.05	1	5%	0.38%	2.55	0.09	13.173	0.0759	0.0038	0.1933	0.7270	3798
0.7	0.05	0.05	1	5%	0.34%	2.91	0.08	14.905	0.0671	0.0034	0.1953	0.7343	3355
0.6	0.05	0.05	1	5%	0.29%	3.40	0.06	17.214	0.0581	0.0029	0.1973	0.7417	2905
0.5	0.05	0.05	1	5%	0.24%	4.08	0.05	20.447	0.0489	0.0024	0.1993	0.7494	2445

Note:

H balance: y=(4+a*3)/2

O balance: x=(y+2)/2

N balance: z=(a+x*2*3.76)/2

where: $CH_4 + aNH_3 + x(O_2+3.76N_2) \rightarrow yH_2O + CO_2 + zN_2$

Rich Conditions

Table A 2 Stoichiometric coefficients for NH_3-CH_4-Air rich mixtures

									mole fraction in reactants				
ϕ	N_{NH3}/N_{CH4}	N_{NH3}	N_{CH4}	N_{NH3}/N_{total}	N_{NH3}/N_{react}	x (moles of air)	(fuel/air)	N_{TReac}	CH_4	NH_3	O_2	N_2	NH_3 ppm
1	0.01	0.01	1	1%	0.09%	2.01	0.11	10.566	0.0946	0.0009	0.1900	0.7144	946
1.1	0.01	0.01	1	1%	0.10%	1.83	0.12	9.697	0.1031	0.0010	0.1882	0.7076	1031
1.2	0.01	0.01	1	1%	0.11%	1.67	0.13	8.973	0.1114	0.0011	0.1864	0.7010	1114
1.3	0.01	0.01	1	1%	0.12%	1.54	0.14	8.361	0.1196	0.0012	0.1847	0.6945	1196
1.4	0.01	0.01	1	1%	0.13%	1.43	0.15	7.836	0.1276	0.0013	0.1830	0.6881	1276
1.5	0.01	0.01	1	1%	0.14%	1.34	0.16	7.380	0.1355	0.0014	0.1813	0.6818	1355
1	0.02	0.02	1	2%	0.19%	2.02	0.11	10.611	0.0942	0.0019	0.1899	0.7140	1885
1.1	0.02	0.02	1	2%	0.21%	1.83	0.12	9.739	0.1027	0.0021	0.1881	0.7072	2054
1.2	0.02	0.02	1	2%	0.22%	1.68	0.13	9.013	0.1110	0.0022	0.1863	0.7005	2219
1.3	0.02	0.02	1	2%	0.24%	1.55	0.14	8.398	0.1191	0.0024	0.1846	0.6940	2382
1.4	0.02	0.02	1	2%	0.25%	1.44	0.15	7.871	0.1270	0.0025	0.1829	0.6876	2541
1.5	0.02	0.02	1	2%	0.27%	1.34	0.16	7.414	0.1349	0.0027	0.1812	0.6812	2698
1	0.03	0.03	1	3%	0.29%	2.02	0.11	10.662	0.0938	0.0029	0.1898	0.7135	2908
1.1	0.03	0.03	1	3%	0.32%	1.84	0.12	9.786	0.1022	0.0032	0.1880	0.7067	3168
1.2	0.03	0.03	1	3%	0.34%	1.69	0.13	9.057	0.1104	0.0034	0.1862	0.7000	3423
1.3	0.03	0.03	1	3%	0.37%	1.56	0.14	8.439	0.1185	0.0037	0.1844	0.6934	3673
1.4	0.03	0.03	1	3%	0.39%	1.45	0.15	7.910	0.1264	0.0039	0.1827	0.6870	3919
1.5	0.03	0.03	1	3%	0.42%	1.35	0.16	7.451	0.1342	0.0042	0.1810	0.6806	4160
1	0.04	0.04	1	4%	0.37%	2.03	0.11	10.703	0.0934	0.0037	0.1897	0.7132	3737
1.1	0.04	0.04	1	4%	0.41%	1.85	0.12	9.824	0.1018	0.0041	0.1878	0.7063	4072
1.2	0.04	0.04	1	4%	0.44%	1.69	0.13	9.092	0.1100	0.0044	0.1861	0.6996	4399
1.3	0.04	0.04	1	4%	0.47%	1.56	0.14	8.473	0.1180	0.0047	0.1843	0.6930	4721
1.4	0.04	0.04	1	4%	0.50%	1.45	0.15	7.942	0.1259	0.0050	0.1826	0.6865	5037
1.5	0.04	0.04	1	4%	0.53%	1.35	0.16	7.482	0.1337	0.0053	0.1809	0.6801	5346
1	0.05	0.05	1	5%	0.47%	2.04	0.11	10.749	0.0930	0.0047	0.1896	0.7128	4652
1.1	0.05	0.05	1	5%	0.51%	1.85	0.12	9.867	0.1013	0.0051	0.1877	0.7059	5067
1.2	0.05	0.05	1	5%	0.55%	1.70	0.13	9.132	0.1095	0.0055	0.1859	0.6991	5475
1.3	0.05	0.05	1	5%	0.59%	1.57	0.14	8.510	0.1175	0.0059	0.1842	0.6925	5875
1.4	0.05	0.05	1	5%	0.63%	1.46	0.15	7.978	0.1254	0.0063	0.1824	0.6859	6268
1.5	0.05	0.05	1	5%	0.67%	1.36	0.16	7.516	0.1331	0.0067	0.1807	0.6796	6653

Note:

H balance: $y=(4+a*3)/2$

O balance: $x=(y+2)/2$

N balance: $z=(a+x*2*3.76)/2$

where: $CH_4 + aNH_3 + x(O_2+3.76N_2) \rightarrow yH_2O + CO_2 + zN_2$

Appendix B: The GRI Mechanism Version 3.0

Number	Reaction	Rate Coefficient A T^n exp(-E/RT)		
		A (mol,cm3,s)	n (T in K)	E (cal/mol)
1	O + O + M -> O2 + M	1.20E+17	-1.0	
2	O + H + M -> OH + M	5.00E+17	-1.0	
3	**O + H2 -> H + OH**	3.87E+04	2.7	6260
4	O + HO2 -> OH + O2	2.00E+13		
5	O + H2O2 -> OH + HO2	9.63E+06	2.0	4000
6	O + CH -> H + CO	5.70E+13		
7	O + CH2 -> H + HCO	8.00E+13		
8	O + CH2(S) -> H2 + CO	1.50E+13		
9	O + CH2(S) -> H + HCO	1.50E+13		
10	**O + CH3 -> H + CH2O**	5.06E+13		
11	**O + CH4 -> OH + CH3**	1.02E+09	1.5	8600
12	O + CO + M -> CO2 + M	1.80E+10		2385
13	O + HCO -> OH + CO	3.00E+13		
14	O + HCO -> H + CO2	3.00E+13		
15	**O + CH2O -> OH + HCO**	3.90E+13		3540
16	O + CH2OH -> OH + CH2O	1.00E+13		
17	O + CH3O -> OH + CH2O	1.00E+13		
18	O + CH3OH -> OH + CH2OH	3.88E+05	2.5	3100
19	O + CH3OH -> OH + CH3O	1.30E+05	2.5	5000

20	O + C2H -> CH + CO	5.00E+13		
21	**O + C2H2 -> H + HCCO**	1.35E+07	2.0	1900
22	O + C2H2 -> OH + C2H	4.60E+19	-1.4	28950
23	O + C2H2 -> CO + CH2	6.94E+06	2.0	1900
24	O + C2H3 -> H + CH2CO	3.00E+13		
25	O + C2H4 -> CH3 + HCO	1.25E+07	1.8	220
26	O + C2H5 -> CH3 + CH2O	2.24E+13		
27	**O + C2H6 -> OH + C2H5**	8.98E+07	1.9	5690
28	O + HCCO -> H + CO + CO	1.00E+14		
29	O + CH2CO -> OH + HCCO	1.00E+13		8000
30	O + CH2CO -> CH2 + CO2	1.75E+12		1350
31	O2 + CO -> O + CO2	2.50E+12		47800
32	**O2 + CH2O -> HO2 + HCO**	1.00E+14		40000
33	**H + O2 + M -> HO2 + M**	2.80E+18	-0.9	
34	**H + O2 + O2 -> HO2 + O2**	2.08E+19	-1.2	
35	H + O2 + H2O -> HO2 + H2O	1.13E+19	-0.8	
36	**H + O2 + N2 -> HO2 + N2**	2.60E+19	-1.2	
37	**H + O2 + AR -> HO2 + AR**	7.00E+17	-0.8	
38	**H + O2 -> O + OH**	2.65E+16	-0.7	17041
39	H + H + M -> H2 + M	1.00E+18	-1.0	
40	H + H + H2 -> H2 + H2	9.00E+16	-0.6	
41	**H + H + H2O -> H2 + H2O**	6.00E+19	-1.2	
42	H + H + CO2 -> H2 + CO2	5.50E+20	-2.0	
43	**H + OH + M -> H2O + M**	2.20E+22	-2.0	
44	H + HO2 -> O + H2O	3.97E+12		671

45	H + HO2 -> O2 + H2	4.48E+13		1068
46	H + HO2 -> OH + OH	8.40E+13		635
47	H + H2O2 -> HO2 + H2	1.21E+07	2.0	5200
48	H + H2O2 -> OH + H2O	1.00E+13		3600
49	H + CH -> C + H2	1.65E+14		
50	**H + CH2 (+M) -> CH3 (+M)**	pressure dependent		
51	H + CH2(S) -> CH + H2	3.00E+13		
52	H + CH3 (+M) -> CH4 (+M)	pressure dependent		
53	**H + CH4 -> CH3 + H2**	6.60E+08	1.6	10840
54	**H + HCO (+M) -> CH2O (+M)**	pressure dependent		
55	**H + HCO -> H2 + CO**	7.34E+13		
56	H + CH2O (+M) -> CH2OH (+M)	pressure dependent		
57	**H + CH2O (+M) -> CH3O (+M)**	pressure dependent		
58	**H + CH2O -> HCO + H2**	5.74E+07	1.9	2742
59	H + CH2OH (+M) -> CH3OH (+M)	pressure dependent		
60	H + CH2OH -> H2 + CH2O	2.00E+13		
61	**H + CH2OH -> OH + CH3**	1.65E+11	0.7	-284
62	H + CH2OH -> CH2(S) + H2O	3.28E+13	-0.1	610
63	H + CH3O (+M) -> CH3OH (+M)	pressure dependent		
64	H + CH3O -> H + CH2OH	4.15E+07	1.6	1924
65	H + CH3O -> H2 + CH2O	2.00E+13		
66	H + CH3O -> OH + CH3	1.50E+12	0.5	-110
67	H + CH3O -> CH2(S) + H2O	2.62E+14	-0.2	1070
68	H + CH3OH -> CH2OH + H2	1.70E+07	2.1	4870
69	H + CH3OH -> CH3O + H2	4.20E+06	2.1	4870

70	H + C2H (+M) -> C2H2 (+M)	pressure dependent		
71	H + C2H2 (+M) -> C2H3 (+M)	pressure dependent		
72	H + C2H3 (+M) -> C2H4 (+M)	pressure dependent		
73	H + C2H3 -> H2 + C2H2	3.00E+13		
74	H + C2H4 (+M) -> C2H5 (+M)	pressure dependent		
75	H + C2H4 -> C2H3 + H2	1.32E+06	2.5	12240
76	**H + C2H5 (+M) -> C2H6 (+M)**	pressure dependent		
77	**H + C2H5 -> H2 + C2H4**	2.00E+12		
78	**H + C2H6 -> C2H5 + H2**	1.15E+08	1.9	7530
79	H + HCCO -> CH2(S) + CO	1.00E+14		
80	H + CH2CO -> HCCO + H2	5.00E+13		8000
81	H + CH2CO -> CH3 + CO	1.13E+13		3428
82	H + HCCOH -> H + CH2CO	1.00E+13		
83	**H2 + CO (+M) -> CH2O (+M)**	pressure dependent		
84	**OH + H2 -> H + H2O**	2.16E+08	1.5	3430
85	**OH + OH (+M) -> H2O2 (+M)**	pressure dependent		
86	**OH + OH -> O + H2O**	3.57E+04	2.4	-2110
87	OH + HO2 -> O2 + H2O	1.45E+13		-500
88	OH + H2O2 -> HO2 + H2O	2.00E+12		427
89	OH + H2O2 -> HO2 + H2O	1.70E+18		29410
90	OH + C -> H + CO	5.00E+13		
91	OH + CH -> H + HCO	3.00E+13		
92	OH + CH2 -> H + CH2O	2.00E+13		
93	OH + CH2 -> CH + H2O	1.13E+07	2.0	3000
94	OH + CH2(S) -> H + CH2O	3.00E+13		

95	OH + CH3 (+M) -> CH3OH (+M)	pressure dependent		
96	**OH + CH3 -> CH2 + H2O**	5.60E+07	1.6	5420
97	**OH + CH3 -> CH2(S) + H2O**	6.44E+17	-1.3	1417
98	**OH + CH4 -> CH3 + H2O**	1.00E+08	1.6	3120
99	**OH + CO -> H + CO2**	4.76E+07	1.2	70
100	OH + HCO -> H2O + CO	5.00E+13		
101	**OH + CH2O -> HCO + H2O**	3.43E+09	1.2	-447
102	OH + CH2OH -> H2O + CH2O	5.00E+12		
103	OH + CH3O -> H2O + CH2O	5.00E+12		
104	OH + CH3OH -> CH2OH + H2O	1.44E+06	2.0	-840
105	OH + CH3OH -> CH3O + H2O	6.30E+06	2.0	1500
106	OH + C2H -> H + HCCO	2.00E+13		
107	OH + C2H2 -> H + CH2CO	2.18E-04	4.5	-1000
108	OH + C2H2 -> H + HCCOH	5.04E+05	2.3	13500
109	OH + C2H2 -> C2H + H2O	3.37E+07	2.0	14000
110	OH + C2H2 -> CH3 + CO	4.83E-04	4.0	-2000
111	OH + C2H3 -> H2O + C2H2	5.00E+12		
112	**OH + C2H4 -> C2H3 + H2O**	3.60E+06	2.0	2500
113	OH + C2H6 -> C2H5 + H2O	3.54E+06	2.1	870
114	OH + CH2CO -> HCCO + H2O	7.50E+12		2000
115	HO2 + HO2 -> O2 + H2O2	1.30E+11		-1630
116	**HO2 + HO2 -> O2 + H2O2**	4.20E+14		12000
117	HO2 + CH2 -> OH + CH2O	2.00E+13		
118	**HO2 + CH3 -> O2 + CH4**	1.00E+12		
119	HO2 + CH3 -> OH + CH3O	3.78E+13		

120	HO2 + CO -> OH + CO2	1.50E+14		23600
121	HO2 + CH2O -> HCO + H2O2	5.60E+06	2.0	12000
122	C + O2 -> O + CO	5.80E+13		576
123	C + CH2 -> H + C2H	5.00E+13		
124	C + CH3 -> H + C2H2	5.00E+13		
125	CH + O2 -> O + HCO	6.71E+13		
126	CH + H2 -> H + CH2	1.08E+14		3110
127	**CH + H2O -> H + CH2O**	5.71E+12		-755
128	CH + CH2 -> H + C2H2	4.00E+13		
129	**CH + CH3 -> H + C2H3**	3.00E+13		
130	CH + CH4 -> H + C2H4	6.00E+13		
131	CH + CO (+M) -> HCCO (+M)	pressure dependent		
132	CH + CO2 -> HCO + CO	1.90E+14		15792
133	CH + CH2O -> H + CH2CO	9.46E+13		-515
134	CH + HCCO -> CO + C2H2	5.00E+13		
135	**CH2 + O2 -> OH + H + CO**	5.00E+12		1500
136	**CH2 + H2 -> H + CH3**	5.00E+05	2.0	7230
137	CH2 + CH2 -> H2 + C2H2	1.60E+15		11944
138	**CH2 + CH3 -> H + C2H4**	4.00E+13		
139	**CH2 + CH4 -> CH3 + CH3**	2.46E+06	2.0	8270
140	CH2 + CO (+M) -> CH2CO (+M)	pressure dependent		
141	CH2 + HCCO -> C2H3 + CO	3.00E+13		
142	**CH2(S) + N2 -> CH2 + N2**	1.50E+13		600
143	**CH2(S) + AR -> CH2 + AR**	9.00E+12		600
144	**CH2(S) + O2 -> H + OH + CO**	2.80E+13		

145	**CH2(S) + O2 -> CO + H2O**	1.20E+13		
146	**CH2(S) + H2 -> CH3 + H**	7.00E+13		
147	CH2(S) + H2O (+M) -> CH3OH (+M)	pressure dependent		
148	**CH2(S) + H2O -> CH2 + H2O**	3.00E+13		
149	CH2(S) + CH3 -> H + C2H4	1.20E+13		-570
150	**CH2(S) + CH4 -> CH3 + CH3**	1.60E+13		-570
151	CH2(S) + CO -> CH2 + CO	9.00E+12		
152	CH2(S) + CO2 -> CH2 + CO2	7.00E+12		
153	CH2(S) + CO2 -> CO + CH2O	1.40E+13		
154	CH2(S) + C2H6 -> CH3 + C2H5	4.00E+13		-550
155	CH3 + O2 -> O + CH3O	3.56E+13		30480
156	CH3 + O2 -> OH + CH2O	2.31E+12		20315
157	CH3 + H2O2 -> HO2 + CH4	2.45E+04	2.5	5180
158	CH3 + CH3 (+M) -> C2H6 (+M)	pressure dependent		
159	CH3 + CH3 -> H + C2H5	6.84E+12	0.1	10600
160	CH3 + HCO -> CH4 + CO	2.65E+13		
161	CH3 + CH2O -> HCO + CH4	3.32E+03	2.8	5860
162	CH3 + CH3OH -> CH2OH + CH4	3.00E+07	1.5	9940
163	CH3 + CH3OH -> CH3O + CH4	1.00E+07	1.5	9940
164	CH3 + C2H4 -> C2H3 + CH4	2.27E+05	2.0	9200
165	**CH3 + C2H6 -> C2H5 + CH4**	6.14E+06	1.7	10450
166	HCO + H2O -> H + CO + H2O	1.50E+18	-1.0	17000
167	**HCO + M -> H + CO + M**	1.87E+17	-1.0	17000
168	HCO + O2 -> HO2 + CO	1.35E+13		400
169	CH2OH + O2 -> HO2 + CH2O	1.80E+13		900

170	**CH3O + O2 -> HO2 + CH2O**	4.28E-13	7.6	-3530
171	C2H + O2 -> HCO + CO	1.00E+13		-755
172	C2H + H2 -> H + C2H2	5.68E+10	0.9	1993
173	C2H3 + O2 -> HCO + CH2O	4.58E+16	-1.4	1015
174	C2H4 (+M) -> H2 + C2H2 (+M)	pressure dependent		
175	**C2H5 + O2 -> HO2 + C2H4**	8.40E+11		3875
176	HCCO + O2 -> OH + CO + CO	3.20E+12		854
177	HCCO + HCCO -> CO + CO + C2H2	1.00E+13		
178	**N + NO -> N2 + O**	2.70E+13		355
179	**N + O2 -> NO + O**	9.00E+09	1.0	6500
180	N + OH -> NO + H	3.36E+13		385
181	N2O + O -> N2 + O2	1.40E+12		10810
182	N2O + O -> NO + NO	2.90E+13		23150
183	N2O + H -> N2 + OH	3.87E+14		18880
184	N2O + OH -> N2 + HO2	2.00E+12		21060
185	N2O (+M) -> N2 + O (+M)	pressure dependent		
186	HO2 + NO -> NO2 + OH	2.11E+12		-480
187	NO + O + M -> NO2 + M	1.06E+20	-1.4	
188	NO2 + O -> NO + O2	3.90E+12		-240
189	NO2 + H -> NO + OH	1.32E+14		360
190	**NH + O -> NO + H**	4.00E+13		
191	**NH + H -> N + H2**	3.20E+13		330
192	NH + OH -> HNO + H	2.00E+13		
193	NH + OH -> N + H2O	2.00E+09	1.2	
194	NH + O2 -> HNO + O	4.61E+05	2.0	6500

195	NH + O2 -> NO + OH	1.28E+06	1.5	100
196	NH + N -> N2 + H	1.50E+13		
197	NH + H2O -> HNO + H2	2.00E+13		13850
198	NH + NO -> N2 + OH	2.16E+13	-0.2	
199	NH + NO -> N2O + H	3.65E+14	-0.5	
200	NH2 + O -> OH + NH	3.00E+12		
201	**NH2 + O -> H + HNO**	3.90E+13		
202	**NH2 + H -> NH + H2**	4.00E+13		3650
203	NH2 + OH -> NH + H2O	9.00E+07	1.5	-460
204	NNH -> N2 + H	3.30E+08		
205	NNH + M -> N2 + H + M	1.30E+14	-0.1	4980
206	NNH + O2 -> HO2 + N2	5.00E+12		
207	NNH + O -> OH + N2	2.50E+13		
208	NNH + O -> NH + NO	7.00E+13		
209	NNH + H -> H2 + N2	5.00E+13		
210	NNH + OH -> H2O + N2	2.00E+13		
211	NNH + CH3 -> CH4 + N2	2.50E+13		
212	H + NO + M -> HNO + M	4.48E+19	-1.3	740
213	HNO + O -> NO + OH	2.50E+13		
214	HNO + H -> H2 + NO	9.00E+11	0.7	660
215	HNO + OH -> NO + H2O	1.30E+07	1.9	-950
216	HNO + O2 -> HO2 + NO	1.00E+13		13000
217	CN + O -> CO + N	7.70E+13		
218	**CN + OH -> NCO + H**	4.00E+13		
219	**CN + H2O -> HCN + OH**	8.00E+12		7460

220	CN + O2 -> NCO + O	6.14E+12		-440
221	**CN + H2 -> HCN + H**	2.95E+05	2.5	2240
222	NCO + O -> NO + CO	2.35E+13		
223	NCO + H -> NH + CO	5.40E+13		
224	NCO + OH -> NO + H + CO	2.50E+12		
225	NCO + N -> N2 + CO	2.00E+13		
226	NCO + O2 -> NO + CO2	2.00E+12		20000
227	NCO + M -> N + CO + M	3.10E+14		54050
228	**NCO + NO -> N2O + CO**	1.90E+17	-1.5	740
229	**NCO + NO -> N2 + CO2**	3.80E+18	-2.0	800
230	HCN + M -> H + CN + M	1.04E+29	-3.3	126600
231	HCN + O -> NCO + H	2.03E+04	2.6	4980
232	HCN + O -> NH + CO	5.07E+03	2.6	4980
233	HCN + O -> CN + OH	3.91E+09	1.6	26600
234	**HCN + OH -> HOCN + H**	1.10E+06	2.0	13370
235	HCN + OH -> HNCO + H	4.40E+03	2.3	6400
236	HCN + OH -> NH2 + CO	1.60E+02	2.6	9000
237	H + HCN (+M) -> H2CN (+M)	pressure dependent		
238	H2CN + N -> N2 + CH2	6.00E+13		400
239	C + N2 -> CN + N	6.30E+13		46020
240	CH + N2 -> HCN + N	3.12E+09	0.9	20130
241	CH + N2 (+M) -> HCNN (+M)	pressure dependent		
242	CH2 + N2 -> HCN + NH	1.00E+13		74000
243	CH2(S) + N2 -> NH + HCN	1.00E+11		65000
244	C + NO -> CN + O	1.90E+13		

245	C + NO -> CO + N	2.90E+13		
246	CH + NO -> HCN + O	4.10E+13		
247	CH + NO -> H + NCO	1.62E+13		
248	CH + NO -> N + HCO	2.46E+13		
249	**CH2 + NO -> H + HNCO**	3.10E+17	-1.4	1270
250	**CH2 + NO -> OH + HCN**	2.90E+14	-0.7	760
251	CH2 + NO -> H + HCNO	3.80E+13	-0.4	580
252	CH2(S) + NO -> H + HNCO	3.10E+17	-1.4	1270
253	CH2(S) + NO -> OH + HCN	2.90E+14	-0.7	760
254	CH2(S) + NO -> H + HCNO	3.80E+13	-0.4	580
255	**CH3 + NO -> HCN + H2O**	9.60E+13		28800
256	CH3 + NO -> H2CN + OH	1.00E+12		21750
257	HCNN + O -> CO + H + N2	2.20E+13		
258	HCNN + O -> HCN + NO	2.00E+12		
259	HCNN + O2 -> O + HCO + N2	1.20E+13		
260	HCNN + OH -> H + HCO + N2	1.20E+13		
261	HCNN + H -> CH2 + N2	1.00E+14		
262	HNCO + O -> NH + CO2	9.80E+07	1.4	8500
263	HNCO + O -> HNO + CO	1.50E+08	1.6	44000
264	HNCO + O -> NCO + OH	2.20E+06	2.1	11400
265	HNCO + H -> NH2 + CO	2.25E+07	1.7	3800
266	HNCO + H -> H2 + NCO	1.05E+05	2.5	13300
267	HNCO + OH -> NCO + H2O	3.30E+07	1.5	3600
268	HNCO + OH -> NH2 + CO2	3.30E+06	1.5	3600
269	HNCO + M -> NH + CO + M	1.18E+16		84720

270	**HCNO + H -> H + HNCO**	2.10E+15	-0.7	2850
271	**HCNO + H -> OH + HCN**	2.70E+11	0.2	2120
272	HCNO + H -> NH2 + CO	1.70E+14	-0.8	2890
273	HOCN + H -> H + HNCO	2.00E+07	2.0	2000
274	HCCO + NO -> HCNO + CO	9.00E+12		
275	**CH3 + N -> H2CN + H**	6.10E+14	-0.3	290
276	**CH3 + N -> HCN + H2**	3.70E+12	0.1	-90
277	NH3 + H -> NH2 + H2	5.40E+05	2.4	9915
278	NH3 + OH -> NH2 + H2O	5.00E+07	1.6	955
279	NH3 + O -> NH2 + OH	9.40E+06	1.9	6460
280	NH + CO2 -> HNO + CO	1.00E+13		14350
281	CN + NO2 -> NCO + NO	6.16E+15	-0.8	345
282	NCO + NO2 -> N2O + CO2	3.25E+12		-705
283	N + CO2 -> NO + CO	3.00E+12		11300
284	**O + CH3 -> H + H2 + CO**	3.37E+13		
285	O + C2H4 -> H + CH2CHO	6.70E+06	1.8	220
286	O + C2H5 -> H + CH3CHO	1.10E+14		
287	OH + HO2 -> O2 + H2O	5.00E+15		17330
288	OH + CH3 -> H2 + CH2O	8.00E+09	0.5	-1755
289	CH + H2 (+M) -> CH3 (+M)	pressure dependent		
290	**CH2 + O2 -> H + H + CO2**	5.80E+12		1500
291	CH2 + O2 -> O + CH2O	2.40E+12		1500
292	CH2 + CH2 -> H + H + C2H2	2.00E+14		10989
293	CH2(S) + H2O -> H2 + CH2O	6.82E+10	0.2	-935
294	C2H3 + O2 -> O + CH2CHO	3.03E+11	0.3	11

295	C2H3 + O2 -> HO2 + C2H2	1.34E+06	1.6	-384
296	O + CH3CHO -> OH + CH2CHO	2.92E+12		1808
297	O + CH3CHO -> OH + CH3 + CO	2.92E+12		1808
298	O2 + CH3CHO -> HO2 + CH3 + CO	3.01E+13		39150
299	H + CH3CHO -> CH2CHO + H2	2.05E+09	1.2	2405
300	H + CH3CHO -> CH3 + H2 + CO	2.05E+09	1.2	2405
301	OH + CH3CHO -> CH3 + H2O + CO	2.34E+10	0.7	-1113
302	HO2 + CH3CHO -> CH3 + H2O2 + CO	3.01E+12		11923
303	CH3 + CH3CHO -> CH3 + CH4 + CO	2.72E+06	1.8	5920
304	H + CH2CO (+M) -> CH2CHO (+M)	pressure dependent		
305	O + CH2CHO -> H + CH2 + CO2	1.50E+14		
306	O2 + CH2CHO -> OH + CO + CH2O	1.81E+10		
307	O2 + CH2CHO -> OH + HCO + HCO	2.35E+10		
308	H + CH2CHO -> CH3 + HCO	2.20E+13		
309	H + CH2CHO -> CH2CO + H2	1.10E+13		
310	OH + CH2CHO -> H2O + CH2CO	1.20E+13		
311	OH + CH2CHO -> HCO + CH2OH	3.01E+13		
312	CH3 + C2H5 (+M) -> C3H8 (+M)	pressure dependent		
313	O + C3H8 -> OH + C3H7	1.93E+05	2.7	3716
314	**H + C3H8 -> C3H7 + H2**	1.32E+06	2.5	6756
315	OH + C3H8 -> C3H7 + H2O	3.16E+07	1.8	934
316	C3H7 + H2O2 -> HO2 + C3H8	3.78E+02	2.7	1500
317	CH3 + C3H8 -> C3H7 + CH4	9.03E-01	3.6	7154
318	CH3 + C2H4 (+M) -> C3H7 (+M)	pressure dependent		
319	O + C3H7 -> C2H5 + CH2O	9.64E+13		

320	H + C3H7 (+M) -> C3H8 (+M)	pressure dependent		
321	H + C3H7 -> CH3 + C2H5	4.06E+06	2.2	890
322	OH + C3H7 -> C2H5 + CH2OH	2.41E+13		
323	HO2 + C3H7 -> O2 + C3H8	2.55E+10	0.3	-943
324	HO2 + C3H7 -> OH + C2H5 + CH2O	2.41E+13		
325	CH3 + C3H7 -> C2H5 + C2H5	1.93E+13	-0.3	

Appendix C: Flat Flame Burner Design

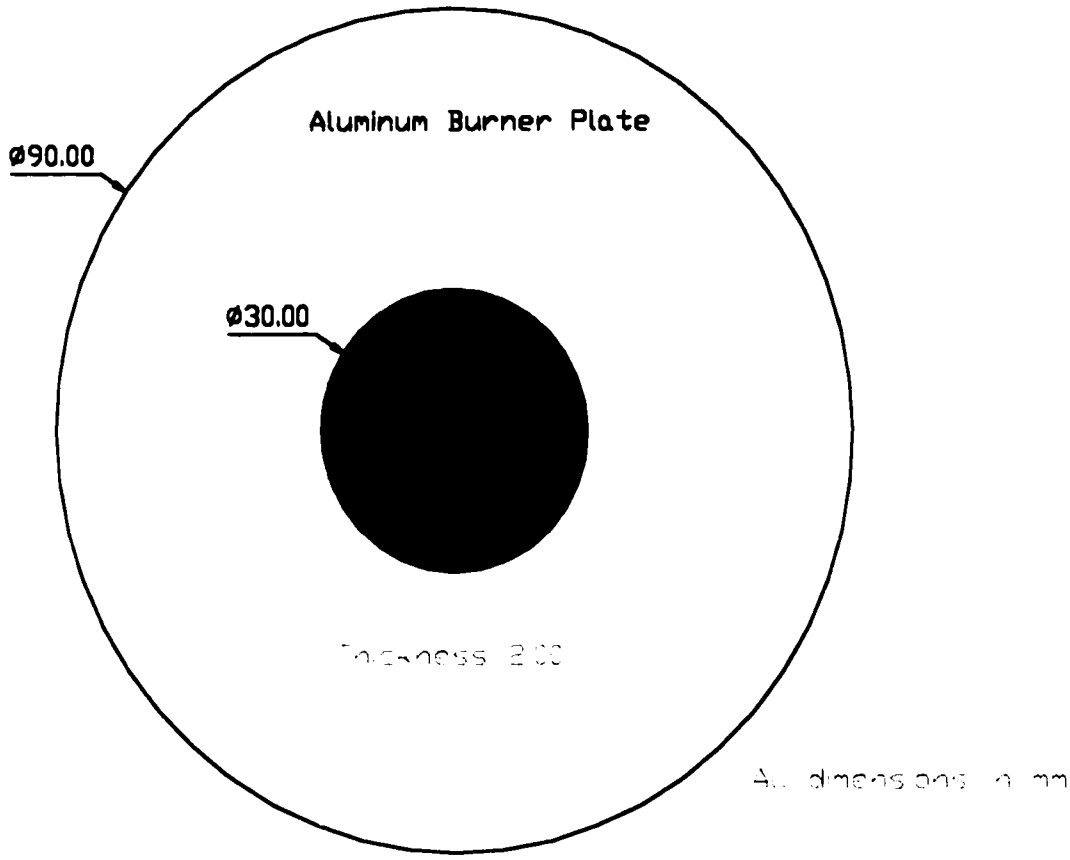

Figure C 1 Aluminum Burner Plate

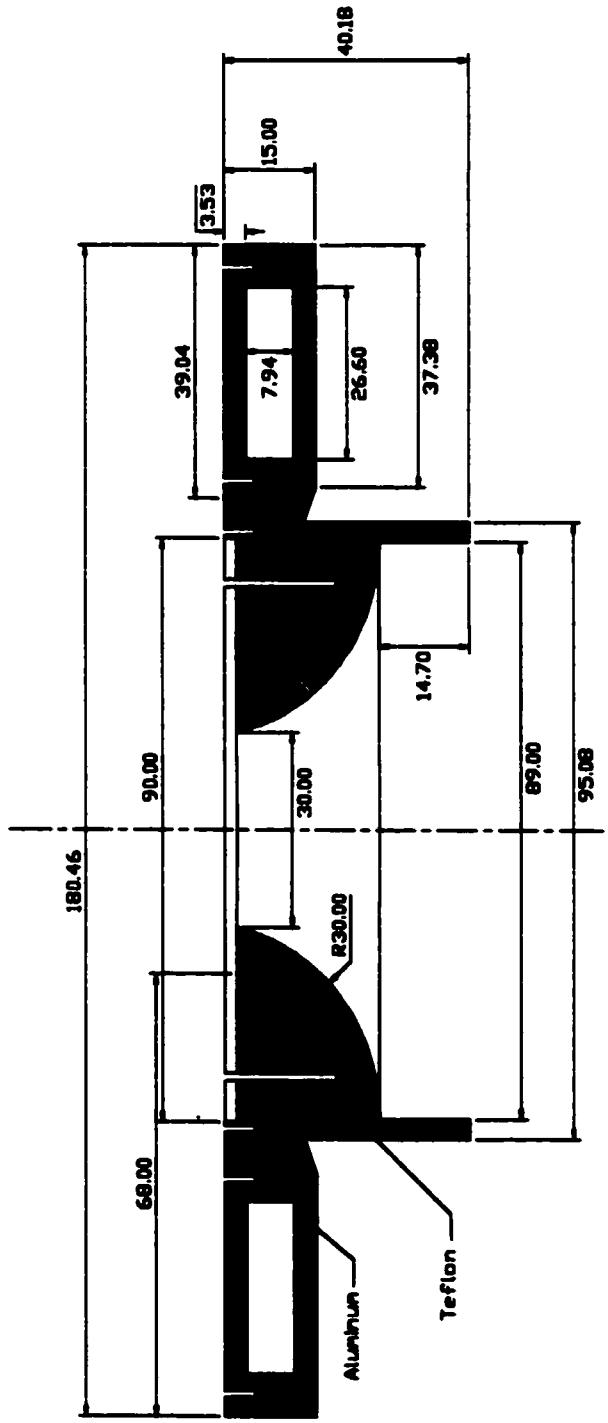

Figure C 2 Burner Head

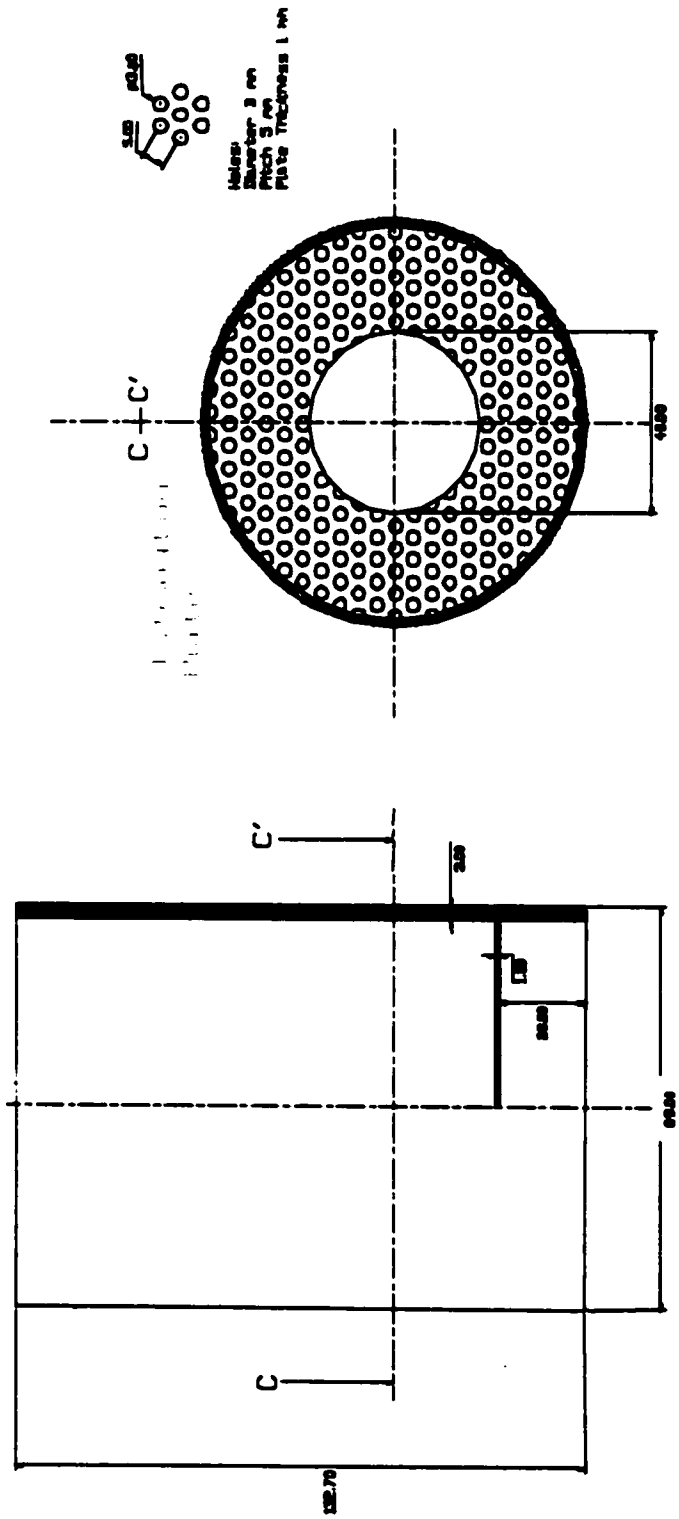

Figure C 3 Burner mixing chamber and distribution plate

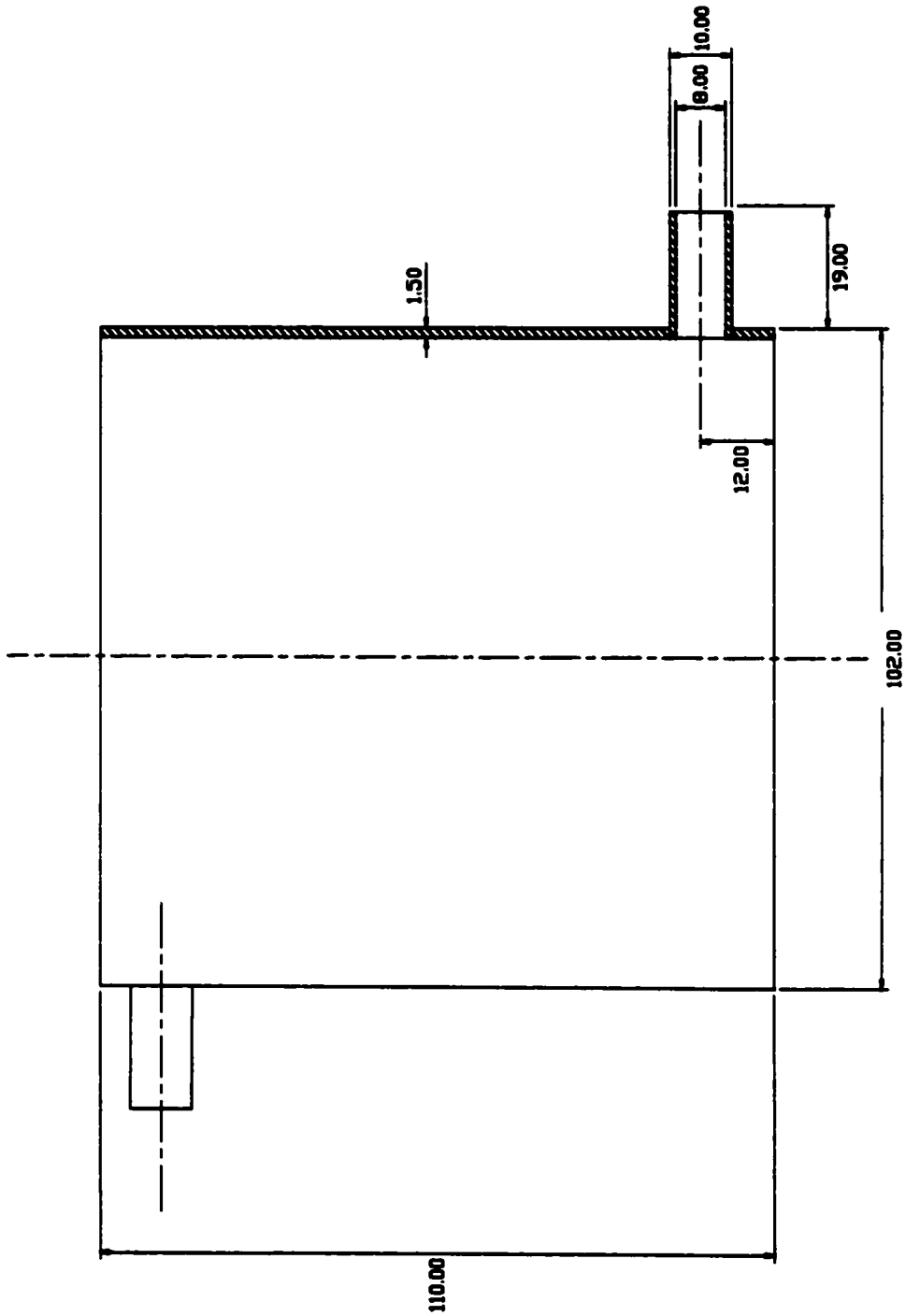

Figure C 4 Burner cooling jacket

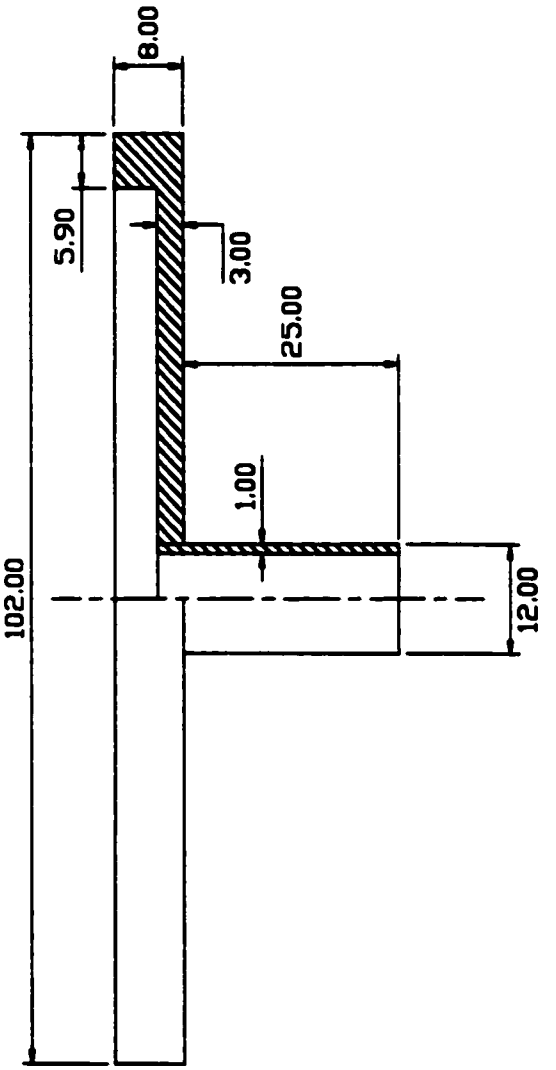

Figure C 5 Burner bottom cover plate

Appendix D: Sample Calculations

Equivalence Ratio, ϕ

The following steps describe a typical calculation of ϕ given the data recorded for an experimental data point.

1. Data at adiabatic condition:

Table D 1 Sample data for calculation of equivalence ratio.

	Ball Reading	T_{exp} [°C]	P_{exp} [in H_2O]
Air	9.55	19	15.4
CH_4	39.7	19	2.6
5%NH_3-air	3.4	19	2.8

T_{exp}= Temperature of gas stream in-line with the flowmeter [°C]
P_{exp}= pressure measured above atmospheric pressure, $P_{bar,exp}$ in-line with the flowmeter [°C]
$P_{bar,exp}$= 393.8 in H_2O

2. Calibration conditions for above ball readings:

At this point it is necessary to calculate the pressure in the gas streams above atmospheric pressure, P_{cal} and the flow rate of each gas, Q_{cal}. Substituting the value for the ball reading into the equations obtained from the calibration curves (see Appendix F for more information on calibration conditions), the following data is generated.

Table D 2 Flow rate calculation.

	Ball Reading	T_{cal} [°C]	P_{cal} [in H_2O]	Q_{cal} [L/min]
Air	9.55	21.5	15.9	10.76
CH_4	39.7	21.5	0.5	1.06
5%NH_3-air	3.4	21.1	0.5	0.66

3. Now a pressure and temperature correction is applied to obtain the actual in-line flow rates of the individual gas streams based on the following equation and dependent on operating in-line pressure and temperature, P_{exp} and $P_{bar,exp}$ and T_{exp}, and the pressure and temperature at calibration conditions, P_{cal} and $P_{bar,cal}$, T_{cal}:

$$Q_{actual} = Q_{cal}\sqrt{\frac{P_{bar,cal} + P_{cal}}{T_{cal}} \cdot \frac{T_{exp}}{P_{bar,exp} + P_{exp}}} \qquad \text{(D.1)}$$

Table D 3 summarizes the values of Q_{actual} obtained by equation D.1:

Table D 3 Pressure and temperature corrected flowrates.

	Q_{actual} [L/min]
Air	10.08
CH_4	0.99
5%NH_3-air	0.62

From Chapter 4, using equations 4.5, 4.6 and 4.2 with the values of Q_{actual} in the above table, ϕ is calculated as follows:

$$\left(\frac{F}{A}\right)_{stoich.} = \frac{1 + 0.05Q_{actual,5\%NH_3+Air}}{Q_{actual,5\%NH_3+Air}(4.522) + \left[\frac{2 + \left(\frac{4 + 0.15Q_{actual,5\%NH_3+Air}}{2}\right) - 1.9Q_{actual,5\%NH_3+Air}}{2}\right]} \qquad (4.76)$$

$$= 0.1070$$

$$\left(\frac{F}{A}\right)_{exp.} = \frac{Q_{actual,CH_4} + 0.05Q_{actual,5\%NH_3+Air}}{Q_{actual,Air} + 0.95Q_{actual,5\%NH_3+Air}}$$

$$= 0.096$$

$$\phi = \frac{\left(\frac{F}{A}\right)_{exp}}{\left(\frac{F}{A}\right)_{stoich}}$$

$$= 0.90$$

Adiabatic Burning Velocity, S_u

Using the same data point used to demonstrate the calculation of ϕ, the calculation of S_u is as follows:

$$S_u = Q_{actual,CH_4}\left(\frac{T_{exp}}{T_u}\frac{P_u}{P_{bar,exp}+P_{exp}}\right)_{CH_4} + Q_{actual,Air}\left(\frac{T_{exp}}{T_u}\frac{P_u}{P_{bar,exp}+P_{exp}}\right)_{Air} + Q_{actual,5\%NH_3+Air}\left(\frac{T_{exp}}{T_u}\frac{P_u}{P_{bar,exp}+P_{exp}}\right)_{5\%NH_3+Air} \quad \text{(D.2)}$$

where Q_{actual} for the three gas streams are given in the previous section along with their respective P_{exp}, $P_{bar,exp}$ and T_{exp} values. T_u is the unburned gas temperature measured in the mixing chamber before the flame front and P_u is assumed to be equal to atmospheric pressure.

For this case T_u= 23.6 °C and P_u=393.8 in H_2O

Thus,

S_u= 20.8 cm/s

Calculation of Ammonia Content in the Fuel

The percent NH_3 in the fuel (CH_4+NH_3) is calculated based in on the actual flowrates as follows:

$$\%NH_3 \text{ in the fuel} = \frac{0.05Q_{actual,5\%NH_3+Air}}{Q_{actual,CH_4}+0.05Q_{actual,5\%NH_3+Air}} \times 100 \quad \text{(D.3)}$$

for the case shown in the previous two calculations, and substituting in the required values,

%NH3 in the fuel = 3.0 %

Appendix E: Uncertainty Analysis

Uncertainty in Measuring ϕ

For NH_3-CH_4-air mixtures used in this thesis, the uncertainty in measuring ϕ was based on the uncertainty in measuring the unburned gas flowrates of the individual gas streams. Determining the unburned gas flowrates depended on the following quantities:

Flowmeter ball reading, X
Line pressure at calibration conditions, P_{cal} and $P_{bar,cal}$
Line pressure at experimental conditions, P_{exp} and $P_{bar,exp}$
Line temperature at calibration conditions, T_{cal}
Line temperature at experimental conditions, T_{exp}

The uncertainties in measuring each quantity are:

$uX_{CH4} = \pm 0.5$ of reading
$uP_{cal} = \pm 0.2$ mmHg
$uP_{bar,cal} = \pm 0.5$ mmHg
$uP_{exp} = \pm 0.2$ mmHg
$uP_{bar,exp} = \pm 0.1$ mmHg
$uT_{cal} = \pm .85\%$ of reading
$uT_{exp} = \pm .85\%$ of reading

The equivalence ratio was calculated by:

$$\phi = \frac{\left(\frac{Q_{actual,CH_4} + Q_{actual,NH_3}}{Q_{actual,Air}}\right)_{exp.}}{\left(\frac{F}{A}\right)_{stoich}} \qquad \text{(E.1)}$$

where $Q_{actual,CH4}$, $Q_{actual,NH3}$ and $Q_{actual,Air}$ are the actual pressure and temperature corrected volumetic flowrates of CH_4, NH_3 and Air. Since the $(F/A)_{stoich}$ term in the denominator is a theoretical number without uncertainy, the uncertainty in ϕ can be expressed as:

$$\frac{u\phi}{\phi} = \left[\left(\frac{uQ_{actual,CH_4}}{Q_{actual,CH_4}}\right)^2 + \left(\frac{uQ_{actual,NH_3}}{Q_{actual,NH_3}}\right)^2 + \left(-\frac{uQ_{actual,Air}}{Q_{actual,Air}}\right)^2\right]^{\frac{1}{2}} \qquad \text{(E.2)}$$

$Q_{actual,CH4}$, $Q_{actual,NH3}$ and $Q_{actual,Air}$ are calculated from equations of the form:

$$Q_{actual,i} = Q_{cal,i} \times \left(\frac{P_{cal} + P_{bar,cal}}{T_{cal}} \cdot \frac{T_{exp}}{P_{exp} + P_{bar,exp}} \right)^{\frac{1}{2}} \qquad \text{(E.3)}$$

where $Q_{cal,i}$ is the flowrate of the desired gas, i, at calibration conditions based on the ball reading and the linear calibration equation as shown in Appendix F. Knowing that the calculation of $Q_{cal,i}$ depends on a linear relationship with ball reading, X, the uncertainty of $Q_{cal,i}$ can be found by the following:

let $y = (P_{cal} + P_{bar,cal})$

$z = (P_{exp} + P_{bar,exp})$

thus, the uncertainty in these terms becomes,

$$uy = \left[(uP_{cal})^2 + (uP_{bar,cal})^2 \right]^{\frac{1}{2}} \longrightarrow \frac{uy}{y} = \frac{\left[(uP_{cal})^2 + (uP_{bar,cal})^2 \right]^{\frac{1}{2}}}{P_{cal} + P_{bar,cal}} \qquad \text{(E.4), (E.5)}$$

where uP_{cal} is the uncertainty in the pressure measurement, P_{cal} and $uP_{bar,cal}$ is the uncertainty in the calibration atmospheric pressure measurement, $P_{bar,cal}$.

$$uz = \left[(uP_{exp})^2 + (uP_{bar,exp})^2 \right]^{\frac{1}{2}} \longrightarrow \frac{uz}{z} = \frac{\left[(uP_{exp})^2 + (uP_{bar,exp})^2 \right]^{\frac{1}{2}}}{P_{exp} + P_{bar,exp}} \qquad \text{(E.6), (E.7)}$$

where uP_{exp} is the uncertainty in the pressure measurement, P_{exp} and $uP_{bar,exp}$ is the uncertainty in the experimental atmospheric pressure measurement, $P_{bar,exp}$.

and thus,

$$\frac{uQ_{actual,i}}{Q_{actual,i}} = \left[\left(\frac{uX}{X} \right)^2 + \left(\frac{1}{2} \frac{uy}{y} \right)^2 + \left(-\frac{1}{2} \frac{uT_{cal}}{T_{cal}} \right)^2 + \left(\frac{1}{2} \frac{uT_{exp}}{T_{exp}} \right)^2 + \left(-\frac{1}{2} \frac{uz}{z} \right)^2 \right]^{\frac{1}{2}} \qquad \text{(E.8)}$$

where uX is the uncertainty in ball reading, X, uy/y is the uncertainty in the calibration pressure measurement, uT_{cal} is the uncertainty in the calibration in-line temperature measurement, T_{cal}, uT_{exp} is the uncertainty in the experimental in-line temperature measurement, T_{exp}, and uz/z is the uncertainty in the experimental pressure measurement.

Table E 1 summarizes the results of applying the above analysis to lean, near stoichiometric and rich CH_4-air combustion.

Table E 1 Typical uncertainty in equivalence ratio.

				Error Range in ϕ	
Calculated ϕ	$u\phi/\phi$	$u\phi/\phi$ [%]	+/-	+	-
0.65	0.03	3.4	0.02	0.67	0.63
1.08	0.01	1.4	0.02	1.10	1.06
1.55	0.04	3.8	0.06	1.61	1.49

Table E 2 show the uncertainty analysis performed on lean, near stoichiometric and rich NH_3-CH_4-air mixtures.

Table E 2 Typical uncertainty in equivalence ratio with ammonia addition

					Error Range in ϕ	
% NH_3 in fuel	Calculated ϕ	$u\phi/\phi$	$u\phi/\phi$ [%]	+/-	+	-
4.1% NH3	0.68	0.08	7.9	0.05	0.73	0.63
4.3% NH3	1.01	0.02	2.1	0.02	1.03	0.99
3.8% NH3	1.40	0.04	3.7	0.05	1.45	1.35
4.4% NH3	1.47	0.06	5.9	0.09	1.56	1.38

Uncertainty in Measuring S_u

Similar to the previous section, the uncertainty in measuring S_u depends on the uncertainty in measuring the unburned gas flowrate. As shown in the following equation, Su is calculated based on the total flowrate of the unburned gas stream, with the necessary pressure and temperature corrections.

$$S_u = Q_{actual,CH_4}\left(\frac{T_{exp}}{T_{burner}}\frac{P_u}{P_{bar,exp}+P_{exp}}\right)_{CH_4} + Q_{actual,Air}\left(\frac{T_{exp}}{T_{burner}}\frac{P_u}{P_{bar,exp}+P_{exp}}\right)_{Air} + Q_{actual,5\%NH_3+Air}\left(\frac{T_{exp}}{T_{burner}}\frac{P_u}{P_{bar,exp}+P_{exp}}\right)_{5\%NH_3+Air} \quad \text{(E.9)}$$

The uncertainty in measuring S_u then becomes:

$$\frac{uS_u}{S_u} = \left[\begin{array}{l} \left(\frac{uQ_{actual,CH_4}}{Q_{actual,CH_4}}\right)^2 + \left[\left(\frac{uT_{exp}}{T_{exp}}\right)^2 + \left(-\frac{uT_u}{T_u}\right)^2 + \left(\frac{uP_u}{P_u}\right)^2 + \left(-\frac{uz}{z}\right)^2\right]_{CH_4} + \\ \left(\frac{uQ_{actual,Air}}{Q_{actual,Air}}\right)^2 + \left[\left(\frac{uT_{exp}}{T_{exp}}\right)^2 + \left(-\frac{uT_u}{T_u}\right)^2 + \left(\frac{uP_u}{P_u}\right)^2 + \left(-\frac{uz}{z}\right)^2\right]_{Air} + \\ \left(\frac{uQ_{actual,NH_3}}{Q_{actual,NH_3}}\right)^2 + \left[\left(\frac{uT_{exp}}{T_{exp}}\right)^2 + \left(-\frac{uT_u}{T_u}\right)^2 + \left(\frac{uP_u}{P_u}\right)^2 + \left(-\frac{uz}{z}\right)^2\right]_{NH_3} \end{array} \right]^{\frac{1}{2}} \quad \text{(E.10)}$$

where the expressions for $\left(\frac{uQ_{actual,i}}{Q_{actual,i}}\right)$ are given in the previous section, uT_{exp} is the uncertainty in the experimental in-line temperature measurement, T_{exp}, uT_u is the uncertainty in the experimental unburned gas temperature measurement, T_u, uP_u is the uncertainty in the experimental unburned gas pressure measurement, P_u (P_u was assumed to be atmospheric pressure), uz/z is the uncertainty in the experimental in-line pressure measurement.

The results for the uncertainty analysis for the same data points used in the previous section are shown in Table E 3 and Table E 4.

Table E 3 Uncertainty in measuring S_u.

					Error Range in Su	
ϕ	Calculated Su	uSu/Su	uSu/Su [%]	+/-	+	-
0.65	12.5	0.04	3.8	0.5	13.0	12.0
1.08	34.7	0.02	2.2	0.8	35.5	33.9
1.55	8.6	0.04	4.2	0.4	9.0	8.3

Table E 4 Uncertainty in S_u with ammonia addition.

% NH_3 in fuel	ϕ	Calculated Su	uSu/Su	uSu/Su [%]	+/-	Error Range in Su	
						+	-
4.1% NH3	0.68	13.0	0.06	6.4	0.8	13.9	12.2
4.3% NH3	1.01	28.9	0.03	2.8	0.8	29.7	28.1
3.8% NH3	1.40	19.3	0.04	3.7	0.7	20.0	18.6
4.4% NH3	1.47	8.2	0.05	5.3	0.4	8.6	7.7

Uncertainty in NH_3% in fuel

The percent of NH_3 in the fuel (CH_4+NH_3) is determined be the following expression:

$$\%NH_3 \text{ in the fuel} = \frac{0.05Q_{actual,5\%NH_3+Air}}{Q_{actual,CH_4} + 0.05Q_{actual,5\%NH_3+Air}} \times 100 \qquad \text{(E.11)}$$

The uncertainty in this calculation is,

$$\frac{u\%NH_3}{\%NH_3} = \left[\left(\frac{uQ_{NH_3}}{Q_{NH_3}}\right)^2 + \left(-\frac{uQ_{CH_4}}{Q_{CH_4}}\right)^2 + \left(-\frac{uQ_{NH_3}}{Q_{NH_3}}\right)^2\right]^{\frac{1}{2}} \qquad \text{(E.12)}$$

Table E 5 Uncertainty in measuring the ammonia content of the fuel.

$\%NH_3$	ϕ	$u\%NH_3/\%NH_3$	%u	+/-	Error Range in $\%NH_3$	
					+	-
3.8	1.40	0.03	3.3	0.1	3.9	3.7
4.4	1.47	0.05	5.0	0.2	4.6	4.2
4.1	0.68	0.08	7.7	0.3	4.4	3.8
4.3	1.01	0.02	1.7	0.1	4.4	4.2

Appendix F: Calibration of Flowmeters

The flowmeters used in this study were calibrated using a bubble meter as a primary standard (Mini-Buck Calibrator). The calibrations were performed using the actual gases (CH_4, 5%NH_3-air, Air) that were used in the experiments. Thus only operating temperature and pressure corrections were needed when determining actual flowrates in experiments from the calibration data. For each flowmeter, calibration was performed according to the following steps:

1. With experimental layout as per usual, i.e. all flowmeters and apparatus in place, disconnect the burner from the sampling train and connect the Buck Calibrator in its place.
2. Set the desired calibration gas to a desired flowrate and record:
    - Ball reading
    - Line temperature (T_{cal}) and pressure (P_{cal})
    - Atmospheric pressure at calibration conditions ($P_{bar,cal}$)
    - Average of three bubble meter flow measurements (Q_{cal}) in L/min
3. Repeat steps 1 and 2 for the entire working range of the flowmeter
4. Plot ball reading vs. Q_{cal} and use linear regression to create an equation for flowrate, Q_{cal}, in terms of ball reading.
5. Plot ball reading vs. P_{cal} and use curve fit to create an equation for pressure, P_{cal}, in terms of ball reading.

The calibration curves for the flowmeters used in this study are show in Figures F.1 to F.4. The following table summarizes the calibration curve equations used for the three gasses used in these experiments. With these equations, flowrates and pressure at varying ball readings can be determined.

Table F 1 Flowrate calibration equations.

Gas	Flowmeter	Flowrate Calibration Equation	Pressure Calibration Equation
Air	Brooks No. 5	Q_{cal}=1.1178x+ 0.0812	P_{cal}=0.1497x^2+0.0943x+1.3116
CH_4	Gilmont No. 23403	Q_{cal}=0.0327x - 0.2394	P_{cal}=0.0002x^2+0.0002x+0.1879
5%NH_3-Air	Matheson No. 603	Q_{cal}= 0.179x + 0.0497	P_{cal}=0.0073x^2+0.0321x + 0.34

Note: x represents the ball reading in these equations.

Table F 2 Atmospheric pressure at calibration conditions.

Gas	$P_{bar,cal}$ [in H_2O]
Air	397.0
CH_4	393.8
5%NH_3-Air	393.8

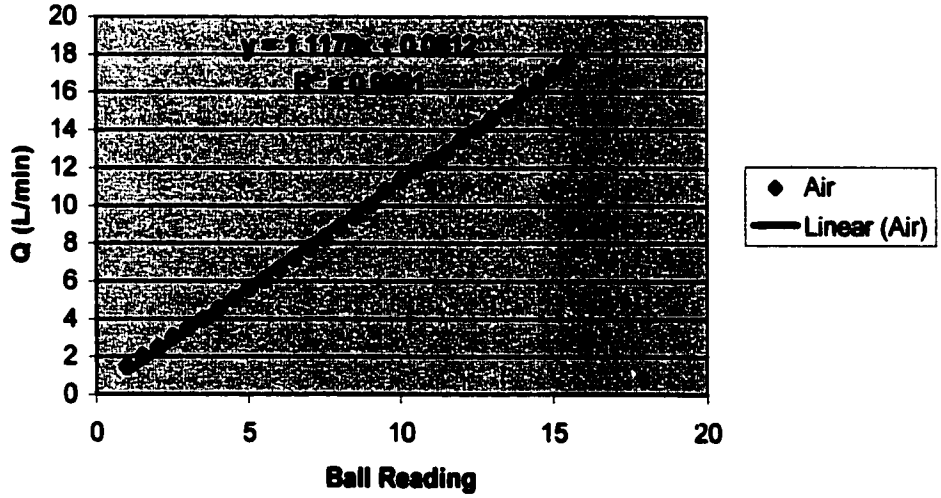

Figure F. 1 Flowrate calibration curve for the air flow.

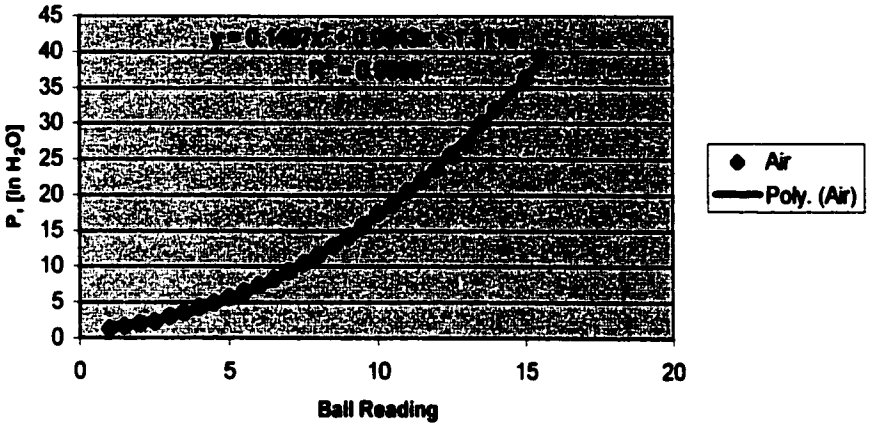

Figure F. 2 Pressure calibration curve for air.

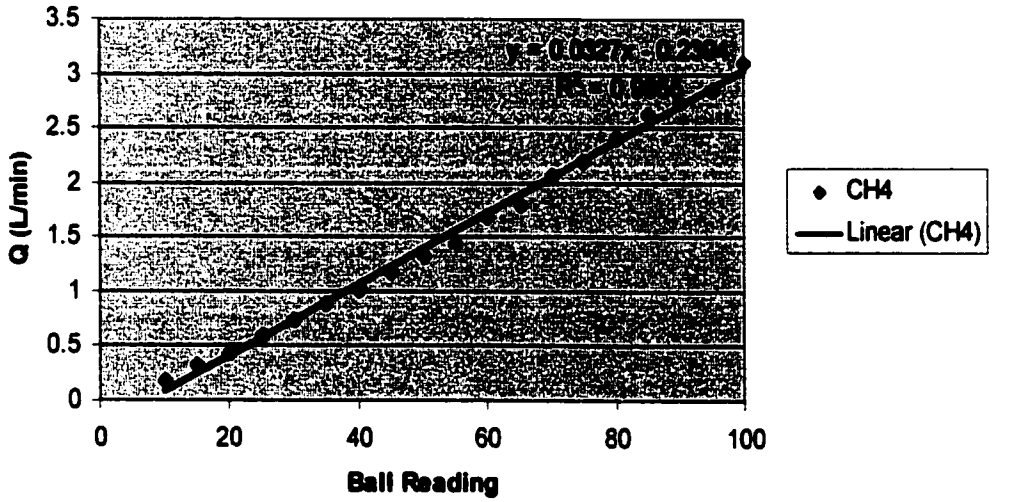

Figure F. 3 Flowrate calibration curve for methane.

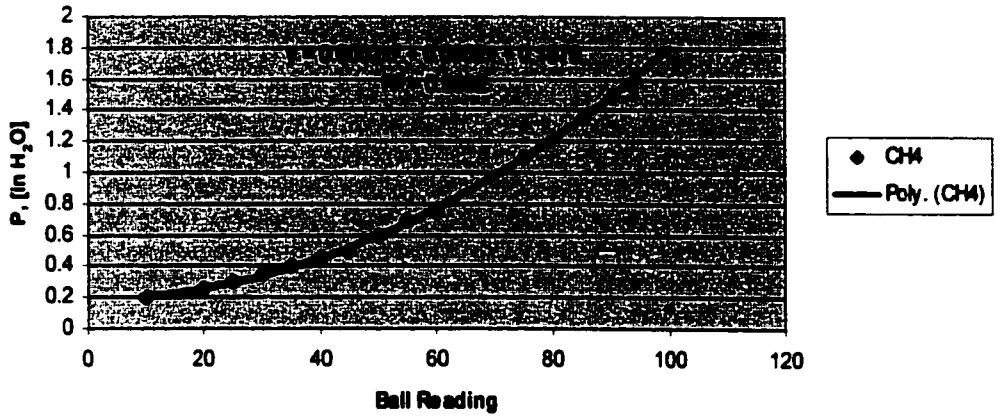

Figure F. 4 Pressure calibration curve for methane.

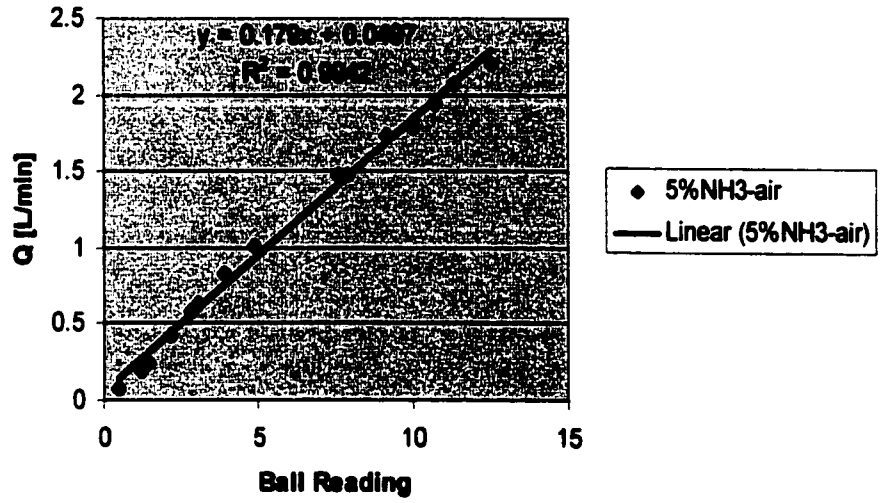

Figure F. 5 Flowrate calibration curve for 5%-NH_3-air

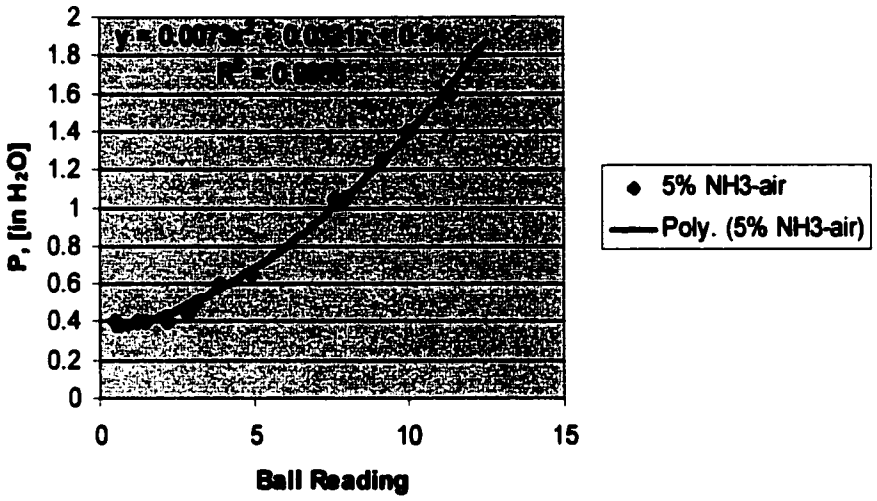

Figure F. 6 Pressure calibration curve for 5%-NH_3-air.

Appendix G: Measurement Range and Accuracy of the IMR 5-Gas Analyzer

Table G 1 IMR 5-Gas Analyzer accuracy and measurement range.

Species	Measurement Principle	Resolution	Accuracy	Measurement Range
O_2	Electrochem. Sensor	0.1 vol. %	Z	0 – 20.9 %
CO	Electrochem. Sensor	1 ppm	Z	0 – 100000 ppm
CO_2	Calculated	0.1 vol. %	Z	Calculated
NO	Electrochem. Sensor	1 ppm	Z	0 – 4000 ppm
NO_2	Electrochem. Sensor	1 ppm	Z	0 – 100 ppm

Z = 0 – 20% of whole measurement range ± 1% of maximum measurement
20 – 100% of whole measurement range ±5% of displayed measurement

Calibrated by IMR June 05, 2000

Appendix H: Observed Flame Properties

Table H 1 Observed characteristics for CH_4-Air and NH_3-CH_4-Air flames

	Condtion	Flame Appearance	Post Flame Appearance
Pure CH_4	Lean	Flat, blue	none
	Stoichiometric	Small corrugations, blue	~ 15 cm bright cone
	Rich	Flat, blue	none
Ammonia Addition	Lean	Flat, pinkish-orange	~ 2.5 cm orange cone
	Stoichiometric	Small corrugations, pinkish-orange	~ 12 cm orange cone
	Rich	Flat, pinkish-orange	~ 2.5 cm dark orange cone

Flame Photographs

Figure H 1 Photograph of a CH_4-air adiabatic flat flame at ϕ=0.7.

Figure H 2 Photograph of a CH_4-air adiabatic flat flame at ϕ=0.9.

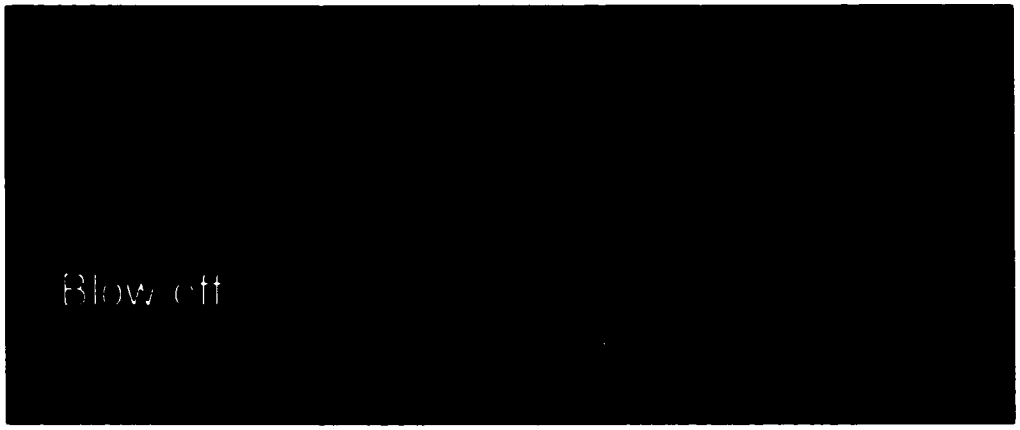

Figure H 3 Photograph of a CH_4-air flame with the unburned gas velocity > S_u.

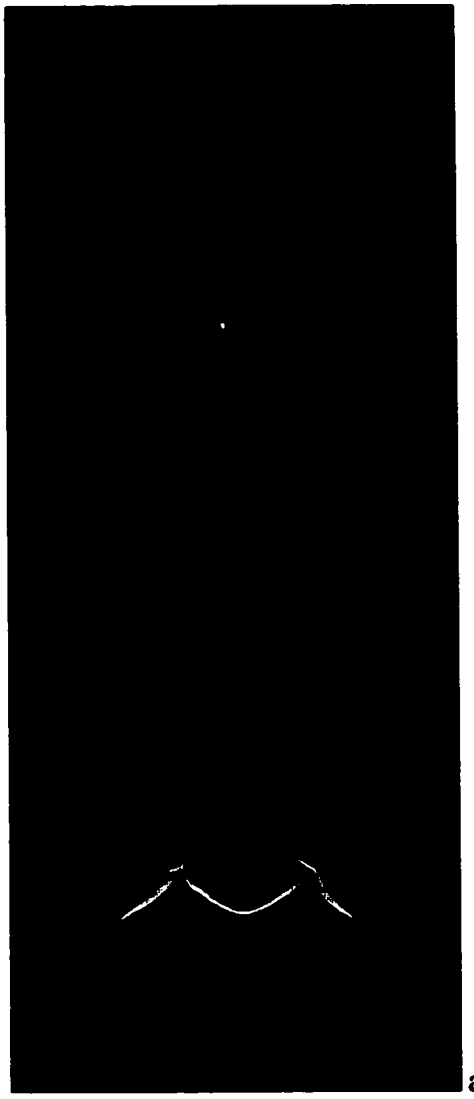

a)

b)

Figure H 4 Unburned gas flowrate greater than Su for a) CH_4-air rich flame, b) CH_4-air lean flame.

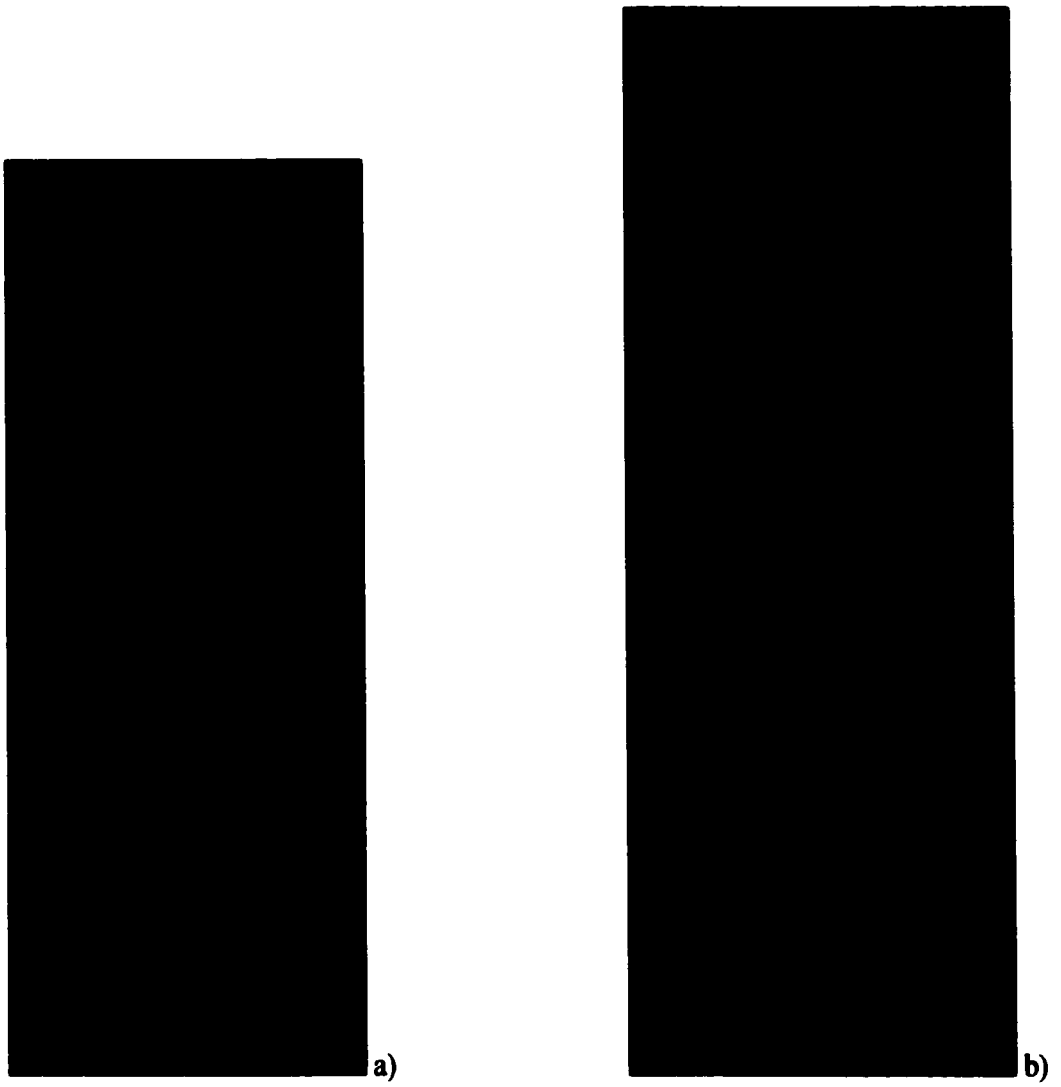

Figure H 5 Photograph of 4% NH_3 addition flame for a) lean conditions and b) rich conditions

Appendix I: Thermodynamic Comparison of CH_4-air and NH_3-CH_4-air Combustion

Stoichiometric Methane-Air

$CH_4 + 2(O_2 + 3.76N_2) \rightarrow CO_2 + 2\,H_2O + 7.52N_2$

$\Delta H_{comb} = \Delta H_{fCO2} + 2\Delta H_{fH2O} - \Delta H_{fCH4}$
$= -802.31$ kJ/molCH_4 (at 298K)

From STANJAN equilibrium data (table E1), [NO] =2195ppm/molCH_4

Thus, $\dfrac{2195\ \text{ppmNO/mol}CH_4}{802.31\ \text{kJ/mol}CH_4} = 2.74$ ppmNO/kJ

Stoichiometric Ammonia-Air

$NH_3 + 0.75(O_2 + 3.76N_2) \rightarrow 1.5H_2O + 6.64N_2$

$\Delta H_{comb} = 1.5\Delta H_{fH2O} - \Delta H_{fNH3}$
$= -316.78$ kJ/molNH_3 (at 298K)

From STANJAN equilibrium (data table E2), [NO] =821ppm/molNH_3

Thus, $\dfrac{821\ \text{ppmNO/mol}NH_3}{316.78\ \text{kJ/mol}NH_3} = 2.59$ ppmNO/kJ

Table I 1 STANJAN equilibrium products for stoichiometric CH_4-Air

Product Species	mol fraction	[ppm]
H2O	1.85190E-01	185190
CO2	8.53440E-02	85344
N2	7.09150E-01	709150
H2	3.70420E-03	3704.2
O2	5.30650E-03	5306.5
CO	9.10470E-03	9104.7
NO	2.19520E-03	2195.2
NO2	3.89170E-07	0.38917

Table I 2 STANJAN equilibrium products for stoichiometric NH_3-Air

Product Species	mol fraction	[ppm]
H2O	3.06560E-01	306560
CO2	0.00000E+00	0
N2	6.87000E-01	687000
H2	4.01510E-03	4015.1
O2	1.59680E-03	1596.8
CO	0.00000E+00	0
NO	8.21350E-04	821.35
NO2	1.00720E-07	0.10072

Table I 3 STANJAN equilibrium products for stoichiometric $0.2NH_3$-CH_4-Air

Product Species	mol fraction	[ppm]	% reduction on a wet basis compared to CH_4-Air
H2O	1.95300E-01	195300	-5.46%
CO2	7.84930E-02	78493	8.03%
N2	7.07390E-01	707390	0.25%
H2	3.78980E-03	3789.8	-2.31%
O2	4.90120E-03	4901.2	7.64%
CO	8.06810E-03	8068.1	11.39%
NO	2.05480E-03	2054.8	6.40%
NO2	3.55710E-07	0.35571	8.60%

CO_2 Reduction with Consideration to Useful Energy

As an example, consider the following:

$1\ CH_4 + Air \longrightarrow 1\ CO_2 + other\ products$ $\quad CO_2/Energy = 1$
$\Delta Hcomb = 1$ energy

$1\ NH3 + Air \longrightarrow 0\ CO_2 + other\ products$ $\quad CO_2/Energy = 0$
$\Delta Hcomb = 0.4$ energy (compared to methane-air) (ie. no CO_2 produced)

Upon mixing,

Assume 1 mole of fuel,

$1(NH_3 + CH_4) + Air \longrightarrow Products$

Thus, in a 20% NH_3, 80% CH_4 fuel mixture, burned in air:

Energy Produced = 0.2(0.4) + 0.8(1) = 0.88 energy

CO_2 produced $\longrightarrow$ 0.8 CO_2 (since fuel contains 20% less Carbon)

$$\frac{CO_2}{Energy} = \frac{0.8\ CO_2}{0.88\ Energy} = 0.9\ \frac{CO_2}{Energy}$$

This means that with 20% ammonia in methane there is a 10% reduction in CO_2 emissions for the same energy output.

Appendix J: Ammonia Break-through Lower Limit of Detection

Based on Standard Methods, Method number 4500-NH_3 C, ammonia by boric acid titration [APHA, AWWA, WEF, 1995], the lower limit of detection of NH_3 was determined by the following:

Indirect Titimetric Analysis:

Knowing at the endpoint, the number of equivalents of H_2SO_4 is equal to the number of equivalents of NH_3. It can be written that,

$$\#eq\ H_2SO_4 = \#eq\ NH_3 \tag{J.1}$$

or,

$$(N \cdot V)_{H_2SO_4} = \frac{m_{NH_3}}{EW_{NH_3}} \tag{J.2}$$

thus,

$$m_{NH_3} = EW_{NH_3}(N \cdot V)_{H_2SO_4} \tag{J.3}$$

where,

m_{NH3} = mass of NH_3 [g]
EW_{NH3} = 17 = equivalent weight of NH_3 [g/equiv]
N_{H2SO4} = 0.114 = Normality of the H_2SO_4 solution used for titration
V_{H2SO4} = volume of H_2SO_4 used to titrate to the endpoint

The lower limit of detection for this method is determined by assuming that just enough ammonia is captured in the impinger to require only one drop of the H_2SO_4 solution to

reach the endpoint. A drop of this size is approximately 0.05mL (V_{H2SO4} =0.05 mL). Since typically 25 L of sample was collected, the lower limit of detection is found by using equation J.3,

$$m_{NH_3} = 17\left(0.114 \cdot 0.05 \times 10^{-3}\right) = 9.69 \times 10^{-5}\ g \tag{J.4}$$

since 25 L of sample was collected,

$$[NH_3] = \frac{9.69 \times 10^{-5}}{30} = 3.23 \times 10^{-6}\ \frac{g}{L} = 3.23\ \frac{mg}{m^3}$$

this concentration is expressed in ppm_v by,

$$ppm_v = \frac{[NH_3] \cdot (22.4) \cdot (T)}{MW_{NH_3} \cdot (273) \cdot (P)} \tag{J.5}$$

where

$[NH_3]$ = the concentration of NH_3 in mg/m^3
T = the temperature of the sample in K
P = the pressure of the sample in atm

thus,

$$ppm_v = \frac{(3.23) \cdot (22.4) \cdot (298)}{17 \cdot (273) \cdot (1)} = 4.6\ ppm$$

Therefore the lower limit of detection for the measurement of ammonia break-through is approximately 5 ppm.

Vita Auctoris

Name: Kenneth R.C. Mann

Place of Birth: Windsor Ontario

Year of Birth: 1974

Education: Sandwich Secondary School, La Salle
1989 – 1993

University of Windsor, Windsor, Ontario
1993 – 1998, B.A.Sc.

University of Windsor, Windsor, Ontario
1998 – 2000, M.A.Sc.